ENHANCEMENT OF FINE PARTICLE DEPOSITION TO PERMEABLE SEDIMENTS

By

Jerry Stephen Fries

B.A., Carnegie Mellon University, 1994

Submitted in partial fulfillment of the requirements of the degree of

Doctor of Philosophy

at the

MASSACHUSETTS INSTITUTE OF TECHNOLOGY

and the

WOODS HOLE OCEANOGRAPHIC INSTITUTION

February 2002

Signature of Author

_____

Joint Program in Oceanography
Massachusetts Institute of Technology and Woods Hole Oceanographic Institution
February 2002

Certified by

_____

John H. Trowbridge
Thesis Supervisor

Accepted by

_____

Ole S. Madsen
Professor of Civil and Environmental Engineering
Thesis Committee Chairman

Accepted by

_____

Oral Buyukozturk
Chairman, Departmental Committee on Graduate Studies

Accepted by

_____

Michael Triantafyllou
Chair, Joint Committee for AOSE

ENHANCEMENT OF FINE PARTICLE DEPOSITION TO PERMEABLE SEDIMENTS

by

Jerry Stephen Fries

Submitted to the Joint Program in Applied Ocean Science and Engineering
and the Department of Civil and Environmental Engineering
on October 16, 2001 in Partial Fulfillment of the Requirements
for the Degree of Doctorate of Philosophy in Civil and Environmental
Engineering and Oceanographic Engineering

ABSTRACT

Predictions of deposition rate are integral to the transport of many constituents including contaminants, organic matter, and larvae. Review of the literature demonstrates a general appreciation for the potential control of deposition by bed roughness, but no direct tests involving flat sediment beds. Understanding the mechanisms at work for flat sediment beds would provide the basis for exploring more complicated bed conditions and the incorporation of other transport processes, such as bioturbation and bedload transport.

Generally, fine particle deposition rates are assumed to be equivalent to the suspension settling velocity, therefore, deposition rates in excess of settling are considered enhanced. Flume observations of deposition were made using treatments that covered a wide range of flow, particle, and bed conditions. Specific treatments demonstrated large enhancements (up to eight times settling). Delivery of particles to the interface is important, but models based on delivery alone failed to predict the observed enhancement.

This necessitated the development of a new model based on a balance between delivery and filtration in the bed. Interfacial diffusion was chosen as a model for particle delivery. Filtration of particles by the bed is a useful framework for retention, but the shear in the interstitial flow may introduce additional factors not included in traditional filtration experiments.

The model performed well in prediction of flow conditions, but there remained a discrepancy between predictions and observed deposition rate, especially for treatments with significant enhancement. Fluid flow predictions by the model, such as slip at the sediment water interface and fluid penetration into the sediment, appeared to be supported by flume experiments. Therefore, failure to predict the magnitude of enhancement was attributed to far greater filtration efficiencies for the sediment water interface than those measured in sediment columns. Emerging techniques to directly measure fluid and particle motion at the interface could reveal these mechanisms. The observation of enhanced deposition to flat sediment beds reinforces the importance of permeable sediments to the mediation of transport from the water column to the sediment bed.

Thesis Supervisor: John Trowbridge, Woods Hole Oceanographic Institution

Acknowledgements

I could not of completed this work without loving support from my family. They have been waiting quite a while for this. I have also needed the support of many friends over the years. Rebecca Thomas has been the best housemate, thank you for putting up with me for six years. It's hard to express how much I appreciate the times I've spent with my best friends: Dave Garcia, Susan Parks, Mak Saito, Yale Passamaneck, and Ben Gutierrez. Sarah Marsh has done so much for me and I can't think of any way to simply write down how much it means. Last, but not least, are the pups (Jasmine and Mudslide) who were always happy to take me for walks. Y'all are the best; I love you and thank you so much.

While this thesis only lists one author, many scientists, all of whom I respect and thank for their contribution, guided the work within it by serving on my thesis committee. John Trowbridge let me pursue this topic and generously gave his time to advise me through some tough spots. Ole Madsen provided the MIT perspective on the workings of a thesis and always managed to keep me honest. Rob Wheatcroft jump started my graduate studies and kept me from drifting into too many disciplines. Wade McGillis has shown great generosity in time and space through the years, even as our professional interests have diverged. Cheryl Ann Zimmer left the committee two years ago, but left an energy and drive for interdisciplinary work that was not forgotten. Thank you all for putting in the time to support my desire to complete this degree.

The WHOI Education Office and AOPE Education coordinator Mark Grosenbaugh provided advice and help with keeping my head on straight, paper work in order, and late fees as small as possible. I feel privileged to have had the opportunity to work in COFDL. To be surrounded by a diverse, interactive, and productive group, makes graduate study more interesting. Of particular note, Jim Price and Jack Whitehead, provided me with advice during tough times. I'd like to thank all of you.

I am deeply indebted to the Reinhardt Coastal Research Center (RCRC) for providing access to the flume facilities necessary to complete this thesis. Jay Sisson provided essential assistance during experimentation. The RCRC staff was very helpful and generous hosts (when I camped out in the offices). I'd also like to thank the Mullineaux and Zimmer Labs for letting me assist in the flume aspects of their projects and exposing me to the demands of other research questions.

Use of a Coulter Counter was an essential part of the analysis in this thesis. I received time on the instrument, help using it, and lots of patience from Rob Olsen and Alexi Shalapyonok. Additional advice in getting started was provided by the Sediment Lab at USGS.

Life at WHOI is five parts work and two parts fun. I am going to miss this place and would like to mention a few of the groups that participated in the fun parts: fellow Joint Program students (hope you weren't looking for a list, it would be quite long), USGS folks (Shannon McDaniel, Dave Walsh, Peter Gill and Michael Casso), the Ketten Lab, MBL folks (Keri Holland and Genevieve Nowicki), lab and officemates (Melissa Bowen, Bill Shaw, Erik Anderson, Chris Zappa, and Sean McKenna), WHUF, and the AOPE Softball Team.

Funding for my graduate studies came from many sources. In particular, the Education Office at the Woods Hole Oceanographic Institution coordinated and provided funding for much of my time here. Additional support has been provided by the Andrew W. Mellon Foundation, the Cooperative Institute for Climate and Ocean Research (CICOR), and the Office of Naval Research under grant numbers N00014-97-1-0556 (STRATAFORM Plume Study Moored Observations: Data Analysis and Modeling), N00014-96-1-0953 (Graduate Student Training in Engineering: Instrumenting the Continental Shelf Wave Bottom Boundary Layer), and N00014-94-1-0713 (Coupled Biological, Geological and Hydrodynamical Processes Associated with Fine-Particle Transport & Accumulation in the Coastal Ocean).

Table of Contents

Figures and Tables

---

1. Review of previous research and the significance of fine particle deposition

1.1. Introduction

This thesis will present a model for predicting the deposition rate of fine particles to permeable sediment beds under turbulent boundary layer flows (Figure 1.1). This model allows for the identification of boundary and flow conditions under which deposition rates exceed the settling velocity of the suspended particles. Rates greater than settling are described as enhanced deposition within this thesis. By identifying conditions that enhance deposition, predictions of deposition could be greatly improved.

The most common assumption in fine particle deposition is that particles are simply settling under gravity. This idea is primarily based on the results of Einstein's (1968) flume study of fine particle deposition to gravel beds, where particle deposition rate was approximately the same as the settling velocity of the suspension. An alternate explanation for these results is possible if we consider that deposition comprises two steps: delivery and retention. Although the fluid may have been delivering large amounts of particles into the bed, poor bed retention allows a majority of this material to be returned to the flow. Therefore, gravity provided the only net flux of particles. Identification of the controls for both delivery and retention of fine particles would improve models of fine particle deposition.

Discussion in this chapter will focus on the significance and mechanics of fine particle deposition. In particular, oceanographic problems that would benefit from

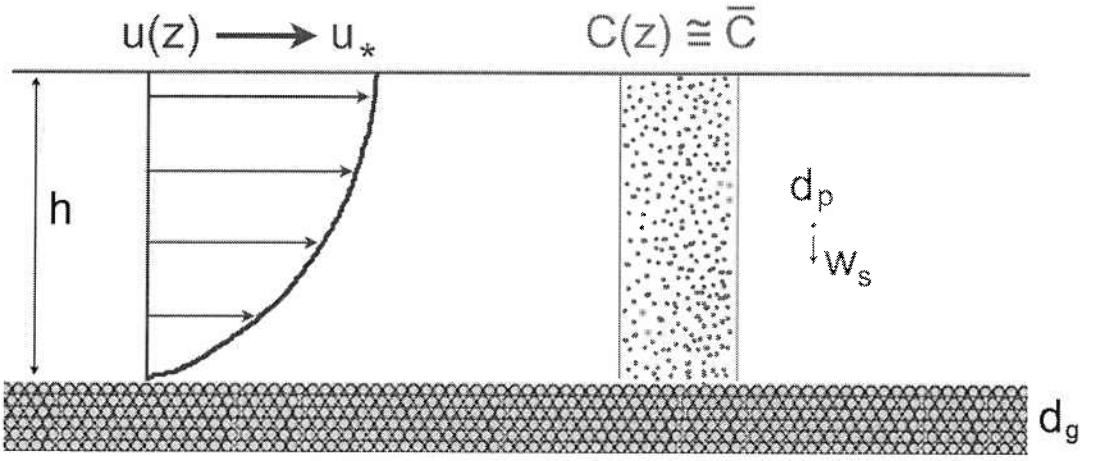

Figure 1.1. Schematic of the fine particle deposition system targeted in this study. All variables are described in the text.

improved predictions of deposition will be presented. The relevant parameters to include in any deposition model will be introduced. From this, two controlling mechanisms, interfacial diffusion and bed filtration, will be discussed in more detail, including review of previous studies of these processes. Lastly, an outline of the remainder of this thesis will be presented.

1.2. Significance on fine particle deposition

Dispersal of fine particles depends critically on the deposition rate (e.g., Nittrouer and Wright, 1994). After the release of contaminants into a water flow, the long-term concern is localization of the areas of sediment bed where contaminated particles have deposited. If deposition rates are enhanced in specific areas of the sea floor, then these areas become centers of deposition and would be the focus of cleanup efforts. Dispersal

of non-contaminated sediments could also be important with respect to sediment budgets and input to offshore sediments from rivers or coastal marshes (e.g., Wheatcroft et al., 1996).

Changes in sediment matrix properties can radically change the fluid environment at the grain scale. As particles deposit, matrix properties such as porosity, permeability, and critical erosion threshold change (e.g., Carling, 1984). Sediment properties are essential to the bottom flow conditions and the mechanisms of filtration within the bed. Changes in the granular structure of a sediment column eventually lead to clogging (e.g., Sakthivadivel and Einstein, 1970; Schalchi, 1992). Studies that focus on filtration mechanisms have shown changes in the mode of particle capture due to the accumulation of material in the pore spaces (e.g., Gruesbeck and Collins, 1982). The eventual goal of linking deposition to matrix properties would be to predict the fate of deposited material within the sediment based on the flow and starting matrix properties.

The particles of interest in some cases are the larvae of the local benthic population. In this case, similar to that of contaminated sediment, the dispersal of larvae may be described by a fine particle deposition model. The treatment of larvae as particles is not completely accurate, but is appropriate in cases where ambient flows are much greater than the swimming speeds of the larvae (Butman, 1989). The incorporation of some behavior is possible if a parallel between settlement and filtration is used when discriminating delivery and retention.

Assemblages of benthic organisms are usually associated with biogenic structures. This type of topography is capable of greatly enhancing interfacial solute flux and

deposition of fine particles (e.g., Huettel et al., 1996). While different in forcing, the study of flux due to topography could provide insights into the mechanisms of capture of colloidal and fine particles in the near-bed flow (e.g., Eylers et al., 1995; Packman et al., 1997). Particles transported to the bed could provide valuable food resources to benthic organisms. In this case, enhanced deposition could be beneficial to benthic assemblages. Food-quality particles are usually rich in organic matter. These particles represent a potential pathway for carbon to be delivered to the seabed. If fine particle deposition were a significant carbon sink with respect to the global budget, then an accurate model would be a valuable contribution to understanding the global carbon cycle.

1.3. Parameters for describing fine particle deposition

Identification of the relevant parameters to explore in experiments of fine particle deposition will be conducted in two stages. First, the variables influencing fluid flow will be introduced. Second, the mechanics of deposition and the attributes of particles in suspension will be discussed. Within each section, a dimensional analysis will be conducted that results in an expression for the variable of interest in terms of the other parameters.

1.3.1. Boundary layer flows over permeable sediments

Fluid flow over a solid boundary has been studied thoroughly over the last century (e.g., Prandtl, 1925; Einstein and Li, 1956; Eckelmann, 1974; Nino and Garcia, 1996). A specific class of boundary layer is open channel flows, where the depth of the

channel limits the boundary layer. Research on boundary layer flows has been applied to the open channel case as well (e.g., Keulegan, 1938; Nezu and Rodi, 1986). These studies have revealed the structure of the flow, providing insight into how the solid boundary influences the fluid. The following discussion provides the basics of open channel boundary layer flow over smooth and rough solid boundaries.

Boundary layer flows over flat sediment beds in wide, rectangular, open channels can be characterized in terms of eight parameters: mean flow velocity (U), channel depth (h), bed grain size (d_g), bed permeability (K), fluid density (ρ), shear velocity ($u_* \equiv \sqrt{\tau_b/\rho}$ where τ_b is the bed shear stress), fluid viscosity (ν), and gravitational acceleration (g). These variables can be reorganized into five dimensionless variables:

$$\text{drag coefficient} = C_D = \left(\frac{u_*}{U}\right)^2, \tag{1.1a}$$

$$\text{Froude number} = Fr = \frac{U}{\sqrt{gh}}, \tag{1.1b}$$

$$\text{channel Reynolds number } R_h = \frac{Uh}{\nu}, \tag{1.1c}$$

$$\text{grain Reynolds number } R_* = \frac{u_* d_g}{\nu}. \tag{1.1d}$$

$$\text{and bed Reynolds number } R_K = \frac{u_* \sqrt{K}}{\nu}. \tag{1.1e}$$

Each of these parameters defines the conditions of the boundary layer. The drag coefficient is a dimensionless representation of the bottom stress. The measured drag coefficient will serve as the primary parameter for momentum flux estimates. Each of

the remaining parameters needs to be considered in light of its contribution to describing drag in the channel within the range of values relevant to this study. The Froude number defines the relative contributions of kinetic and potential energy to the system. This study is restricted to values of Fr less than unity, representing "subcritical" conditions where this parameter has limited influence on flow structure. The value of the channel Reynolds number is indicative of the type of boundary layer in the channel. This study considers turbulent boundary layers where $R_h > 2000$ (Nezu and Rodi, 1986). The grain Reynolds number compares the roughness scale of the bed to the viscous scales in the fluid. A boundary layer is called smooth turbulent when $R_* < 10$ (e.g., Grass, 1971). Bed permeability is commonly expressed as a function of bed porosity (ϕ) often called the Carman-Kozeny equation (Kozeny, 1927; see Boudreau, 1997),

$$K = \frac{\phi^3}{180(1-\phi)^2} d_g^2, \tag{1.2}$$

Therefore, the bed Reynolds number could be replaced by another dimensionless parameter that represents the packing of the bed,

$$\frac{\sqrt{K}}{d_g} = \frac{R_K}{R_*}. \tag{1.3}$$

Typical values for sediments are $O(10^{-2})$. By considering the list of parameters presented in this section (and neglecting Fr), a four variable description of momentum transport to a boundary is possible,

$$C_D = f\left(R_*, R_h, \frac{\sqrt{K}}{d_g}\right). \tag{1.4}$$

1.3.2. Fine particle deposition to sediment beds

Prior work in pursuit of a general description of particle deposition covers a wide range of media, particle types, boundary roughness and flows. The bulk of these studies were done in wind tunnels with droplets or spores depositing to regular roughness or vegetation (see review by Nicholson, 1988). Most investigators were particularly interested in deposition via impaction (Davies, 1966; Browne, 1974; Cleaver and Yates, 1975). Few investigations of particle deposition have been conducted in water (e.g., Self et al., 1989). In these cases, deposition has been measured primarily in water tanks with sand roughness on walls (Shimada et al., 1987; Hoyal et al., 1997) or grid-stirred tanks (Nielsen, 1993). All of these studies were designed to investigate the processes that control fine particle deposition.

Deposition of particles from a suspension can be defined in terms of the depositional flux (F), suspension concentration ($\overline{C}$), particle diffusivity (D), diameter (d_p) and density (ρ_p). These parameters can be normalized to fit the dimensionless framework developed so far,

$$\text{enhancement factor} = E_D = \frac{F}{\overline{C} w_s} = \frac{w_d}{w_s}, \tag{1.5a}$$

$$\text{suspension density anomaly} = \rho' = \frac{\overline{C}}{\rho}, \tag{1.5b}$$

$$\text{particle relaxation time} = t_{p+} = \frac{\rho_p}{\rho_p - \rho} \frac{w_s u_*^2}{g \nu}, \tag{1.5c}$$

$$\text{Schmidt number} = Sc = \frac{\nu}{D}, \tag{1.5d}$$

$$\text{and grain diameter ratio} = D_R = \frac{d_g}{d_p}. \tag{1.5e}$$

where w_d is the deposition velocity and w_s is the particle settling velocity,

$$w_S = \frac{\rho_p - \rho}{\rho} \frac{g d_p^2}{18\nu}. \tag{1.6}$$

Use of (1.6) to determine settling velocity limits this discussion to fine particles. The normalization of deposition velocity by the settling velocity is sensible when considering the omnipresence of gravitational forcing on the system. Values of E_D greater than unity indicate conditions where enhanced deposition occurs. Optimally, deposition models should aim to predict this variable.

As in the case of boundary layer flow, each of the remaining parameters needs to be considered within the range of values relevant to this study. The suspension density anomaly indicates the influence of the particles on the density of the fluid. This study will focus on cases where ρ' is very small and the fluid properties do not depend on the suspension concentration.

In most studies of deposition in air (e.g., Wood, 1981), results are typically plotted against the particle relaxation time. An example of the dependence of deposition on t_{p+} is shown in Figure 1.2. Relaxation time is a measure of how fast a particle responds to changes in the local velocity field. For fine particles in water, t_{p+} is small (of order 10^{-5} to 10^{-3}), indicating that the particles follow the flow and inertia is limited in importance. Another implication of neglecting inertial influences is the profile of

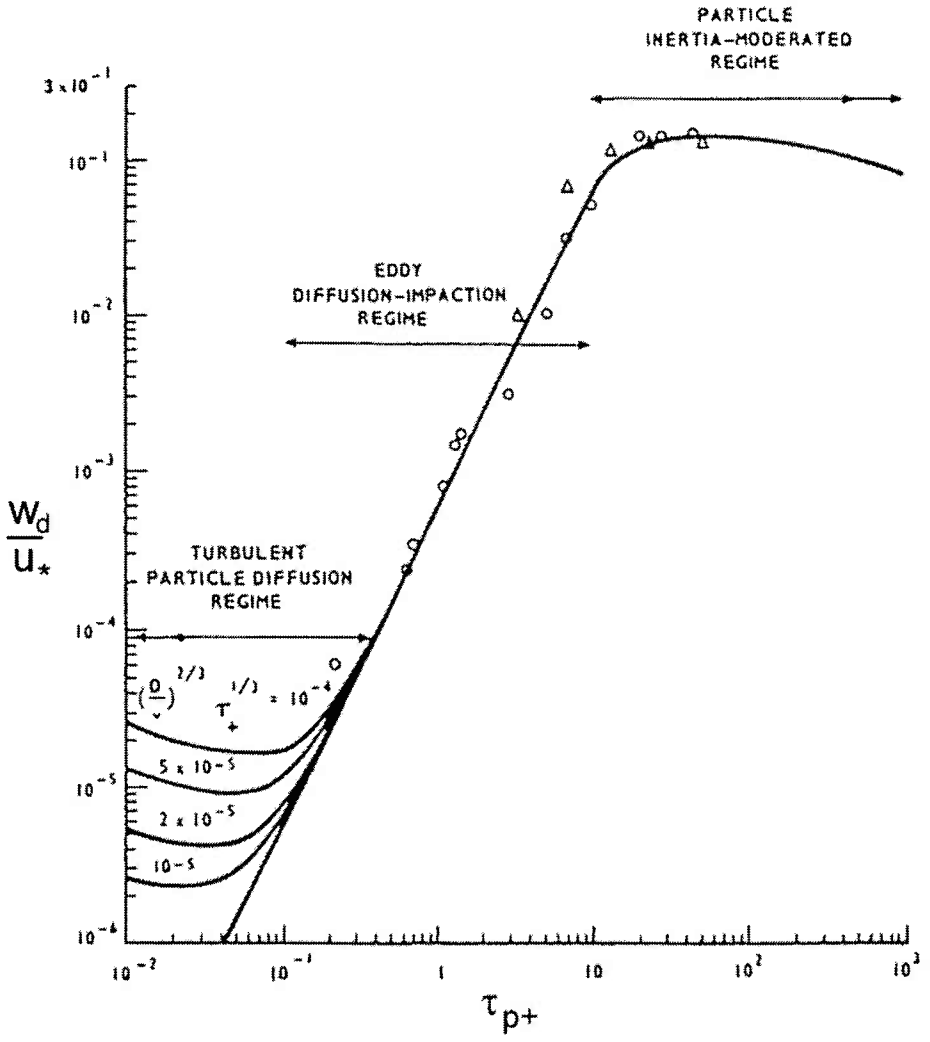

Figure 1.2. Prediction of aerosol deposition in air as a function of relaxation time. The region of oceanographic interest is beyond the left-hand limit of the plot. This figure modified from Wood (1981).

suspended particles. The structure of the concentration profile under equilibrium conditions is typically described as the balance between settling and resuspension by turbulence and can be fit to

$$C(z) = C_r \left(\frac{h - z}{h} \frac{z_r}{h - z_r} \right)^R , \tag{1.7}$$

$$\text{where } R = \frac{w_s}{\kappa u_*}, \tag{1.8}$$

κ is the von Karman constant, and the subscript r denotes values at a reference level (Rouse, 1937). While many models exist for determining the proper choices for z_r and C_r (e.g., Drake and Cacchione, 1989), the profile approaches a constant value for small R. This limit can be assumed to describe most fine particle suspensions; therefore, the water column should be well mixed and the concentration near the bed is the same as the depth averaged value. Note that the constant profile can be radically altered in cases of fine particle aggregation (e.g., Stolzenbach et al., 1992). As aggregates form, the settling velocity increases. The effects of aggregation on fine particle deposition are neglected in this discussion, although we will return to this issue in analysis of experimental results.

Particle diffusion is based on Brownian motion (Einstein, 1906). The resultant diffusivity is typically of the order 10^{-9} cm^2/s for particles larger than a micrometer in water. This diffusivity makes Sc large, indicating that diffusion plays a minimal role. Another way to demonstrate this is to compare the diffusive sublayer thickness, based on arguments by Jorgensen and des Marais (1990), to the particle diameter,

$$\frac{\delta_D}{d_p} = \frac{10\nu}{d_p u_*} \mathrm{Sc}^{-1/3}. \tag{1.9}$$

For diffusive transport control of deposition, the sublayer thickness needs to be significantly bigger than the particle diameter; this occurs only for sub-micrometer particles (Figure 1.3).

Grain diameter ratio describes the relative sizes of the particles and the bed grains. This ratio is important in describing the ability of particles to enter the bed with fluid intrusions as well as the capability of the bed to capture particles in the interstitial flow. Of these parameters, only D_R will continue to be considered. These considerations lead to a final expression for particulate flux conprising five parameters,

$$E_d = f\left(R_*, R_h, \frac{\sqrt{K}}{d_g}, D_R \right). \qquad (1.10)$$

1.4. Mechanics of fine particle deposition

Two processes could be responsible for enhancement of fine particle deposition. First, the diffusion of fluid across the sediment water interface increases delivery of particles relative to settling. Second, the filtration of particles from interstitial flows retains the delivered particles in the bed, preventing resuspension. While these processes, working in concert, could greatly enhance the deposition rate, the literature reflects sporadic and limited interest in their details. This section will present a review of the relevant studies that address interfacial diffusion and bed filtration.

Dispersion of solutes within the sediment matrix is of great importance to the study of porous media flow and the movement of contaminant plumes (e.g., Bear, 1972). List and Brooks (1967) summarized a large set of early work defining this dispersion

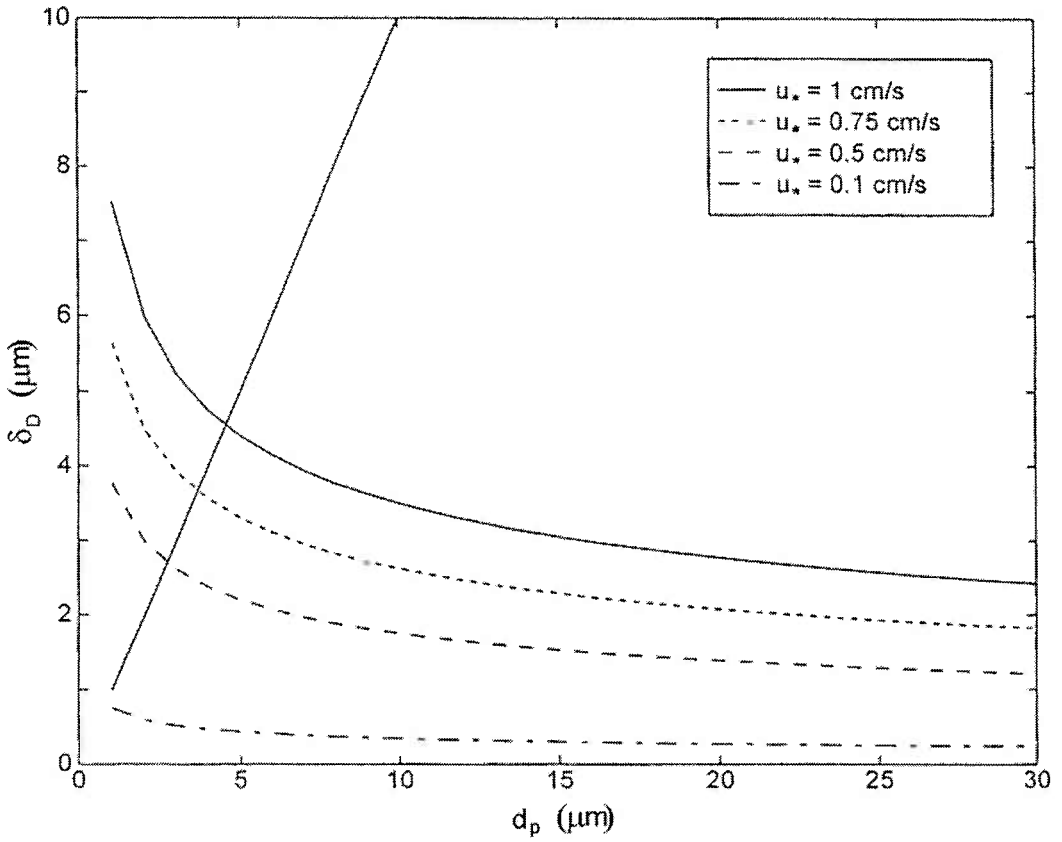

Figure 1.3. Comparison of particle diameter and diffusive sublayer thickness in water. Conditions below 1:1 line indicate conditions where Brownian diffusion may exert some control on particle deposition.

with respect to the flow and sediment characteristics. Their results recognize the dependence of dispersion within sediment on both the local flow velocity and the permeability of the sediment.

In overland flows, contaminants, such as fertilizers, may seep out of sediments into runoff. This situation is elementally different than dispersion within the sediment, but similar mechanisms might still limit exchange. In fact, studies of interfacial solute

exchange have supported models with diffusion between the sediment and flow (e.g., Richardson and Parr, 1988; Nagoka and Ohgaki, 1990). As in the case of dispersion within the sediment, the chosen diffusivity is dependent on scales of flow intensity and bed permeability. These models may prove valuable in predicting the exchange of fluids across the sediment water interface in oceanographic settings. The major limitation is the application of bulk properties (e.g., permeability) to the uppermost layers of sediment grains.

The exchange of fluid across the interface has also been detected through alterations of the flow profile or drag coefficient. Direct measurements of flow profiles within porous boundaries (Ruff and Gelhar, 1972; Nagoka and Ohgaki, 1990) confirm that interstitial velocity may be driven by a downward diffusion of momentum. Beavers and Joseph (1967) pursued another route for detection of fluid flow in the permeable boundary. Their measurements focused on the slip at the interface and a nominal reduction in drag. Along with Richardson and Parr (1991), these observations imply that the subsurface flow may be detected from profile measurements taken above the sediment water interface.

Most studies of solutes near the sediment water interface are designed to ensure that diffusion is the primary control on flux. However, other processes might better describe solute flux, as described in the case of contaminants. Therefore, both the input of particles and solutes must be accurately predicted in order to estimate the removal of carbon from the water column. Recent efforts to estimate the fluid-driven flux of oxygen (Guss, 1998; Hondzo, 1998) and comparisons between fluxes for beds of different

sediment types (e.g., Booij et al., 1991; Booij et al., 1994) are providing data to support the enhancement of solute flux to permeable beds.

Restriction of flow within the sediment may also affect the deposition of particles. Low inertia (t_p) particles should behave the same as solutes, following the fluid motions above and below the sediment water interface. However, particles are solid and, therefore, are subject to the specific geometry of the sediment bed in order to pass through unhindered. Studies exploring the ability of the sediment to mediate particle deposition include those measuring clay capture within ripples (e.g., Eylers et al., 1995; Packman et al., 2000). These works specifically entail the mechanics of colloidal capture in sediment beds. However, these mechanisms, including electrical and chemical forces, are very different than the filtration of fine particles (see review by McDowell-Boyer et al., 1986). In addition, it is unclear whether or not the diffusion of fluid across the sediment water interface has any influence when interfacial flows are being driven by topography (e.g., Thibodeaux and Boyle, 1987).

As in the case of dispersion, controlled laboratory experiments provide some insights into the mechanics of fine particle retention. Experiments have identified the ratio of grain sizes to be very important in describing the ability of particles to infiltrate the bed (Sherard et al., 1984a,b) and the efficiency of bed filtration (e.g., Maroudas and Eisenklam, 1964a,b; Fitzpatrick and Spielman, 1973). The concept of filtration efficiency is analogous to the consumption rate of solutes within the sediment.

Recent investigations of deposition to rough boundaries have introduced the idea of particle filtration in the enhancement of deposition (e.g., Hoyal et al., 1997). In the

case when the boundary is impermeable, the filtration is imposed in the fluid very near the roughness elements. This process is the same as roughness interception, as defined by Dade (1993). Unfortunately, this process is very different than those that would be expected within the sediment bed.

An unexplored area within this body of literature is the measurement of fine particle deposition to flat sediment beds. In this case, the capture of particles will occur within the sediment and delivery would be driven by interfacial diffusion alone, not topography. This study would entail several treatments of flow, sediment beds, and particle types to cover the four parameters identified in the dimensional analysis (1.10).

1.5. Outline of thesis

The idea that the diffusion of fluid across the sediment water interface, combined with filtration by the sediment bed, may mediate the deposition of fine particles has been identified as an unexplored and potentially significant deposition mechanism. The pursuit of this question entailed three steps. First, enhanced deposition was observed within a range of oceanographically relevant conditions with respect to bed, flow, and particles (Chapter 2). Previously devised models of deposition to rough boundaries (e.g., Dade et al., 1991) could not explain these results. Second, a new model for fine particle deposition to permeable beds was derived (Chapter 3). This model couples the intrusion of particle-laden flows (delivery) and filtration of particles by the sediment bed (retention). Both of these processes rely on the structure of the sediment matrix, a clear extension on previous deposition models. Third, the performance of this new model is

evaluated with respect to predicting both particle and fluid transport (Chapter 4). This test of performance involves extensive flume experiments to observe the interfacial diffusivity critical to enhancement of deposition and previous studies of the changes in flow conditions due to permeability of the boundary. The final chapter (Chapter 5) will summarize the thesis results and present a final discussion of how this thesis fits into the body of research regarding the flux of particles to permeable boundaries.

2. Flume observations of enhanced fine particle deposition to permeable sediment beds

2.1. Introduction

Dispersal of fine particles, such as contaminants, depends on the deposition rate (e.g., Nittrouer and Wright, 1994). In many cases, this rate is assumed to be the settling velocity of the particles in still water. However, flow conditions and boundary roughness may alter the deposition rate. Enhancement of deposition has been documented in marsh canopies (Leonard and Luther, 1995), at the air-sea interface (Larsen et al., 1995), and groups of benthic fauna (see review by Butman, 1987). Bed topography can generate interfacial flows, advecting suspended material into the sediment bed (e.g., Thibodeaux and Boyle, 1987; Huettel et al., 1996). Deposition may also be limited by the local bed shear stress (e.g., McCave and Swift, 1976). A general model based on flow, bed roughness and sediment properties would provide predictions of deposition rate.

Prior work in pursuit of a general description of particle deposition covers a wide range of media, particle types, boundary roughness and flows. The bulk of these studies were done in wind tunnels with droplets or spores depositing to regular roughness or vegetation (see review by Nicholson, 1988). Fewer investigations of particle deposition have been conducted in water. In these cases, the ideas generated in the air-side literature are applied over granular beds (e.g., Einstein, 1968), water tanks with grain roughness on walls (Shimada et al., 1987; Hoyal et al., 1997), or grid-stirred tanks (Nielsen, 1993).

Describing the deposition of fine particles to beds of coarser material requires an understanding of many physical processes in both fluid and granular media. A viscous sublayer (VSL), characterized by a spatial pattern of fluctuations called bursts and sweeps (e.g., Grass, 1971; Grass et al., 1991), completely covers smooth boundaries. Flow resistance and turbulent flow structure through changes in roughness type and scale in the transitionally rough turbulent regime (e.g., Nikuradsae, 1933; Bandyopadhyay, 1987). The change from a smooth to transitional boundary layer is due to the onset of eddy formation and shedding from the roughness elements. When a fully rough turbulent boundary layer exists, the roughness-scale eddies stabilize, with a marked decrease in shedding.

Einstein (1968) observed deposition independent of flow conditions for fully rough flows. His experiments involved silica flour (3 - 30 μm) depositing to flat, gravel beds. During his runs, regions in-between grains near the sediment-water interface existed where no fluctuating flows were observed. In these regions, particles settled into the bed. This observation suggests that the contribution of turbulent eddies to deposition is small relative to settling under fully rough turbulent boundary layers.

The porous nature of sediment beds complicates the description of near-bed flows. The sediment bed resists the flow in the channel via drag on the sediment grains. Further increases in drag may occur via transport of turbulent eddies into the sediment matrix (e.g., Nagoka and Ohgaki, 1990; Richardson and Parr, 1991). Material deposited by these eddies will then be subject to filtration in the bed (Hoyal et al., 1997; Packman et al., 1997). The ability of deposited particles to descend into the bed can be described

in terms of the filtration capability of the bed (e.g., Maroudas and Eisenklam, 1961b; Sherard et al., 1984a,b). Generally, the depth in the bed to which particles may travel depends on the particle size relative to the grains in the bed. Particles incorporated into the bed are effectively captured, limiting particle availability for resuspension.

This chapter will extend previous work on the deposition of fine particles to permeable beds by considering a very basic scenario: flat sediment beds (Figure 2.1). This work will include a description and test of the model derived by Dade et al. (1991). The facilities and experimental design will be described. The results of deposition experiments will be presented with a focus on the treatments that demonstrate an enhancement of deposition relative to settling alone. Discussion of these results will include a test of the model from Dade et al. (1991) and identification of success and failure within its application. The final goal of this chapter is to identify the mechanisms responsible for enhancing deposition to permeable sediments.

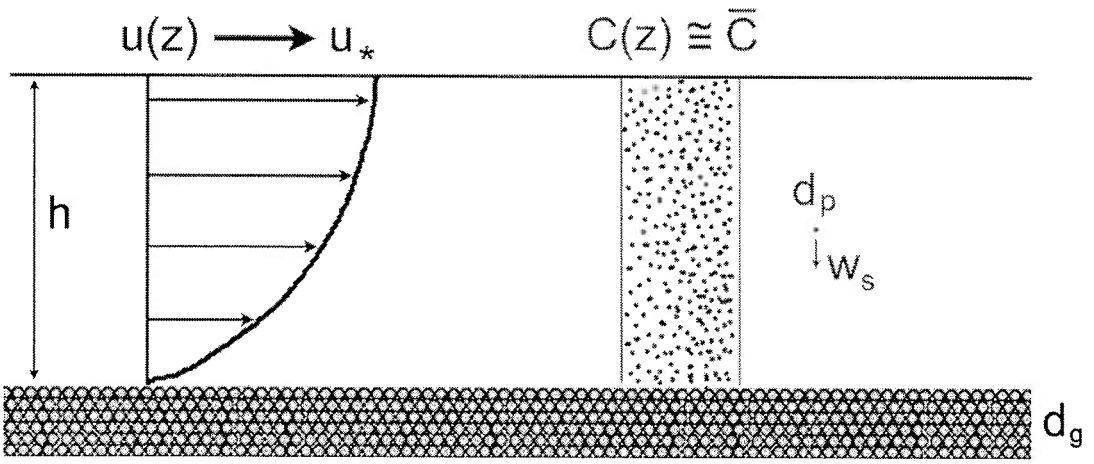

Figure 2.1. Schematic of the fine particle deposition system targeted in this study. All variables are described in the text.

2.2. Methods

2.2.1. Previous model for fine particle deposition

Previous attempts to model the process of fine particle deposition have focused on the delivery of fine particles to the seabed. In particular, the model derived by Dade et al. (1991) targeted the conditions required to enhance deposition relative to settling. It was assumed that delivery limits deposition and was a combination of four mechanisms: gravitational settling, interception, impaction, and diffusion. Their model recognized that these mechanisms depend on the particle, flow, and bed characteristics. For the scenario proposed in this study, only the effects of interception and settling are important (see their Figure 16.1). This restriction of mechanisms leads to an expression for the efficiency of particle capture,

$$\eta_D = \frac{40\nu w_s}{d_g u_*^2} + \frac{d_p}{d_g}, \tag{2.1}$$

where w_s and d_p are the particle settling velocity and diameter, ν is the fluid viscosity, u_* is the shear velocity, and d_g is the bed grain size. The efficiency of capture is limited to values between zero and unity. The boundary conditions for concentration are a nearly uniform concentration ($\overline{C}$) away from the boundary and a reduced concentration at a specified distance above the bed (Δ_D) based on the capture efficiency,

$$C_\Delta = C(\Delta_D) = \left(1 - \eta_D\right)\overline{C}. \tag{2.2}$$

For fine particle deposition to flat sediment beds, the height to apply this boundary condition can be approximated as the bed grain size (from scaling in Dade et al., 1991). By applying this boundary condition to the equation for the flux of particles,

$$F = w_d C = w_s C + \nu_t \frac{\partial C}{\partial z}, \tag{2.3}$$

where w_d is the deposition velocity and ν_t is the turbulent viscosity of the fluid very near the bed (as proposed by Dade et al., 1991),

$$\nu_t = \nu \left(\frac{z u_*}{\nu} \right)^3. \tag{2.4}$$

Integration of the flux equation leads to an exponential concentration profile,

$$C(z) = \overline{C} \exp\left(-500(E_d - 1) \frac{w_s}{u_*} \left(\frac{u_* z}{\nu} \right)^{-2} \right). \tag{2.5}$$

where E_d is the enhancement of deposition calculated from the capture efficiency,

$$E_d - 1 = \frac{u_*}{500 w_s} \left(\frac{u_* \Delta_D}{\nu} \right)^2 \ln\left(\frac{1}{1 - \eta_D} \right) \cong 0.08 R_*^2. \tag{2.6}$$

These predictions will be compared to experimental measurements.

2.2.2. Flume facilities

Observations were made in two flumes: the "17-Meter" (described by Butman and Chapman, 1989) and "Racetrack" flumes located in the Reinhart Coastal Research Laboratory at the Woods Hole Oceanographic Institution (Figure 2.2). Throughout this chapter, these flumes will be referred to by the abbreviations "17M" and "RTF", respectively. The essential difference between the flumes is the method used to

recirculate the water. The 17M directs flow through the channel (17.3 m long, 60 cm wide, 30 cm deep) and into a sump that drains into a centrifugal pump for recirculation. Water depth in the channel is adjustable via a downstream weir. The RTF is an oval design with a linear paddle-drive designed to maintain vertical paddle orientation while in the flow. The test section is positioned on the opposite side (7.5 m long, 75 cm wide, 30 cm deep). All flume experiments used 10 μm filtered seawater. Velocity measurements were made with a Laser Doppler Velocimeter (LDV) (Agrawal and Belting, 1988). Experimental flow data were fit to an expression for open channel, turbulent boundary layers, necessitating collection of several points in elevation (z). The profile expression for a smooth turbulent boundary layer over a permeable boundary can be expressed as

$$u(z) = \frac{u_*}{\kappa}\ln(z_+) + 5.5u_* + W(z) + u_s, \tag{2.7}$$

$$\text{where } z_+ = \frac{u_*(z+\Delta)}{\nu}, \tag{2.8}$$

Δ is the displacement of the profile, κ is the von Karman constant, u_s is the slip velocity, W is the profile due to the wake layer,

$$W(z) = \frac{2\Pi}{\kappa}u_* \sin^2\left(\frac{\pi}{2}\frac{z+\Delta}{h}\right), \tag{2.9}$$

Π is a fit parameter that ranges from 0 to 0.4 (Coles, 1956), and h is the channel depth. Note that smooth boundaries are those that fit the following criterion:

$$R_* = \frac{u_* d_g}{\nu} < 10 \tag{2.10}$$

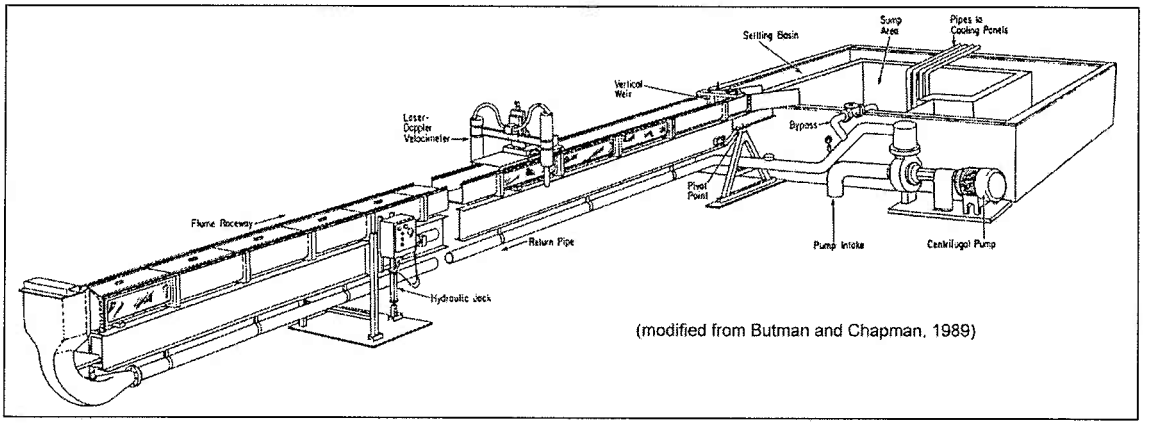

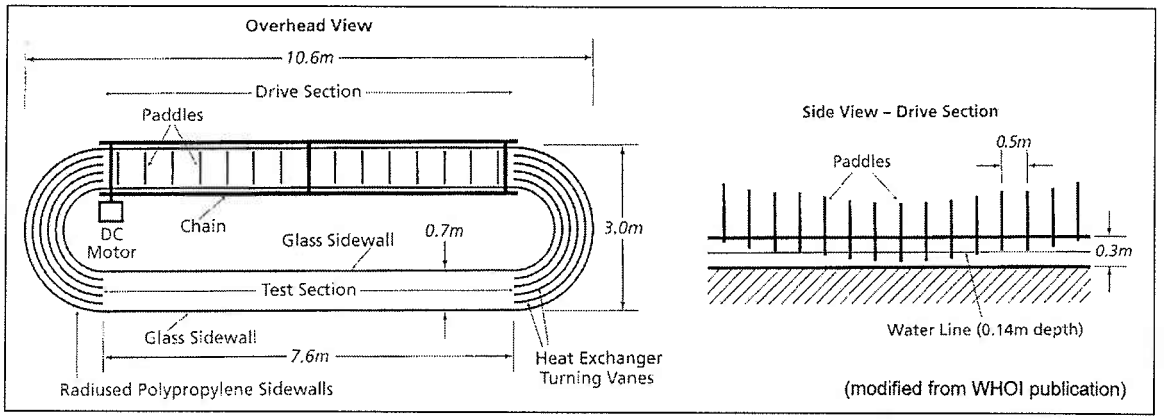

Figure 2.2. Layout of flume facilities. (a) 17-M flume. Sediment beds installed in final 11 m of raceway. (b) Racetrack flume. Sediment beds occupied entire test section. Flow sampling (LDV) located 6 m from start of sediment in both.

---

where R_* is called the roughness Reynolds number. For larger values of R_*, the flow profile approaches the rough turbulent limit,

$$u(z) = \frac{u_*}{\kappa} \ln\left(\frac{z+\Delta}{d_g}\right) + 8.5u_* + W(z) \quad (2.11)$$

A critical measure of flow properties in the channel is the drag coefficient,

$$C_D = \left(\frac{u_*}{U}\right)^2, \quad (2.12)$$

where U is the mean channel velocity. This measure was obtained by fitting the profile data to the expressions above, then integrating to obtain U.

Flat sediment beds were used in a majority of the experiments. In these cases, the channel bottom was covered with sediment to a depth of 2 to 4 cm. Upstream of the sand bed, panels were level with the sediment surface. Table 2.1 details the various sediments used for these experiments. Bottom topography was eliminated using a channel-wide sled. Flat bed conditions were verified by visual inspection from above and through sidewall windows.

Permeability values were determined using falling or constant head permeability tests as described by Al-Khafaji and Andersland (1992). The experimental setup included a head pipe for pressure and porous plastic ends to the core holder (Figure 2.3a). Permeability values obtained for experimental sediment using this method are reported in Table 2.1. The ratio of permeability to the median grain size was lower for the natural sediments than the artificial ones (Figure 2.3b). A lower ratio is consistent with the idea that resistance to flow increases with broader distributions of grain size and tighter packing due to more angular grains. All of the permeability measurements fall within the range of values previously explored in the literature (e.g., List and Brooks, 1967).

For smooth bed experiments in the 17M, a false bottom was installed with a 55-cm square panel with three 8 x 20 x 0.4 cm deep indentations (Figure 2.4). Indentations were filled, flush with the bottom, with one of two classes of glass beads to serve as particle traps. The nominal size ranges for the glass beads supplied by Cataphote (Jackson, MI) were 250 - 350 μm and 420 - 590 μm.

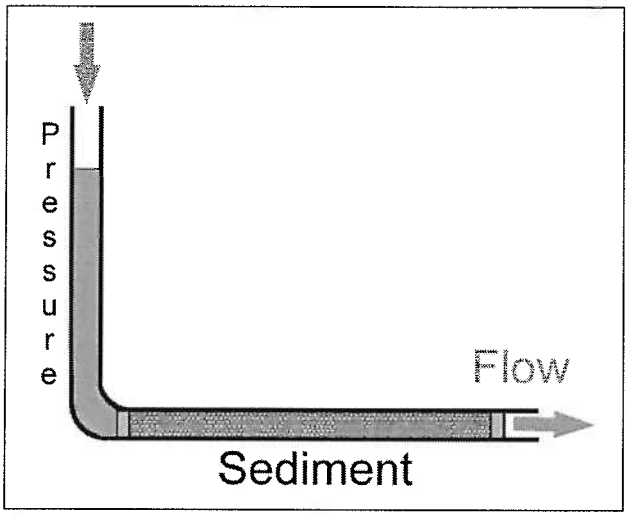

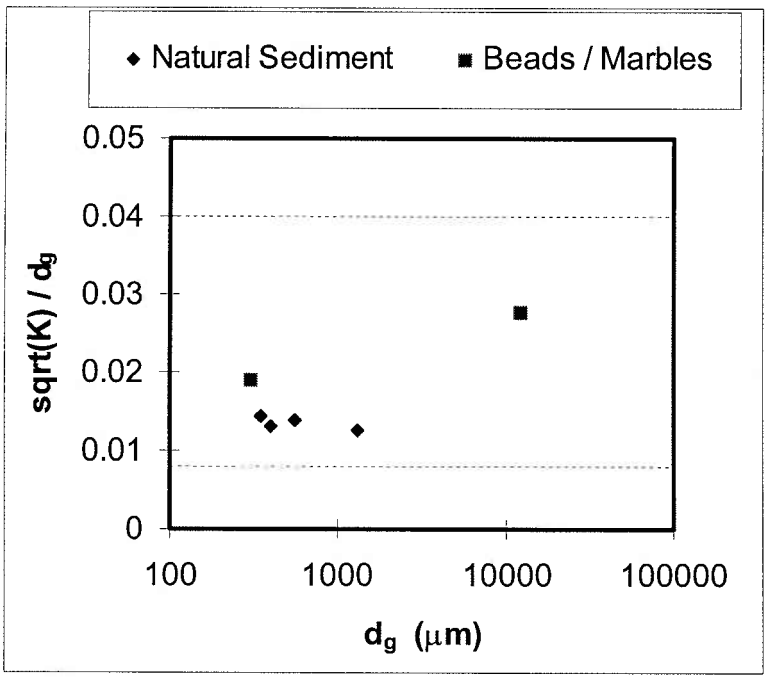

Figure 2.3. Permeability measurement for experimental sediments. (a) Setup for measurement by falling or constant head method. (b) Ratio of permeability to grain size for sediments (diamonds) and well-sorted beads and marbles (squares). The range of values reported by List and Brooks (1967) is marked by dashed lines.

Table 2.1. Treatments used in flume experiments.

Bed	# runs	u_* (cm/s)	h (cm)	d_g	K (cm^2)	d_{g15}
PVC	20	0.10 to 1.38	11.8 to 13.5	---	---	---
Sand	16	0.34 to 1.49	13.0 to 13.2	350 μm	2.5×10^{-7}	210 μm
	4	0.34 to 0.80	12.3 to 13.0	400 μm	2.7×10^{-7}	260 μm
Coarse sand	12	0.23 to 1.05	11.8 to 12.5	550 μm	3.0×10^{-7}	300 μm
Gravel	3	0.43 to 1.25	12.0 to 12.2	1.3 mm	2.8×10^{-6}	700 μm
Marbles	17	0.20 to 4.19	12.3 to 12.8	1.23 cm	1.4×10^{-3}	1.23 cm

Table 2.2. Suspensions used for flume experiments.

	Material	Density (g/cc)	d_p range (μm)	Median d_p (μm)	w_s (cm/s)
I	Solid glass	2.5	5 - 25	12	0.010
II	Solid glass	2.5	3 - 25	8	0.007
III	Solid glass	2.5	20 - 60	30	0.030
IV	Hollow glass	1.4	10 - 30	13.5	0.004

Four suspensions were used in this study (Table 2.2). MoSci Corporation (Rolla, MO) supplied three classes of glass beads. Flow-tracking particles from Sontek (San Diego, CA) were used as the fourth suspension material. Grain size distributions provided by the manufacturer were verified in the laboratory by conducting particle size analysis using a Coulter Counter Model II. Samples were analyzed using a 100-μm orifice that resolves diameters from 1 - 64 μm. The particle size distributions were resolved to 1-μm bins of particle count, not mass (Figure 2.5).

Fine particles were added to the flume after the flow stabilized. Suspensions were mixed with flume water and introduced to the flume sump (17M) or in the turns downstream of the test section over a flume transit time (RTF). Particles were allowed at least two additional transit times through the system prior to sampling to allow particles to mix into the system. Initial suspension concentrations of 4 to 40 mg/L were used.

2.2.3. Total mass analysis

Water samples were collected during flume experiments to monitor the amount of fine particles in suspension over time. For most experiments, 1 L water samples were collected at both ends of the test section. A single siphon tube was used at the upstream end ("head") of the channel. At the downstream end ("tail"), a multi-port siphon was installed on the flume centerline. In most cases, all ports were combined to obtain a depth-averaged sample. Samples were collected at each end prior to fine particle addition as a control. The timing of water sample collection depended on the suspension to be

used (Table 2.3) and was designed to capture significant changes in suspension concentration between samples.

Control samples provided an initial measure of the ambient concentration. To account for the deposition of ambient particles during experimental runs, an estimate of the ambient particle settling velocity was needed. Three experimental runs without fine particle addition were conducted. The results indicated that ambient material settled very slowly (0.0041 ± 0.0018 cm/s) compared to all suspensions except IV. For experiments using suspension IV, efforts were made to limit the ambient concentration to less than 10% of the total suspended concentration. The slow settling velocity allowed for an assumption of a constant ambient concentration for the duration of any flume run. The fraction of the total suspended mass that was ambient varied from 0 to 0.56 with only 8 runs greater than 0.3 (ambient concentrations from 0 to 6 mg/L). Therefore, the

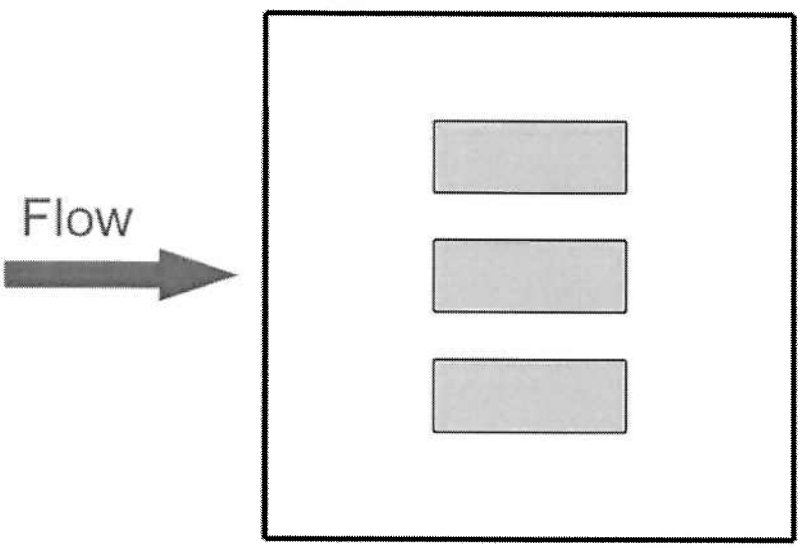

Figure 2.4. Panel for collecting particles during PVC runs. Overall panel was a 55 cm square with three 8 x 20 cm traps.

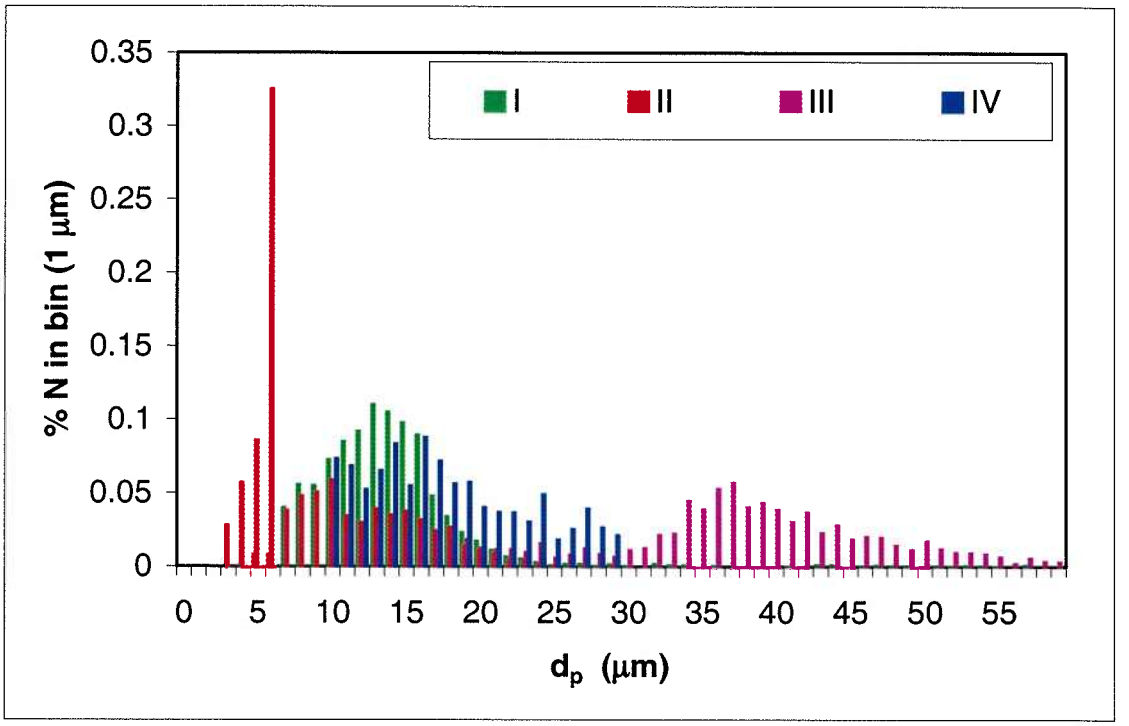

Figure 2.5. Particle size distributions for suspensions. See Table 2.2 for suspension descriptions.

Table 2.3. Schemes for water sampling.

Flume	Suspension	#	Time elapsed at each sample (minutes)
17M	I	10	0, 20, 40, 60, 80, 100, 120, 150, 180 and 225
	II	9	0, 20, 40, 60, 80, 100, 120, 150, and 180
RTF	II	9	0, 20, 40, 60, 80, 100, 120, 150, and 180
	III	7	0, 5, 10, 15, 20, 25, and 30
			0, 3, 6, 9, 12, 15, and 18
	IV	6	0, 30, 60, 90, 135, and 180

assumption of constant ambient concentration should have a minor influence on a majority of the deposition measurements.

Water samples were poured through a 45-μm sieve onto a pre-weighed 1.2 μm membrane for vacuum filtration (Osmonics MCE Membranes). This sieve was not used for experiments with the largest suspension (III) to avoid selective removal of the coarsest fraction. Each filter membrane was weighed to determine the total amount of material in the sample. The total mass measurements were fit to an equation describing the loss of suspended particles to the boundary as an exponential decay,

$$\overline{C}_{H/T}(t) = \overline{C}_o \exp\left(-\alpha_{H/T}(t - t_{o,H/T})\right), \tag{2.13}$$

$$\text{where } \overline{C}_o = \frac{m_{add}}{V_f} + \overline{C}_a, \tag{2.14}$$

the subscript H/T denotes samples from the "head" or "tail", α is the decay rate for the suspension, t_o is the time lag due to mixing in the sump, m_{add} is the mass of particles added to the flume, V_f is the total volume of the flume, $\overline{C}_a$ is the ambient concentration (from control samples), and overbars represent depth-averaged values. The fit to the decay equation involves adjusting the values for t_o and α. Graphically, the adjustment of t_o shifts the decay curve along the time axis and α changes the curvature to obtain the best fit. Curve fits were determined using a least squares method. Comparison between α_H and α_T demonstrate that they are essentially equal (Figure 2.6) and can be replaced by α without a subscript.

Measurements of concentration were converted to deposition velocities through the comparison of time series from the head and tail of the test section. The expression for changes in concentration over the bed in the channel was

$$\overline{C}(x,t) = \overline{C}_H(t)\exp\left(\frac{-w_d}{Uh}x\right), \tag{2.15}$$

where x is the alongstream coordinate. An expression for the TAIL concentration after one transit (x = L, where L is the length of the channel) is

$$\overline{C}_T\left(t+\frac{L}{U}\right) = \overline{C}_H(t)\exp\left(\frac{-w_d L}{Uh}\right). \tag{2.16}$$

This concentration could also be obtained using the time series,

$$\overline{C}_T\left(t+\frac{L}{U}\right) = \overline{C}_o\exp\left(-\alpha\left(t+\frac{L}{U}-t_{o,T}\right)\right), \tag{2.17}$$

Substituting for the head time series and equating the equations for the tail concentration, the expression for deposition velocity from head-tail comparison is

$$w_d = h\alpha\left(\frac{U}{L}\left(t_{o,H}-t_{o,T}\right)+1\right). \tag{2.18}$$

An additional piece of information was drawn from the time series at each end of the flume. By assessing the change from the tail to the head, the loss to the rest of the flume could also be determined. The solution for the loss is nearly the same as that for deposition velocity except for the application of a new length,

$$L_L = \frac{V_f}{b_f h} - L, \tag{2.19}$$

where b_f is the flume width. The loss expression is

$$\overline{C}_H\left(t+\frac{L_L}{U}\right)=\overline{C}_T(t)\exp\left(\frac{-w_L L_L}{Uh}\right)=\overline{C}_o\exp\left(-\alpha\left(t+\frac{L_L}{U}-t_{o,H}\right)\right), \qquad (2.20)$$

and the solution for the loss velocity becomes

$$w_L = h\alpha\left(1-\frac{U}{L_L}\left(t_{o,H}-t_{o,T}\right)\right). \qquad (2.21)$$

For all but 10 early experiments in the 17M, both head and tail sampling was conducted. The loss velocities for the 17M are very small and do not exhibit a significant trend with respect to flow (Figure 2.7). The average value of w_L/w_s for the 17M (0.058 ± 0.012) was applied to runs where either head or tail data was not available. The loss in the RTF shows larger scatter and, possibly, a negative trend with channel Reynolds number. The larger values were expected given the flat design of the flume that creates the potential for settling of particles in areas outside the test section. As flow increases, the vertical flows in the turning sections and under the paddles should exceed the threshold for particles to settle and remain on the flume bottom, decreasing the loss term. For both flumes, all the loss velocities are within one settling velocity of zero. If there was no loss in the flume outside of deposition in the test section ($w_L = 0$), then the deposition velocity becomes directly dependent on the flume geometry,

$$w_d = \frac{\alpha V_f}{b_f L} = \alpha h'. \qquad (2.22)$$

The length h' would be the channel depth if all the flume volume was within the channel.

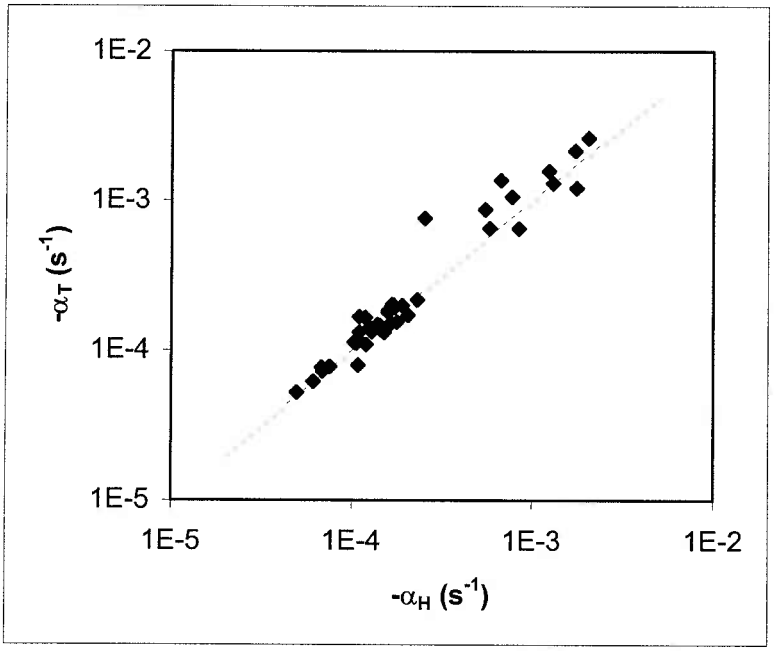

Figure 2.6. Decay from HEAD and TAIL samples. Dashed curve represents 1:1 comparison.

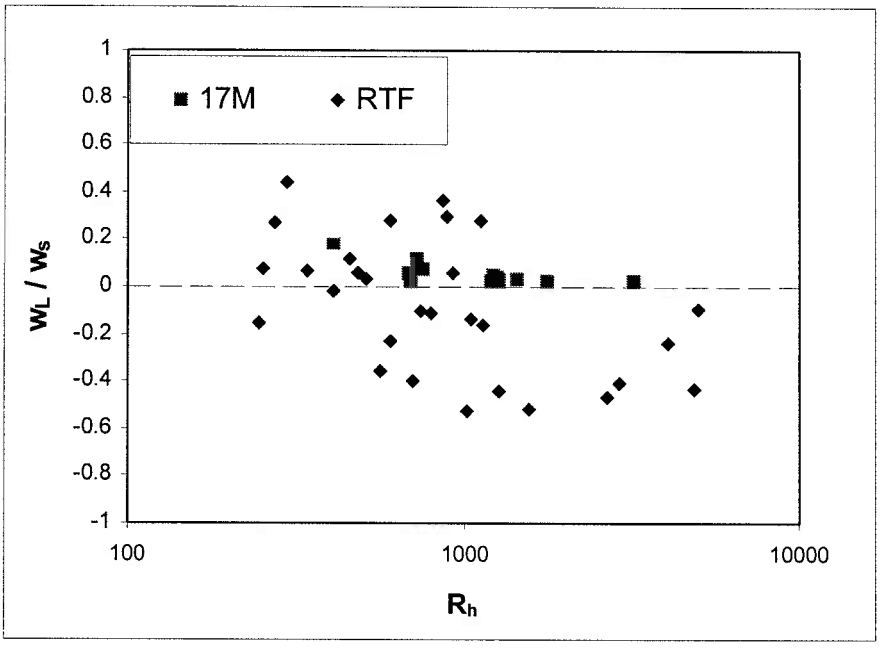

Figure 2.7. Loss velocities outside of test section. Data from both the 17-M Flume (squares) and Racetrack Flume (diamonds) are presented.

In order to assess variability in clean filter weight, 22 membranes were used to vacuum filter 1 L de-ionized water over the course of flume experiments. The results demonstrated a mean loss of 1.2 ± 0.11 mg (12 samples) from each membrane. Error ranges in this study are reported as standard errors unless otherwise noted. A variability of 0.1 mg is consistent with the accuracy of the scale used (Mettler AE163).

The error inherent in the handling of water samples was evaluated in a "spike" experiment. Bottles containing 10-μm filtered seawater were spiked with varying amounts of fine particles. Concentrations from 0.2 to 12 mg/L were targeted in order to cover the range measured in flume experiments. Measured concentration was directly correlated to spike amount (Figure 2.8). An average error of 0.16 mg (4 samples per concentration) was found in this test. Therefore, the level of detection for this method is approximately 0.2 mg/L.

2.2.4. Size fraction analysis

Separation of the suspension into a group of size classes allows for solution of the relative changes in deposition velocity for each class. Two models for the change in median particle size (d_{p50}) were compared to the measured time series. Median particle size satisfies the condition

$$\int_{d_{\min}}^{d_{p50}(t)} n(\sigma,t)d\sigma = \frac{1}{2}, \qquad (2.23)$$

where n is the particle count in each diameter bin, the subscripts 'min' and 'max' refer to the minimum and maximum diameters in the count, and n is the particle count based on

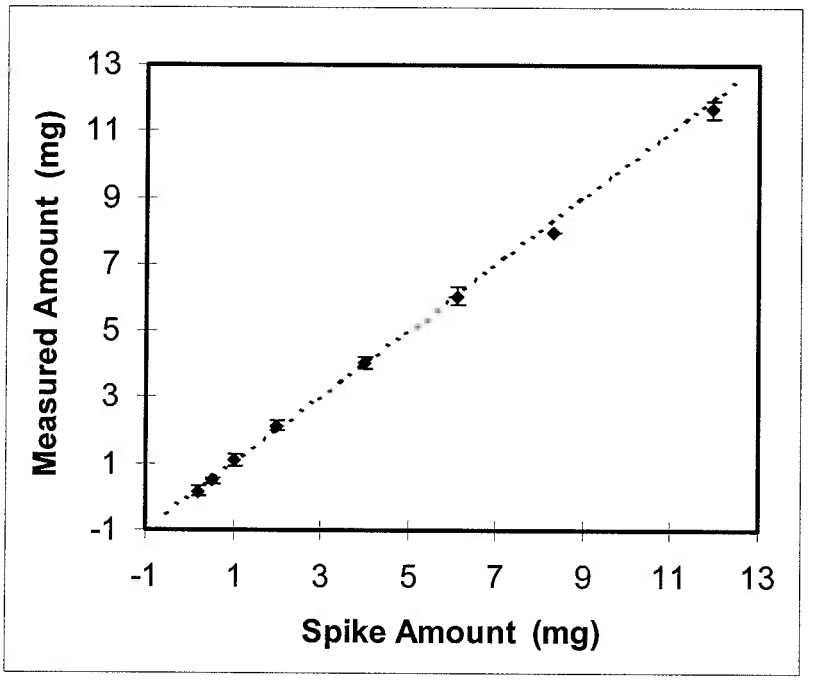

Figure 2.8. Spike test for water samples. Dashed curve represents 1:1 comparison. Error bars represent ±1 SE.

Coulter counter analysis. First, a constant d_{p50} was checked. The median diameter would remain constant if the particle size distribution also remains constant. A constant model would fit observations if deposition velocity were independent of particle size. Second, the changes in d_{p50} were compared to the predicted change for settling-only deposition. Predictions of settling were based on the initial distribution and the assumption of no loss to the rest of the flume,

$$n(d_p,t) = n(d_p,0)\exp\left(\frac{-w_s(d_p)}{h'}t\right). \qquad (2.24)$$

If neither of these models fit the data, then the trend in d_{p50} was assumed to be due to a third process. Other statistics, including an attempt to repeat the mass analysis above for

each size class, were subject to large errors due to small counts in some bins. Using d_{p50} relaxes the error contribution due to small values.

Two types of samples were analyzed for changes of suspension in time. First, the filters from the total mass analysis for some of the early experiments were dissolved to produce a solution for Coulter Counter analysis. Filters were immersed in 3 ml of 37N sulfuric acid, allowed to dissolve, and diluted with 36 ml of de-ionized water. This solution was neutralized with 11 ml of 10N sodium hydroxide. The resultant solution (50 ml) was sub-sampled when analyzed on the Coulter Counter. Second, small water samples (50 ml) were collected directly from the flume along with samples for total mass analysis. In this case, additional chemical treatment of the samples prior to counting was not necessary.

To ensure that all other contaminant particles were detected prior to sample counting, all analyses were run with blanks containing 0.45-μm filtered seawater. Therefore, the primary source of error in Coulter Counter results was the particles derived from the dissolved filter. All of this material was smaller than 10 μm (Figure 2.9) and, coupled with the observed settling velocity, resulted in a density of 1.9 g/cc for ambient material. This density suggests that a majority of the ambient material was not quartz. Results for raw seawater (from flumes) match those of the dissolved filters, consistent with the ambient fraction being dissolved along with the filter. In any case, Coulter analysis focused on material coarser than 10 μm to avoid influences from the ambient material.

Coulter counter analysis also provided a definite measure of the particle size population at the start of all experiments. The settling velocities from the initial size distribution were compared to that from the source material (Figure 2.10). For all the suspensions, a relatively large amount of scatter was evident, mostly in the positive direction. Also, for all but suspension I, no trend is evident with respect to flow. Both of these observations suggest that alteration of the suspension may be due to losses of the finest fractions during handling of the dry particles. A positive trend of settling velocity with flow would support the idea that some of the coarsest fraction may be lost in the flume system depending on the flow.

2.2.5. Sediment core analysis

To verify that particles lost from suspension were deposited to the bed, cores were taken from the sediment bed during experiments. At least seven cores were collected prior to (pre-cores) and following (post-cores) each flume run. In all cases, the cores were placed such that both cross-channel and along-channel lines were collected. Cores were taken with cut 5 cc syringes (1.4 cm diameter). Each core was stored in a centrifuge tube. Mass deposited was measured by diluting each core with de-ionized water then passing the sample through a 45-μm sieve. As in the case for water samples, this sieve was not used for samples from experiments with suspension III to avoid unintended removal of particles. The fluid recovered after repeating his procedure three times was vacuum filtered through a 1.2-μm membrane. The solid fraction remaining from each core was dried and weighed to measure the total core mass. For smooth-bed runs, the

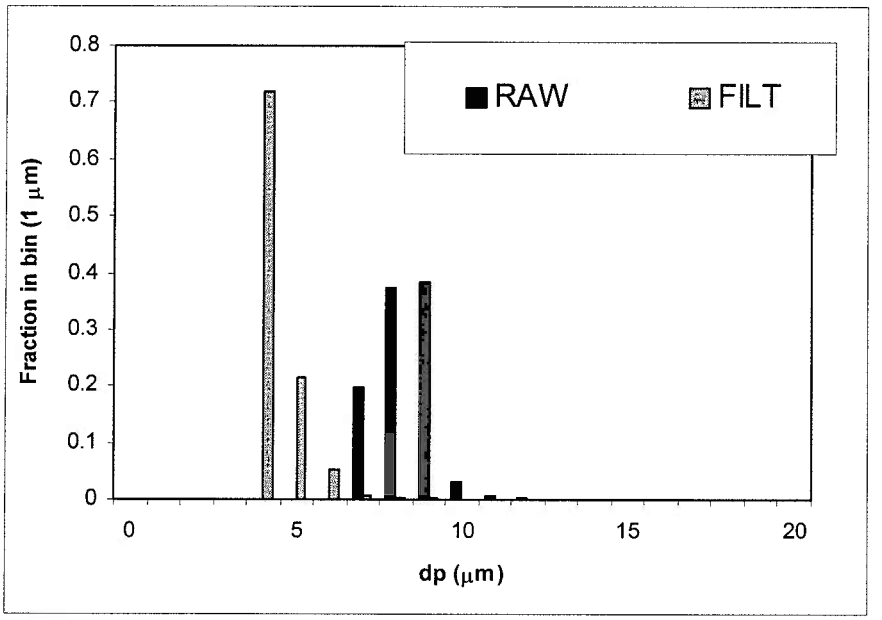

Figure 2.9. Particle size analysis of dissolved filters from Coulter analysis. RAW = seawater sample from flume. FILT = dissolved filter from control sample.

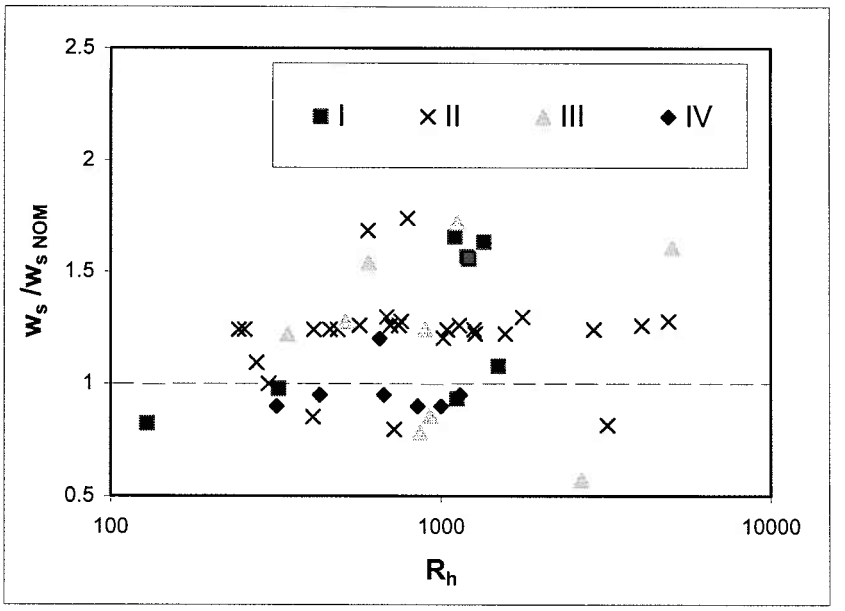

Figure 2.10. Settling velocities from initial water samples. The subscript NOM indicates the nominal settling velocity from the source material.

particle traps were siphoned into a bottle and handled using the same procedure as for water samples. One pre-core and two post-cores were collected for each smooth run.

Calculation of the amount deposited (m_c) was the difference between pre and post cores, adjusted by the core weight,

$$m_c = m_{post} - m_{pre}\frac{M_{post}}{M_{pre}} \quad , \tag{2.25}$$

where m and M are the mass of particles in the fluid from the core and the total mass of the core, respectively, and the subscripts "pre" and "post" denote the core. In cases where the fine particle mass was computed to be negative, the sample was determined to be below the level of detection and a mass of zero was adopted. By integrating the loss from the time series, the total mass deposited can be calculated to predict the amount of fine particles in a core (m_w),

$$m_w = \varepsilon A_c h'\left(\overline{C}(-t_o) - \overline{C}(t_{core} - t_o)\right) \cong \varepsilon A_c h' C_o \exp\left(\frac{-w_d t_{core}}{h'}\right) \quad , \tag{2.26}$$

where ε corrects for the distribution of deposition in the flume, A_c is the area of the core, and t_{core} is the time elapsed between the run start and coring. The value of ε is the ratio of the deposition measured at the sampling location to the deposition averaged over the entire bed. Flume runs were executed in both flumes to compute this correction term and found that it was nearly unity (Table 2.4). Unfortunately, this analysis also confirmed the large scatter that is associated with the core sampling in this study.

For one experimental treatment (400-μm sand and suspension IV), cores were sectioned to determine the vertical distribution of deposited particles in the sediment.

Four sections were isolated: 0 to 2 mm, 2 to 5 mm, 5 to 10 mm, and below 10 mm. The majority of cores were over 3 cm in length. Mass determination for each section was done in the same manner as the whole cores. A control experiment was conducted to ensure that the coring procedure does not significantly alter the profile of concentration within the sediment bed. A suspension of 100 mg/L was allowed to settle under still water conditions to a sand bed. Cores were collected one and three hours after addition. Under still water, all deposited particles should be in the top sediment section (0 - 2 mm). Particles deeper in the bed were assumed to have moved during the coring procedure.

Error analysis for sediment core measurements was conducted by adding a spike of particles to sediment samples. The amounts of fine particles added (0.8, 1.6 and 2.4 mg) span the range of deposition amounts predicted for sand cores. Results from core analysis compared well with spike amounts (Figure 2.11a) with a standard error for all the spike samples of 0.31 mg (4 samples per concentration). For smooth bed cores, error magnitude was estimated using another series of spike tests. In this case, a series of pikes from 25 to 100 mg were tested. The standard error from this analysis was 0.64 mg (3 samples per concentration) coupled with 8 % loss (Figure 2.11b). Both corrections are small compared to the magnitude of deposited mass anticipated in particle traps.

Table 2.4. Correction factors for spatial variability of core results.

Flume	# of runs	# of cores	Correction values (ε)
RTF	1	81	0.95 ± 0.52
17M	3	90	1.01 ± 0.43, 0.55 ± 0.25, 0.92 ± 0.41

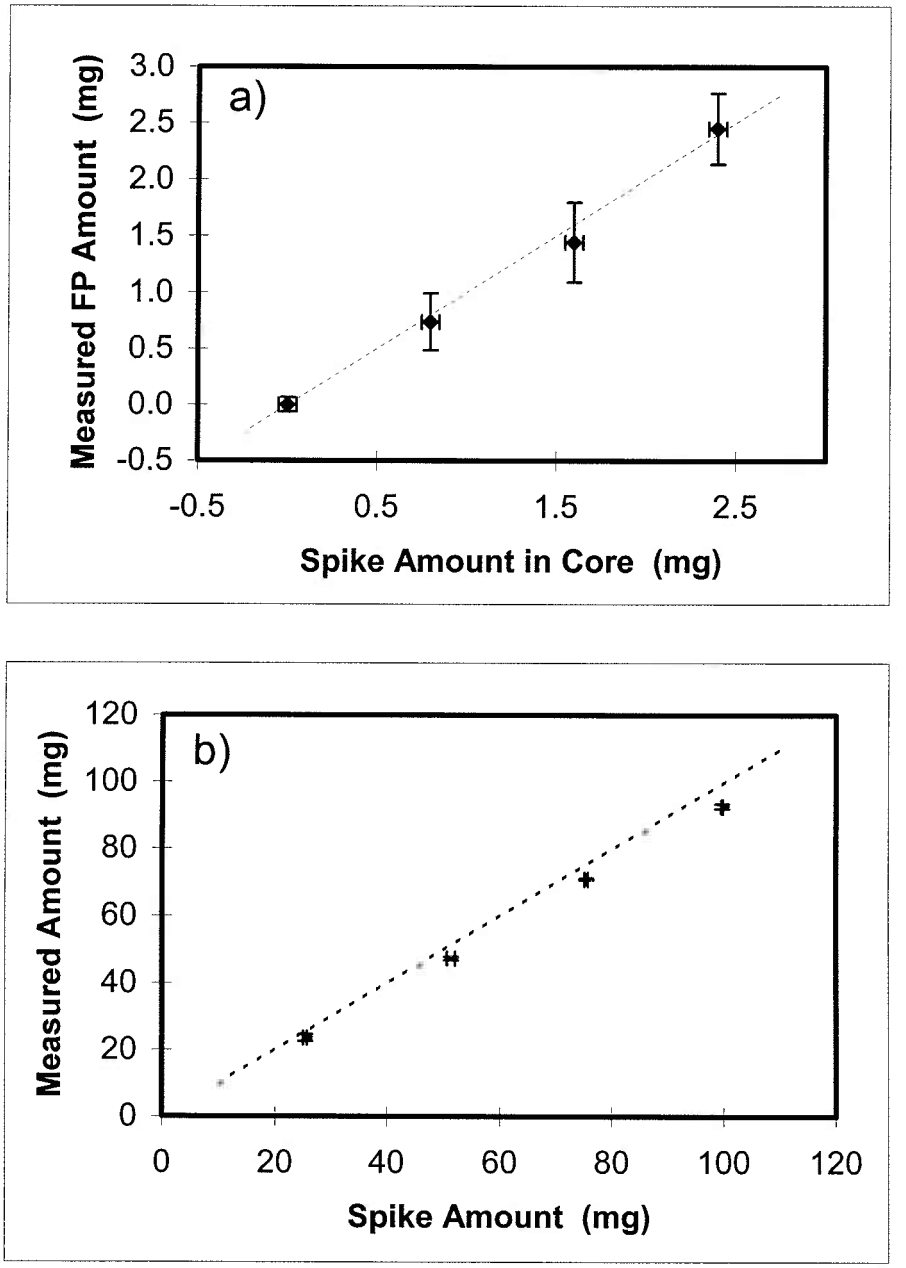

Figure 2.11. Spike test for cores. Samples from (a) sediment and (b) smooth bed traps were tested. Dashed curves represent 1:1 comparison. Error bars represent ±1 SE.

2.3. Results

2.3.1. Deposition to impermeable boundaries

Impermeable boundaries were used as a control treatment for deposition measurements. Results from water samples collected during flume experiments over PVC beds confirmed that the deposition velocity was approximately the same as settling for all suspensions and over the range of flows possible in the flume facilities (Figure 2.12). The total amount of deposition was qualitatively confirmed by the smooth bed particle trap results (Figure 2.13). The traps reproduce the relative magnitudes of the total losses from the water column; however, there is a notable decline for the highest concentration runs. This result confirmed that the flumes could be used to measure deposition rates as small as the settling velocity for the test suspensions. All data from impermeable bed experiments are listed in Table 2.5.

2.3.2. Deposition to sediment from water samples

The results from deposition experiments with sediment beds (Figure 2.14) can be divided into two sets. First, for large grain Reynolds numbers, little to no enhancement was observed to marble beds. This observation is consistent with the results from Einstein (1968) for very rough beds. Second, finer sediment treatments revealed a set of conditions that lead to enhancement. Three specific treatments demonstrated large enhancements and will often be referred to separately in this discussion: suspension I and 350-μm sand, III and 550-μm sand, and IV and 400-μm sand. Other sand and gravel treatments exhibited little to no enhancement. The variety of enhancement values for the

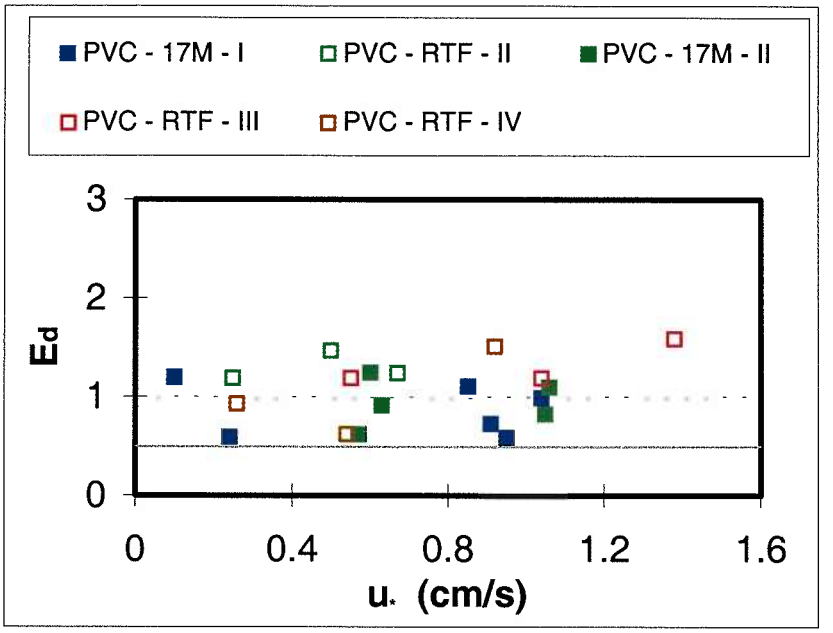

Figure 2.12. Deposition results for all PVC experiments. Horizontal lines denote the adopted range of values for no enhancement ($E_d = 1 \pm 0.5$). Points are organized by both color for suspension and shading for flume. Blue = I, green = II, red = III, and brown = IV. Filled = 17M and open = RTF. Errors (bars omitted for clarity) were typically $\pm$ 0.5 E_d units.

same grain Reynolds number reinforces the idea that additional, particle dependent, parameters are necessary in a model for fine particle deposition. All data from sediment bed experiments are listed in Tables 2.6 and 2.7.

2.3.3. Suspension characteristics

Observations of the median particle diameter over time were usually consistent with both constant and settling models described in Section 2.2.4 (Figure 2.15). In order to compare models, the ratio of data to model predictions was computed over time and

deviations from unity were recorded. The resultant statistic, similar to a root mean square error, is presented for all the treatments analyzed in Table 2.8. The baseline value was calculated based on the same statistic if the two models were compared to each other. In other words, the goal is to identify data that is consistent with either model and ensure that the models are distinct. Values for data-model comparisons smaller than the baseline from model-model comparisons are considered to be reasonable.

Table 2.5. Data from PVC deposition experiments.

Flume	(cm/s) u_*	Suspension	(cm/s) w_s	(cm/s) w_d	(cm/s) w_L	($x10^4$) C_D	(mg) m_c
17M	0.24	I	0.0088	0.0053	---	36	9
17M	0.10	I	0.0074	0.0090	---	43	---
17M	1.04	I	0.0147	0.0147	---	38	---
17M	0.95	I	0.0140	0.0084	0.001	37	60
17M	0.85	I	0.0149	0.0168	---	39	51
17M	0.91	I	0.0141	0.0104	0.000	41	24
RTF	0.50	II	0.0091	0.0135	-0.002	40	---
RTF	0.25	II	0.0054	0.0065	0.002	48	---
RTF	0.67	II	0.0094	0.0118	-0.001	35	---
17M	0.60	II	0.0043	0.0054	0.001	41	58
17M	0.57	II	0.0070	0.0044	0.000	38	59
17M	0.63	II	0.0069	0.0064	0.001	48	27
17M	1.05	II	0.0067	0.0056	0.000	38	34
17M	1.06	II	0.0066	0.0073	0.000	37	45
RTF	1.04	III	0.0150	0.0180	---	24	---
RTF	0.55	III	0.0150	0.0180	---	27	---
RTF	1.38	III	0.0150	0.0240	---	22	---
RTF	0.54	IV	0.0038	0.0024	---	28	---
RTF	0.92	IV	0.0038	0.0058	---	24	---
RTF	0.26	IV	0.0036	0.0034	---	21	---

--- = not measured

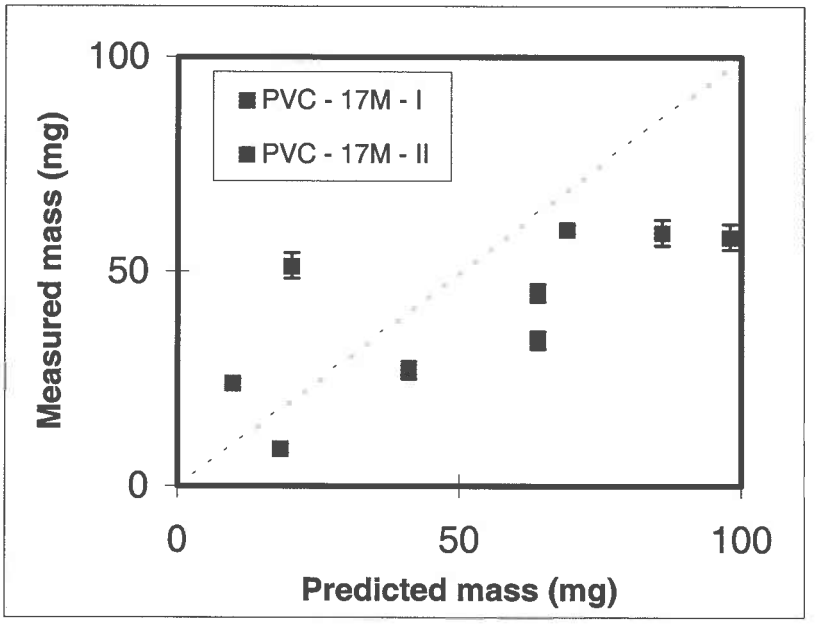

Figure 2.13. Smooth bed particle trap results for all PVC experiments. Dashed line represents 1:1 relationship. All data collected in 17M. Symbols are the same as in Figure 2.12. Error bars represent ±1 SD.

Three treatments demonstrated reasonable fits to at least one model: suspension I over both PVC and 350-μm sand and suspension II over 550-μm sand. For the PVC case, the settling model fits the data well. For the pair of sand experiments above, both the constant model and settling model fit the data well. All data for suspension III are not in agreement with either model due to the fact that the models themselves are not terribly different (low baselines).

2.3.4. Deposition from sediment cores

Results from sediment cores were used to confirm the deposition amounts calculated from water samples. Results from both methods are consistent with few

deviations from a 1 to 1 relationship (Figure 2.16). The points furthest from the 1:1 curve (in box on right-hand side of plot) are results from the first three runs conducted. These experiments were subject to large errors in m_c due to the inclusion of plastic dishes in the filter weights that were not checked for consistent weights through drying. This error was eliminated in all later experiments.

Sectioning of cores was done for the 400-μm sand runs (three experiments). These cores revealed elevated concentrations of fine particles deeper in the sediment bed relative to the still water experiments (Figure 2.17a). Concentrations were normalized to allow for comparison between still water and flume experiments. Profiles taken at 1 and 3 hours show little change in time (Figure 2.17b). The center of mass of each profile shifts 1 mm down, corresponding to a settling velocity of 1.5×10^{-5} cm/s (or < 1 % of w_s in the fluid). Both of these observations support the idea that particles are entering the bed and penetrating into the sediment via interfacial diffusion, not settling.

2.4. Discussion

2.4.1. Comparison of results to Dade model

The model derived by Dade et al. (1991) predicts the enhancement of fine particle deposition to sediment beds. Large enhancements are found in Dade model predictions, but the observations for high R_* do not follow this increasing trend (Figure 2.18). The Dade model is focuses on stable flow structures near large roughness capable of mediating the particle flux. These fluid flows may not be present near flat sediment beds.

Other factors, such as permeability and interstitial flow may prove to be more important to delivery of particles to the seabed.

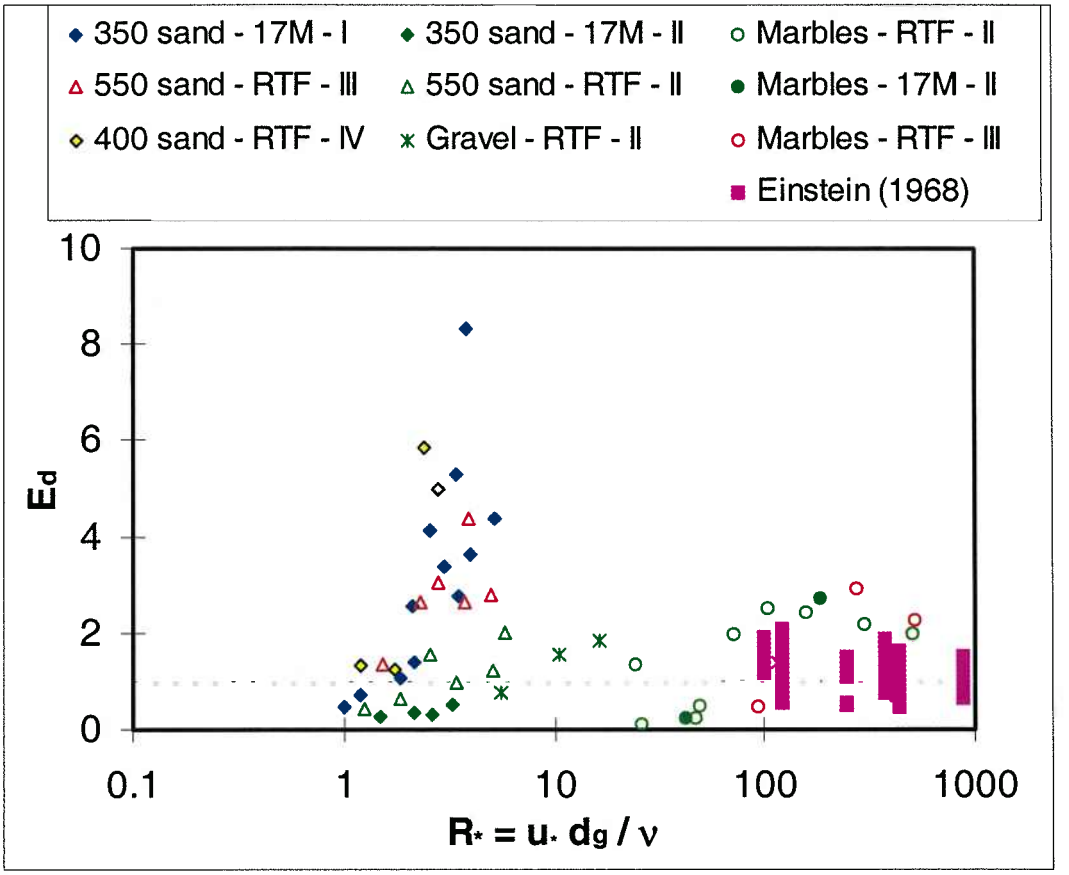

Figure 2.14. Deposition results for all sediment bed experiments. Horizontal line denotes the value for no enhancement ($E_d = 1$). Points are organized by three properties: shape for sediment, color for suspension, and shading for flume. Diamonds = 350- and 400-μm sand, triangles = 550-μm sand, asterisks = 1.3-mm gravel, and circles = 1.2-cm marbles. Blue = I, green = II, red = III, and brown = IV. Filled = 17M and open = RTF. Errors (bars omitted for clarity) were typically ± 0.5 E_d units.

Table 2.6. Data from sand bed deposition experiments. Lightened values estimated from source particle size distribution.

Flume	(μm) d_g	(cm/s) u_*	Suspension	(cm/s) w_s	(cm/s) w_d	(cm/s) w_L	($x10^4$) C_D	(mg) m_c
17M	350	1.49	I	0.0090	0.0396	---	52	0.61
17M	350	1.15	I	0.0097	0.0355	---	60	0.54
17M	350	0.86	I	0.0084	0.0286	---	62	0.57
17M	350	0.29	I	0.0090	0.0043	0.001	68	---
17M	350	1.11	I	0.0090	0.0751	0.000	41	1.41
17M	350	0.98	I	0.0090	0.0478	0.000	45	1.13
17M	350	1.00	I	0.0090	0.0250	---	53	0.99
17M	350	0.62	I	0.0090	0.0126	---	54	1.64
17M	350	0.74	I	0.0090	0.0374	---	42	2.11
17M	350	0.53	I	0.0090	0.0097	0.000	64	1.67
17M	350	0.34	I	0.0090	0.0069	---	60	1.44
17M	350	0.60	I	0.0090	0.0230	---	55	1.06
17M	350	0.50	I	0.0090	0.0026	---	62	1.63
17M	350	0.62	II	0.0054	0.0020	---	52	1.90
17M	350	0.43	II	0.0054	0.0016	---	65	0.54
17M	350	0.76	II	0.0054	0.0017	---	60	0.83
17M	350	0.94	II	0.0054	0.0029	---	62	0.72
RTF	550	0.69	III	0.0227	0.0605	0.008	35	0.97
RTF	550	0.28	III	0.0353	0.0480	0.002	54	0.19
RTF	550	0.42	III	0.0370	0.0975	0.001	45	1.08
RTF	550	0.91	III	0.0500	0.1415	0.014	34	0.72
RTF	550	0.51	III	0.0447	0.1380	0.013	36	1.28
RTF	550	0.72	III	0.0360	0.1580	0.011	38	0.44
RTF	400	0.69	IV	0.0036	0.0210	---	24	1.00
RTF	400	0.34	IV	0.0038	0.0050	---	22	0.54
RTF	400	0.80	IV	0.0036	0.0180	---	24	0.40
RTF	400	0.50	IV	0.0048	0.0060	---	24	0.38

Table 2.7. Data from coarser sediment bed deposition experiments.

Flume	d_g (cm)	u_* (cm/s)	Suspension	w_s (cm/s)	w_d (cm/s)	w_L (cm/s)	C_D ($\times 10^4$)
17M	1.23	0.34	II	0.0046	0.0011	0.001	54
17M	1.23	1.48	II	0.0070	0.0192	0.000	66
17M	1.23	2.67	II	0.0044	0.0255	0.000	67
RTF	1.23	0.84	II	0.0065	0.0165	-0.003	53
RTF	1.23	1.29	II	0.0066	0.0162	-0.003	55
RTF	1.23	2.43	II	0.0067	0.0148	-0.003	55
RTF	1.23	0.87	II	0.0067	0.0095	-0.001	53
RTF	1.23	0.38	II	0.0067	0.0016	0.001	51
RTF	1.23	0.21	II	0.0067	0.0009	0.001	49
RTF	1.23	0.58	II	0.0068	0.0136	-0.003	51
RTF	1.23	3.36	II	0.0068	0.0049	-0.002	58
RTF	1.23	0.40	II	0.0067	0.0033	0.000	35
RTF	1.23	4.08	II	0.0069	0.0136	-0.003	57
RTF	1.23	0.20	II	0.0067	0.0091	-0.001	40
RTF	1.23	0.76	III	0.0249	0.0120	0.001	45
RTF	1.23	2.23	III	0.0166	0.0492	-0.008	51
RTF	1.23	4.19	III	0.0467	0.1060	-0.005	57
RTF	0.13	0.82	II	0.0064	0.0100	---	34
RTF	0.13	0.43	II	0.0064	0.0050	---	33
RTF	0.13	1.25	II	0.0064	0.0120	---	32

Figure 2.15. Median diameter results from Coulter counter. Seven different treatments presented in independent plots. Suspensions denoted with MS# and bed material within each plot title: PVC = impermeable bed, 350 = 350-μm sand, 550 = 550-μm sand, and MRB = marbles. Circles are ratios of data to constant suspension model and asterisks are the ratio of data to the settling model. Horizontal lines at a ratio of 1 represent perfect match between data and model.

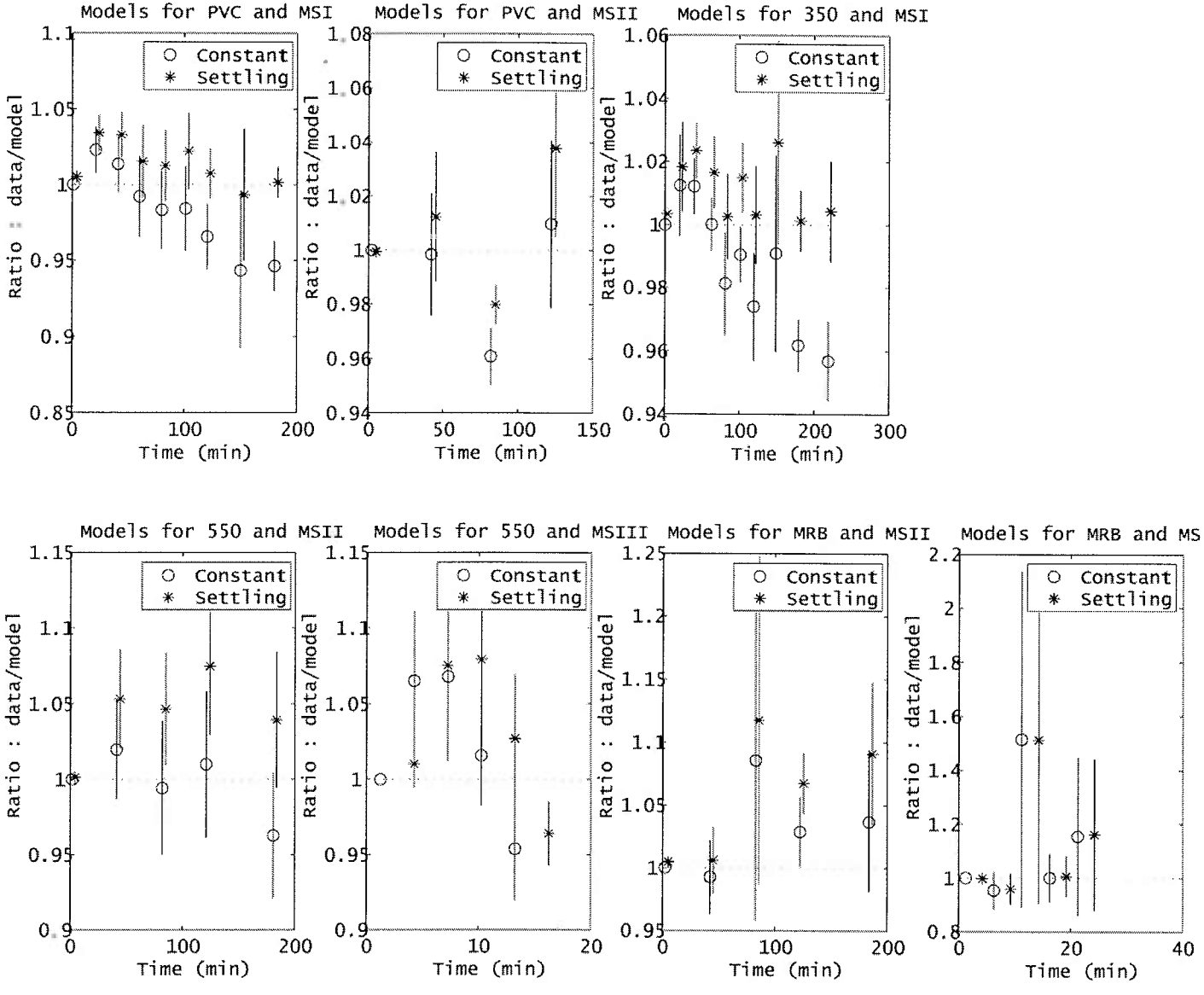
Models for PVC and MSI
Models for PVC and MSII
Models for 350 and MSI
Models for 550 and MSII
Models for 550 and MSIII
Models for MRB and MSII
Models for MRB and MS
Constant
Settling
Ratio : data/model
Time (min)

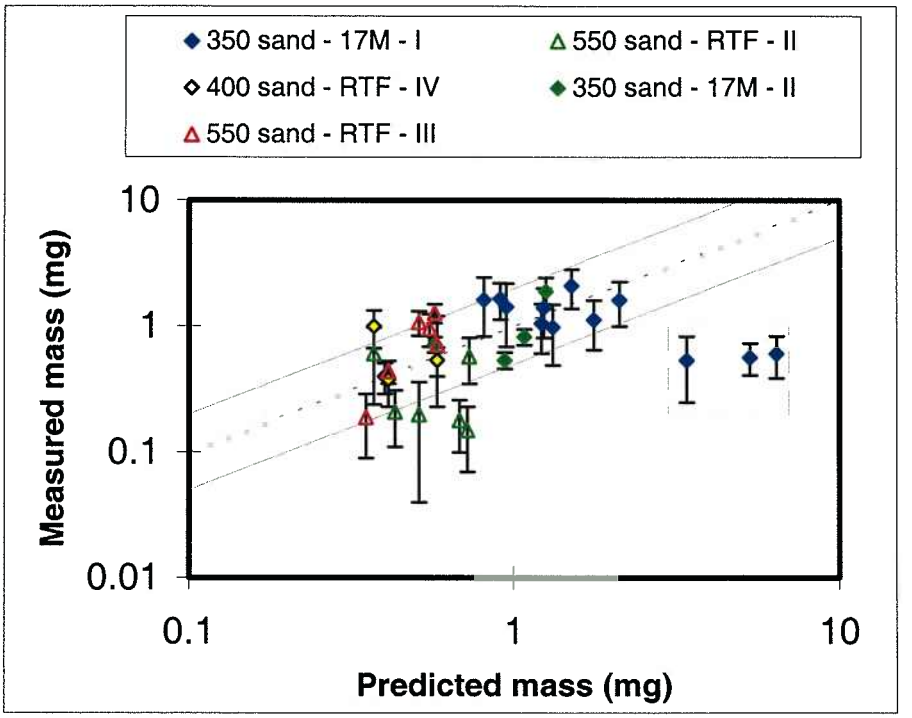

Figure 2.16. Sediment bed core results for all sand experiments. Dashed line represents 1:1 relationship while solid lines represent a factor of 2 difference. Symbols are the same as in Figure 2.14. Error bars represent ±1 SD.

2.4.2. Link between deposition and drag coefficient

Recent studies have highlighted the ability of permeable sediment beds to allow fluid intrusion near topography (e.g., Thibodeaux and Boyle, 1987; Huettel et al., 1996). These studies include observations of the delivery of particles in pressure driven, interfacial flows and some discussion of the potential for sedimentary control of the net deposition rate. A common theme is that the increases in deposition should be directly due to increases in the drag exerted on the fluid by the bed.

Flat sediment beds should not exhibit this correlation between drag and deposition. To test this idea, drag coefficients and deposition velocities for the three

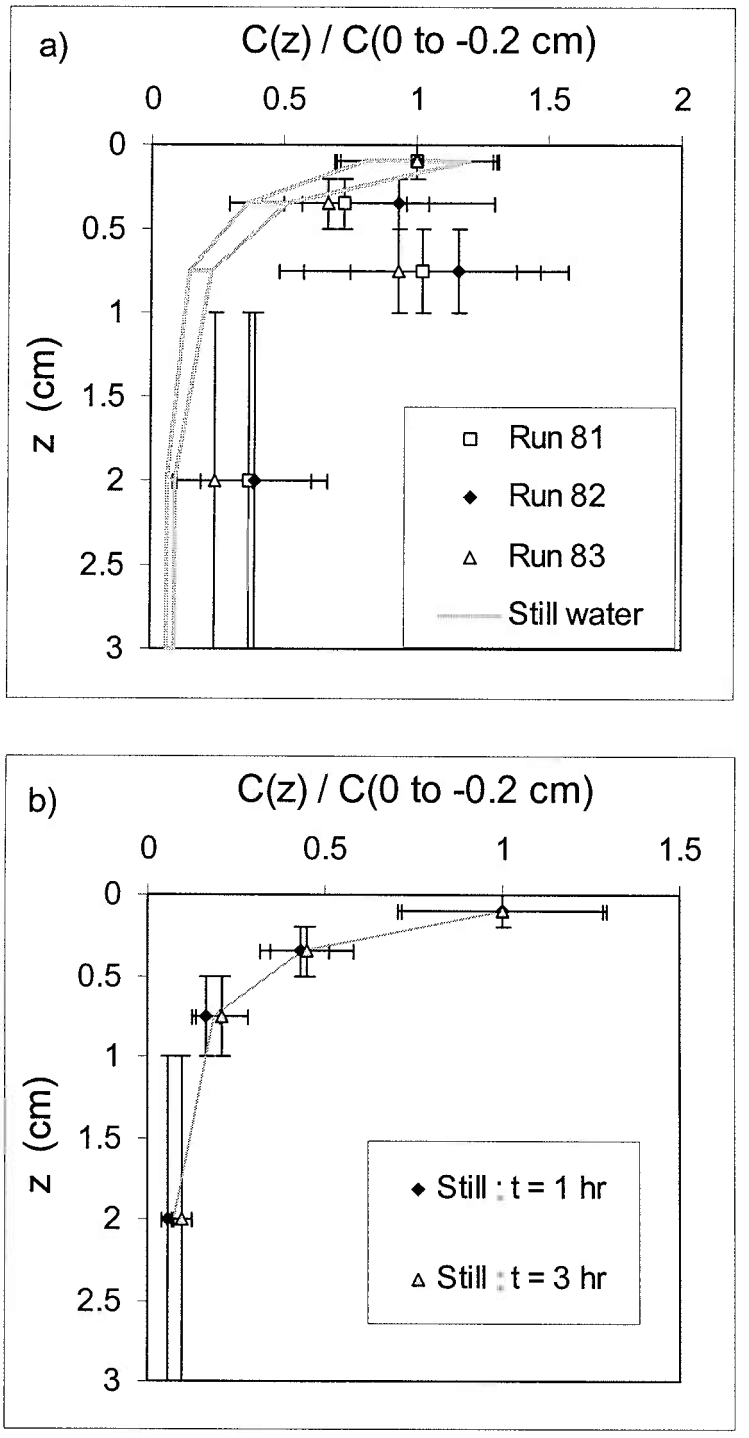

Figure 2.17. Results from sectioned cores for 400-μm sand experiments. Vertical bars denote depth interval for measurement and horizontal error bars represent ±1 SD. Still water data contained in gray box with horizontal bars at data locations.

treatments with significant enhancement were compared (Figure 2.19). In none of these cases was the correlation positive. In fact, the correlations were negative for the treatments with significant variation in C_D (all but 400-μm sand). This correlation suggests that another mechanism, one that reduces drag while increasing interfacial flux, may be responsible for the observed enhancements.

One possibility is the induction of slip at the sediment water interface. Reductions in drag due to flow within a permeable boundary have been observed by other investigators (e.g., Beavers and Joseph, 1967; Richardson and Parr, 1991), but the specifics of the mechanism that drives these flows are poorly understood. To date, the most promising lead is the imposition of a diffusive flux at the sediment water interface. Richardson and Parr (1988) used interfacial diffusion to describe the effusion of solutes from sediments subjected to runoff flow. This scenario can be inverted to describe the transport of particles with diffusive fluid flows into the sediment bed (model developed based on this idea is presented in Chapter 3).

2.4.3. Check for aggregation in flume

The rapid removal of fine particles through deposition is usually assumed to be aggregation controlled. In this study, two assumptions were made in accordance with two common caveats regarding aggregation (e.g., Gonzalez and Hill, 1998). First, formation of aggregates is controlled by concentration. Therefore, particle additions were kept small enough to avoid aggregation. Second, high shear promotes destruction

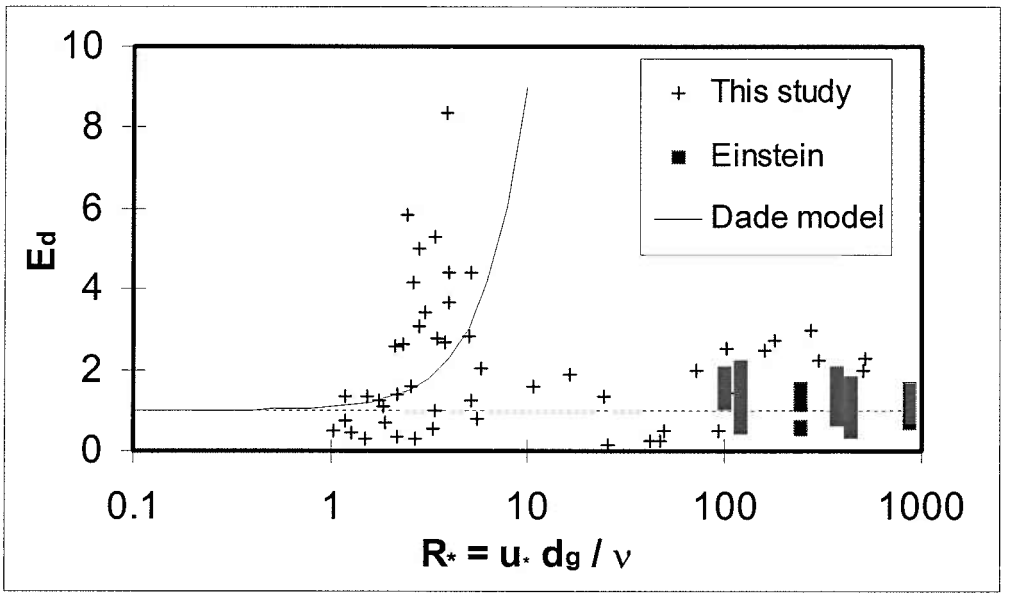

Figure 2.18. Comparison of Dade model predictions and deposition results for all experiments. Measurements from this study (pluses) and Einstein (squares) are included.

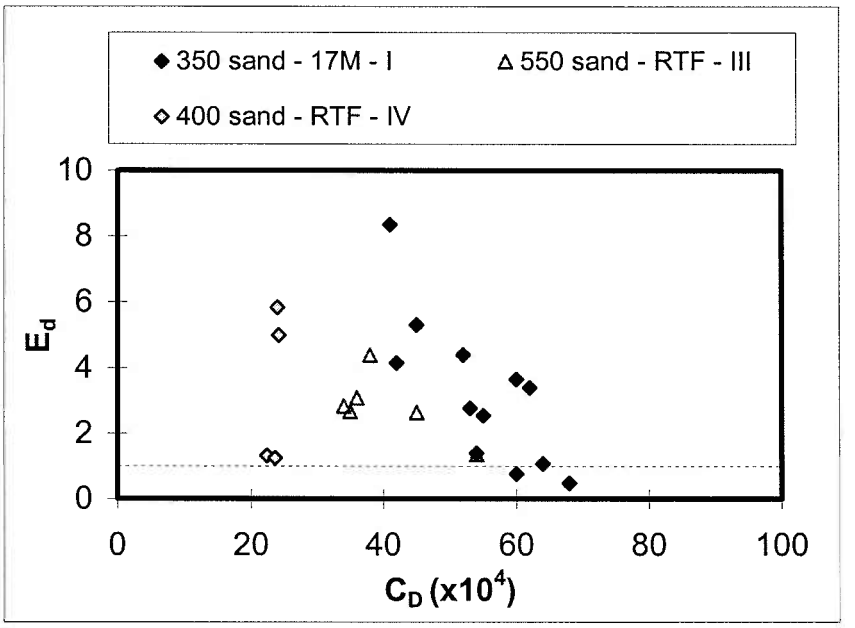

Figure 2.19. Drag coefficient relative to deposition results for all experiments with significant enhancement. Symbols are the same as in Figure 2.14.

of aggregates already formed. The pump and return pipe of the flume provided convenient shear vessels for disrupting those that may have formed in the sump.

To ensure that these assumptions were correct, two sets of experiments were undertaken. First, flume experiments over smooth panels were repeated with both freshwater and seawater suspensions. Three flume experiments with similar flow conditions were executed for each water type. Both the freshwater ($u_* = 0.56 \pm 0.03$ cm/s) and seawater ($u_* = 0.55 \pm 0.01$ cm/s) runs resulted in no enhancement of deposition (Figure 2.20). The w_d values for freshwater and seawater runs were 0.017 ± 0.002 and 0.014 ± 0.003 cm/s, respectively. Second, observations of the concentration profile in the flume were attempted. These measurements were made with a multiple port siphon placed in the flume at the tail location. The ports were individually sampled at 20-minute intervals during a series of smooth bed experiments. Results confirmed that the water

Table 2.8. Fit measures for median diameter models.

Boundary	Suspension	Baseline	Constant	Settling
PVC	I	0.084	0.093	0.057
	II	0.036	0.040	0.045
350-μm sand	I	0.085	0.070	0.046
550-μm sand	II	0.113	0.044	0.110
	III	0.022	0.106	0.119
Marbles	II	0.070	0.098	0.164
	III	0.018	0.538	0.539

Shaded values are considered reasonable fits (see discussion in Section 2.3.3).

column was well mixed (Figure 2.21) as expected for slow settling particles. While this result does not exclude the possibility of slow settling aggregates, the suspension particle size analyses and resultant confirmation of settling velocity (Figure 2.10) precludes significant changes in the particle size distribution. These results strengthen the claim that aggregation played no role in enhancing deposition in this study.

2.4.4. Suspension characteristics and deposition mechanisms

Median diameter models tested in this study were based on the idea that either gravitational settling or a particle independent process (e.g., loss in the flume system) drives fine particle deposition. The general conclusion from this analysis was that the models were not distinct enough to allow for discrimination of which fits the data better. In other words, if the data fit one of the models well, then it usually fit the other well also. Another interpretation of this result would be the adoption of another mechanism that is responsible for the deposition of fine particles.

The primary difference between the constant and settling models introduced is the dependence of each on the particle size. In the case of the settling model, the deposition rate is proportional to the diameter squared. The constant model assumes deposition is independent of particle diameter. If the data truly falls in between these models, it would be anticipated that the new process would depend on particle diameter to a power between 0 and 2.

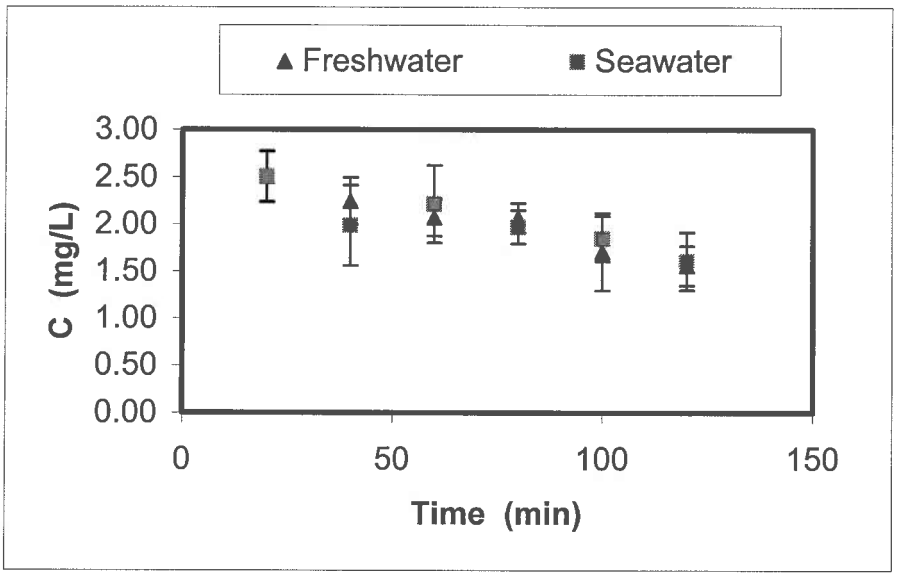

Figure 2.20. Aggregation test results. Two sets of data for freshwater (triangles) and seawater (squares) are presented. Error bars represent ±1 SD.

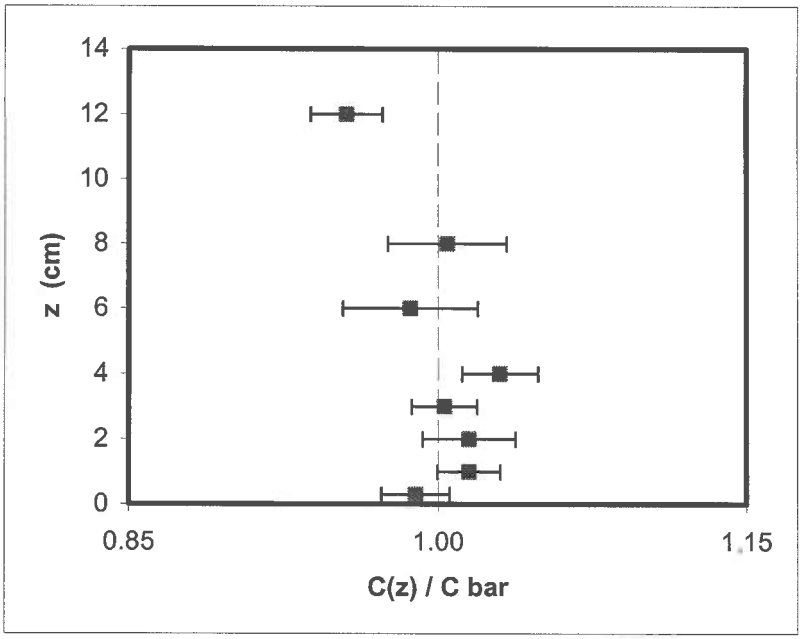

Figure 2.21. Fine particle concentration profile. Concentration profile normalized by the depth averaged concentration. Error bars represent ±1 SE.

2.5. Conclusion

This study presents new observations of fine particle deposition to smooth permeable sediment beds. Enhanced rates for specific treatments of flow, suspension, and bed grain size were measured. Control experiments over impermeable beds resulted in no enhancement relative to settling. A model for enhancement of deposition proposed by Dade et al. (1991) failed to predict the amount of deposition. The reason for this failure lies in the reliance on the small roughness scales for smooth sediment beds. Other potential reasons for the enhancement, such as aggregation or topography, were not responsible for the observed rates. In fact, the inspection of variations in deposition with the drag coefficient revealed that the mechanism that enhances particle delivery to the bed also reduces the drag in the channel. This result inspires a search for a new mechanism that enhances fine particle deposition to permeable sediment beds.

3. A new model for fine particle deposition to permeable sediment beds

3.1. Introduction

Studies aimed at describing the flux of particles to permeable boundaries under turbulent flow conditions are somewhat limited compared to the extensive knowledge accumulated for solid cases (e.g., Cleaver and Yates, 1975; Wood, 1981; Nino and Garcia, 1996). The effect of permeability on the transport to the boundary is important to investigations in many fields, such as geochemical cycling (e.g., Lerman, 1978; Hedges, 1992), sediment transport (i.e., Martin, 1970; Carling, 1984), and agricultural runoff (Ahuja and Lehman, 1983; Parr et al., 1987). The next step is to explore the links between flow within permeable boundaries and the transport of particles across the sediment water interface.

Observations of enhanced fine particle deposition (see Chapter 2) exceed the predictions of deposition models dependent on delivery only (e.g., Dade et al., 1991). The source of this under prediction may be the lack of consideration of the sedimentary controls on deposition (i.e. permeability). Therefore, another model is required to accommodate both sides of the sediment water interface.

This chapter will describe a new model for predicting fine particle deposition to permeable sediment beds (Figure 3.1). The central theme of the proposed model is that both particle delivery and retention are important when predicting deposition rates. Superimposed on these two processes is the gravitational settling of particles. The primary mechanism for delivery is the diffusion of fluid across the sediment-water

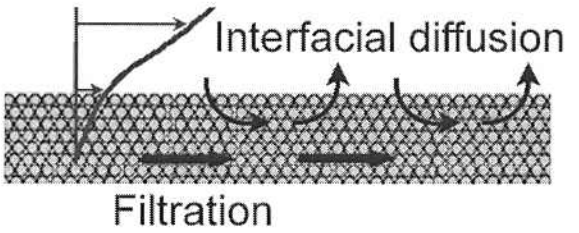

Figure 3.1. Schematic of the fine particle deposition mechanisms within the proposed model.

interface. These flows drive subsurface flows that may be detectable in the flow profile above the boundary. Retention of particles is accomplished via filtration in the bed. Prediction of particle removal should be possible through the application of insights from bed filter research. The mathematical framework for the model will be detailed and a final expression presented. This model expression will provide a means for determining the conditions required to enhance fine particle deposition.

3.2. Model for interstitial flow

3.2.1. Governing equation

Brinkman (1947) was one of the first to consider the coupling between flows across fluid-particle interfaces, where flow resistance is a combination of viscous and turbulent drag on the fluid by the grains. Ruff and Gelhar (1972) made direct measurements of flow profiles in a permeable boundary (foam) and fit these data to models based on an introduced kinematic viscosity for the pore fluid (ν_b),

$$-\frac{\partial p}{\partial x}+\rho\nu_b\frac{\partial^2 u}{\partial z^2}=\frac{\rho\nu}{K}u+\frac{\rho u^2}{c\sqrt{K}}. \qquad (3.1)$$

where p is the pressure driving the flow, and x and z are the horizontal and vertical coordinates, ρ and ν are the fluid density and viscosity, u is the horizontal flow velocity, K is the bed permeability, and c is a constant whose value depends on the boundary structure. The viscosity of the pore fluid is analogous to the turbulent eddy viscosity frequently used in describing turbulent flows (e.g., Prandtl, 1925). The last term is a quadratic drag in the bed. The constant c was found to be 1.8 for granular beds (Ward, 1964) and on the order of 10 for foam (Ruff and Gelhar, 1972). By comparing the two drag terms on the right hand side of (3.1), the criterion for excluding the quadratic term is

$$\frac{u\sqrt{K}}{c\nu}<<1. \qquad (3.2)$$

For natural sediment beds, this criterion is often satisfied and will be considered as a limit for application of the final model.

Another possible limit is that of negligible diffusion, where the pressure gradient is balanced by the drag in the bed. This balance is described by Darcy's equation (Darcy, 1856; see discussion in Bear, 1972), resulting in an expression for the interstitial velocity,

$$u_d=\frac{-K}{\rho\nu}\frac{\partial p}{\partial x}, \qquad (3.3)$$

In open channel flows, the pressure gradient is due to bottom drag and the resultant flow,

$$u_d\cong\frac{K}{\nu}\frac{u_*^2}{h}. \qquad (3.4)$$

This constant profile is appropriate away from the sediment water interface.

The diffusive term becomes more significant very close to the interface. In this case, the pressure gradient becomes negligible as shown by the comparison of the forcing terms,

$$\frac{\left(\frac{\partial p}{\partial x}\right)}{\rho \nu_b \left(\frac{\partial^2 u}{\partial z^2}\right)} \propto \frac{u_*^2}{h} \frac{d_g^2}{\nu_b u_*} = R_* \frac{d_g}{h} \frac{\nu}{\nu_b}, \tag{3.5}$$

where d_g is the sediment grain size. This ratio is much smaller than unity for the sediment and flow scales typical of deposition to sand beds. The differential equation governing interstitial flow near the interface becomes

$$\nu_b \frac{\partial^2 u}{\partial z^2} = \frac{\nu}{K} u, \tag{3.6}$$

where this flow is in addition to the Darcy flow at depth. Two sensible boundary conditions are the extinction of flow deep in the bed,

$$u \to 0 \text{ as } z \to -\infty \tag{3.7}$$

and the matching of momentum fluxes at the interface,

$$\nu_b \left.\frac{\partial u}{\partial z}\right|_{z=0} = u_*^2. \tag{3.8}$$

3.2.2. Diffusion within the sediment

At this point it is necessary to identify the nature of the diffusivity in the bed and any possible dependence on depth. The simplest case is to assume the diffusivity of the sediments is constant with depth. In this case, the solution for the flow profile in the sediment becomes

$$\frac{u(z)}{u_*} = \frac{u_s}{u_*}\exp\left(\sqrt{\frac{\nu}{\nu_b K}}\, z\right), \tag{3.9}$$

where u_s is the slip velocity at the sediment water interface. From the interface boundary condition (3.8), a solution for the slip velocity becomes

$$\frac{u_s}{u_*} = \frac{u_*\sqrt{K}}{\sqrt{\nu\nu_b}} = R_K\sqrt{\frac{\nu}{\nu_b}}. \tag{3.10}$$

where R_K is the bed Reynolds number,

$$R_K = \frac{u_*\sqrt{K}}{\nu}. \tag{3.11}$$

One aspect of this solution is the rapid decay of the profile. From the decay, an estimate of the flow penetration depth (δ) can be made,

$$\delta \propto \sqrt{\frac{K\nu_b}{\nu}}. \tag{3.12}$$

This number is exceedingly small for a majority of natural sediments given the strong dependence on the permeability scale ($\sqrt{K}$).

Another possible way to parameterize diffusivity is to relate the diffusivity to the local flow velocity. Ruff and Gelhar (1972) suggested the use of expressions for lateral dispersion in sediments (e.g., Harleman and Rumer, 1963; List and Brooks, 1967). The appropriate expression for ν_b depends on the bed Reynolds number of the interstitial flow,

$$R_{K,b} = \frac{u\sqrt{K}}{\nu} = \frac{u}{u_*}R_K. \tag{3.13}$$

Two regimes of diffusivity exist (Figure 3.2), defined as follows:

$$\frac{\nu_b}{\nu} = 0.14 R_{K,b}^{2/3} \text{ for } R_{K,b} < 0.1 \tag{3.14a}$$

$$\text{and } \frac{\nu_b}{\nu} = R_{K,b} \text{ for } R_{K,b} \geq 0.1. \tag{3.14b}$$

The remarkable aspect of this transition is the fact that the expression (3.14b) matches that for longitudinal dispersion (Harleman and Rumer, 1963). This indicates that the fluid motions driving diffusion are independent of flow direction for $R_{K,b}$ of order 10^{-1} or greater. These two forms of diffusivity will be referred to as the low and high R_K models. These expressions lead to more complicated solutions to the governing equation that is detailed in Appendix A. The final solution to the low R_K model is

$$\frac{u(z)}{u_*} = \frac{u_s}{u_*}\left(1 + \frac{z}{\delta}\right)^3, \tag{3.15a}$$

$$\text{where } \frac{u_s}{u_*} \cong 2.3 R_K^{1/2} \tag{3.15b}$$

$$\text{and } \frac{\delta}{\sqrt{K}} = 1.2 R_K^{1/2}. \tag{3.15c}$$

The final solution to the high R_K model is

$$\frac{u(z)}{u_*} = \frac{u_s}{u_*}\left(1 + \frac{z}{\delta}\right)^2, \tag{3.16a}$$

$$\text{where } \frac{u_s}{u_*} \cong 1.1 R_K^{1/3} \tag{3.16b}$$

$$\text{and } \frac{\delta}{\sqrt{K}} = 2.6 R_K^{2/3}. \tag{3.16c}$$

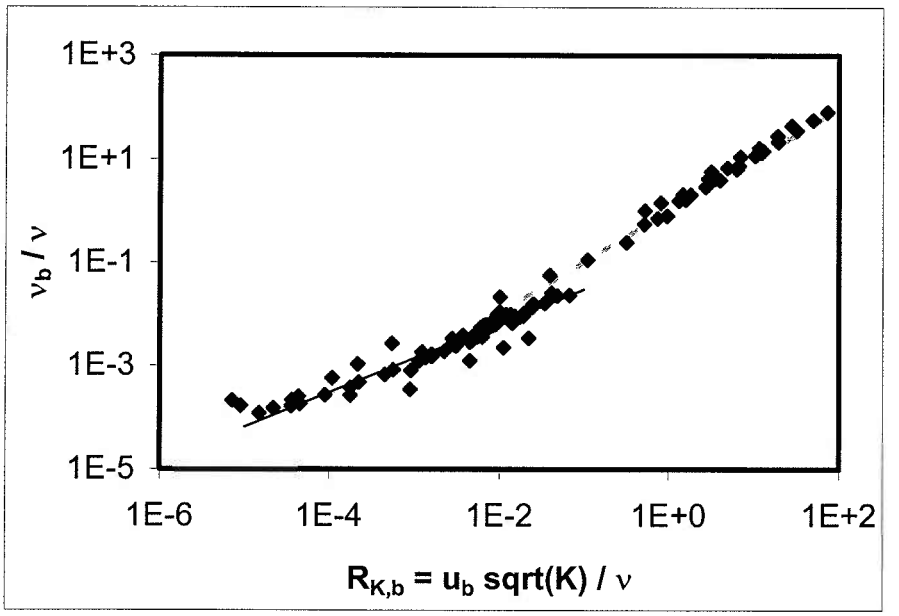

Figure 3.2. Dispersion data summarized by List and Brooks (1967). Regressions based on work by Harleman and Rumer (1963).

These profiles differ markedly from the exponential solution for a constant diffusivity. In these cases, the layer of flow driven by the interfacial diffusion has a definite thickness that remains smaller than the grains in the bed.

Two difficulties arise from the limited layer of fluid flow affected by interfacial diffusion. First, the detection of these flows is difficult, as demonstrated by the efforts made by the few successful direct measurements of flow in permeable boundaries (e.g., Ruff and Gelhar, 1972; Nagoka and Ohgaki, 1990). Note that these observations are for high R_K and may not provide accurate predictions for less permeable beds. Second, it is difficult to argue for the use of flow dependent diffusivity when a thin shear layer may be better represented by an "average" value for the entire bed.

Using a constant diffusivity has the advantage of being detectable using the flux of tracers, like dye or particles, as a proxy for the diffusive exchange of fluid across the sediment water interface. Monitoring the release of a tracer from soil under runoff, Richardson and Parr (1988) observed a large enhancement of interfacial diffusion relative to the diffusivity of the tracer. Analysis of their data reveals a relationship between interfacial diffusion and bed Reynolds number (Figure 3.3),

$$\frac{\nu_b}{\nu} = (0.091 \pm 0.040) R_K^{(1.88 \pm 0.16)} \cong \frac{R_K^2}{10}. \tag{3.17}$$

If this diffusivity is adopted and applied to the expressions for constant ν_b above, then the fluid flow in the bed is defined by three expressions,

$$\frac{u(z)}{u_*} = \frac{u_s}{u_*} \exp\left(\frac{\sqrt{10}}{\mathrm{R_K}} \frac{z}{\sqrt{\mathrm{K}}}\right), \tag{3.18a}$$

$$\text{where } \frac{u_s}{u_*} \cong \sqrt{10} \tag{3.18b}$$

$$\text{and } \delta \propto \sqrt{K} R_K. \tag{3.18c}$$

The applicability of this flow model should be limited to the range of R_K tested by Richardson and Parr (1988), which spans the range of values expected for sediments from fine sand to pea gravel.

An indirect measure of the viscosity in the sediment bed is the depth of fluid penetration into the sediment. Few measurements of this depth for flat sediment beds are reported in the literature. Unfortunately, the community pursuing the topic of interfacial fluxes has chosen to treat the flat sediment bed as a control surface, limiting the diversity

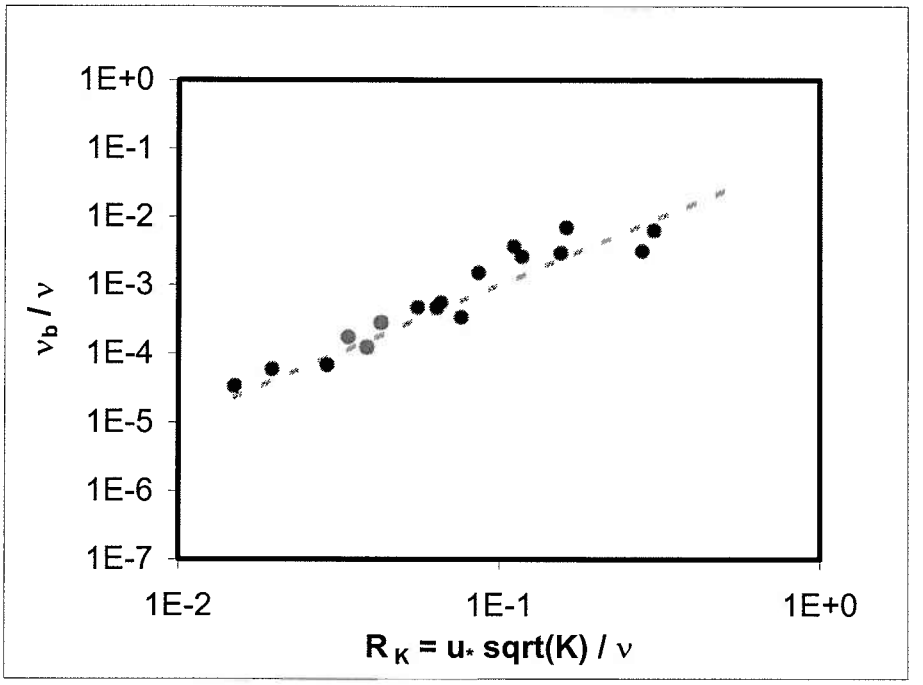

Figure 3.3. Interfacial diffusion data from Richardson and Parr (1988). Regression computed and presented in text.

---

of the experiments conducted. The expression for diffusivity based on fluid penetration (δ_f) is

$$\nu_b = \frac{\delta_f^2}{t_R}, \tag{3.19}$$

where t_R is the total run time. This expression assumes that the diffusivity is constant in time and that the bed is sufficiently thick as to not influence the penetration.

Huettel et al. (1996) made coincident fluid and particle penetration measurements for flat beds and roughened beds (mounds). Their flat bed results are consistent with the results of Richardson and Parr (1988) for fluid exchange and a significant increase of diffusivity due to topography (Figure 3.4). In the particle cases, however, both the

apparent diffusivities and the increases attributable to topography were reduced. A reasonable explanation for these reductions is the filtration of particles from intruding flows.

3.3. Model expression for concentration

3.3.1. Governing equation

Retention of deposited material could provide a means to enhance particle deposition. Carling (1984) demonstrates the rapid enhancement of deposition of sand to gravel when grains were captured in narrow conduits within the sediment matrix. Even in cases of frequent fluid and particle intrusions into the bed, if few particles are retained,

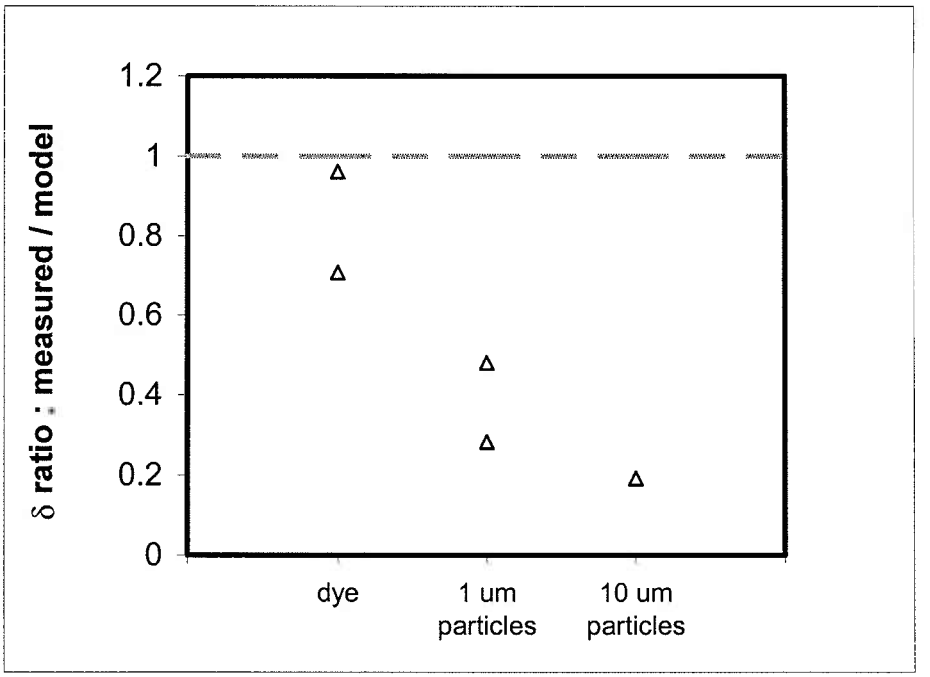

Figure 3.4. Penetration of fluid (dye) and particles into a flat bed compared to diffusion model predictions. Original data reported by Huettel et al. (1996).

then a majority of material transported downwards will also be returned to suspension as the next interfacial flow displaces them. This is a potential explanation for the results obtained by Einstein (1968). The net effect of poor filtration would be to decrease the gradient of concentration across the sediment water interface, negating potential enhancement due to interfacial diffusion.

The governing equation for particle concentration within the bed is based on the loss of particles due to settling and diffusion into the bed and filtration within the sediment,

$$\frac{\partial C(z)}{\partial t} = w_s \frac{\partial C(z)}{\partial z} + \nu_b \frac{\partial^2 C(z)}{\partial z^2} - \lambda_T C(z), \tag{3.20}$$

where λ_T is the decay of concentration due to filtration. The filtration term will be described in detail in the following section (3.3.2). Two boundary conditions are imposed in the concentration model. The first matches the particle concentration at the interface from both the sediment and fluid sides and the second describes the vanishing concentration deep in the bed,

$$C(0) = \overline{C}, \tag{3.21a}$$

$$C \to 0 \text{ as } z \to -\infty. \tag{3.21b}$$

where $\overline{C}$ is the depth averaged concentration. The depositional flux is also defined in terms of the concentration gradient at the interface,

$$\nu_b \left.\frac{\partial C}{\partial z}\right|_{z=0} = (w_d - w_s)\overline{C}. \tag{3.22}$$

The settling of particles within the bed is small compared to the other terms based on the observation of a static profile, in time, for still water conditions (see 2.3.4 and Figure 2.17b). Two additional assumptions can be made to simplify the governing equation for concentration (3.20). First, it is possible that the filtration term is negligible and that the concentration profile simply penetrates the bed diffusively,

$$\frac{\partial C(z)}{\partial t} = \nu_b \frac{\partial^2 C(z)}{\partial z^2} \tag{3.23}$$

Second, the system of fine particle deposition can be treated as quasi-steady, eliminating the time derivative in the governing equation,

$$\nu_b \frac{\partial^2 C(z)}{\partial z^2} = \lambda_T C(z) \tag{3.24}$$

The decision as to which of these expressions to use (3.23 or 3.24) requires some knowledge of the mechanics of filtration.

3.3.2. Bed filtration

Several expressions and parameters for filtration exist, but the general consensus is to state efficiency in terms of an exponential decay in concentration (e.g., Ives, 1967),

$$-\frac{\partial C}{\partial t} = \lambda_T C = \lambda u C . \tag{3.25}$$

where λ is the efficiency in terms of inverse length. The conversion from time to length reflects the use of packed sediment columns for determination of filtration efficiency. Unlike the flow at the sediment water interface, little to no shear in the velocity profile exists in these sediment columns. Based on the extensive past research on particle

filtration in granular columns, McDowell-Boyer et al. (1986) identified three mechanisms: diffusion, interception, and sedimentation. The diffusion of the particles in the subsurface flow should be negligible due to the same scaling arguments presented in Chapter 1 and particle diffusivities (order 10^{-9} cm^2/s) based on Brownian motion (Einstein, 1906). Each of the remaining mechanisms needs to be explored in detail to assess their contribution to fine particle deposition.

Interception of particles within the bed relies on two processes: collisions of particles and grains and the subsequent ability of particles to remain attached,

$$d_g \lambda_I = f_I \left(\frac{e_A}{\rho v d_p^2 u} \right)^{1/8} D_R^{-2}, \tag{3.26}$$

where λ_I is the efficiency of filtration by interception, f_I is a function of porosity,

$$f_I = 0.84 \left(\frac{P^3 - P^8}{1 - 1.5P + 1.5P^5 - P^6} \right), \tag{3.27}$$

$$P = (1 - \phi)^{1/3}, \tag{3.28}$$

e_A is the electrical attraction or affinity between the particles and the bed grains (typically order 10^{-13} erg), ϕ is the bed porosity, and D_R is the grain diameter ratio defined as

$$D_R = \frac{d_{g15}}{d_p}, \tag{3.29}$$

where the subscript 15 indicates that 15 % of the sediment mass is finer than this grain size. The particle-grain affinity requires a significant ionic strength in the fluid to reduce repulsion between grains and particles (e.g., Fitzpatrick and Spielman, 1973). In these cases, this term is of orders 0.1 to 1 for particle-grain interactions. Contrasting results

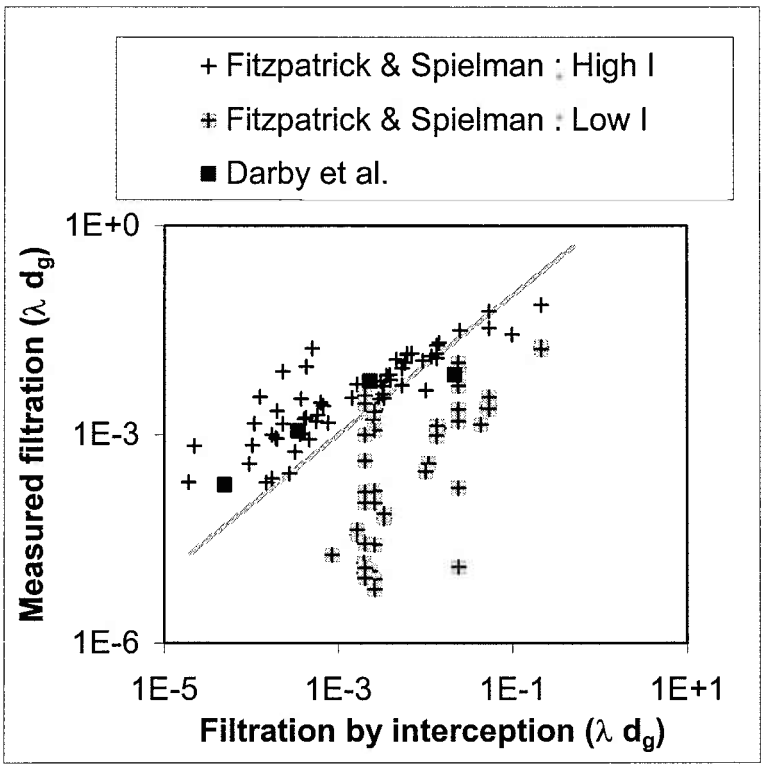

Figure 3.5. Efficiency of filtration via interception. Line represents 1:1 correlation between (3.26) and measured efficiency. The distinction between low I (shaded pluses) and high I (pluses) is based on the threshold in Fitzpatrick and Speilman (1973) for their data. Additional measurements by Darby et al. (1992) for high ionic strength also included.

from experiments with low and high ionic strength (using the criterion proposed by Fitzpatrick and Spielman, 1973) reveals a clear reduction in interception efficiency due to the action of double layer repulsion between grains and particles (Figure 3.5). Seawater has high ionic strength; therefore, the expression is appropriate (3.26).

Another requirement for enhanced deposition is particle penetration of the sediment bed. This is not possible when particles are incapable of fitting into the pores at the interface. A general rule proposed by Sherard et al. (1984) suggests that sediment

beds are virtual sieves with a mesh size of 0.11 d_{g15}. Another way to state this is that the grain diameter ratio must be larger than 9. This study will only address particles small enough to enter the bed (i.e., $D_R > 9$).

Sedimentation can be important for particles with significant density. While the scaling in Chapter 1 demonstrated that fine particles have small inertia in water, as measured by relaxation time, the impact of gravitational settling may be important in the slower flows within the sediment bed. The model expression presented in McDowell-Boyer et al. (1986) reflects competition between settling and the interstitial flow,

$$d_g \lambda_S = f_S \frac{w_s}{u} \sqrt{D_R}\,, \tag{3.30}$$

where λ_S is the efficiency of filtration by sedimentation, f_S is a function of porosity,

$$f_S = 0.0036 \left(\frac{P^3 - P^8}{1 - 1.5P + 1.5P^5 - P^6} \right). \tag{3.31}$$

To ensure that the filtration expressions (3.26 and 3.30) are applicable to the experiments conducted in Chapter 2, the range of grain and particle sizes were compared to those of previous investigations that contributed to the development of the expressions. The grain-particle geometries for all natural sediment treatments from this study are adequately reproduced in previous experiments (lower box in Figure 3.6a). Marble treatments are unique in this respect. In addition to the grain and particle sizes, two dimensionless parameters are also important in describing the efficiency of filtration: w_s/u_* and D_R. All treatments are consistent with previous experiments with respect to these dimensionless parameters (Figure 3.6b). Given the overlap in both sets of

parameters, the results of column experiments should be applicable to the treatments used in this study.

3.3.3. Model expressions for particle deposition

Given the two possible governing equations (3.23 and 3.24), two corresponding solutions for the concentration profile exist. Each of these profiles was solved analytically. Numerical modeling of the complete governing equation (3.20) is presented in the next section of this chapter.

Richardson and Parr (1988) described effusion of fluid with a conservative tracer (i.e., no decay or filtration) from a sediment bed in terms of a well-known solution for time-dependent diffusion (see Hildebrand, 1976). The error function (erf) solution modified to describe diffusion into the sediment is

$$\frac{C(z,t)}{\overline{C}} \cong 1 - erf\left\{\frac{z}{2\sqrt{\nu_b t}}\right\}. \qquad (3.32)$$

This function describes a region of fluid that deepens in time and clearly depends on the diffusivity in the sediment. This profile solution predicts a time-dependent flux into the sediment using (3.22),

$$E_d - 1 \cong \sqrt{\frac{\nu_b}{4\pi t w_S^2}}. \qquad (3.33)$$

This solution is not consistent with the apparently constant deposition velocities over time observed during flume experiments (Chapter 2).

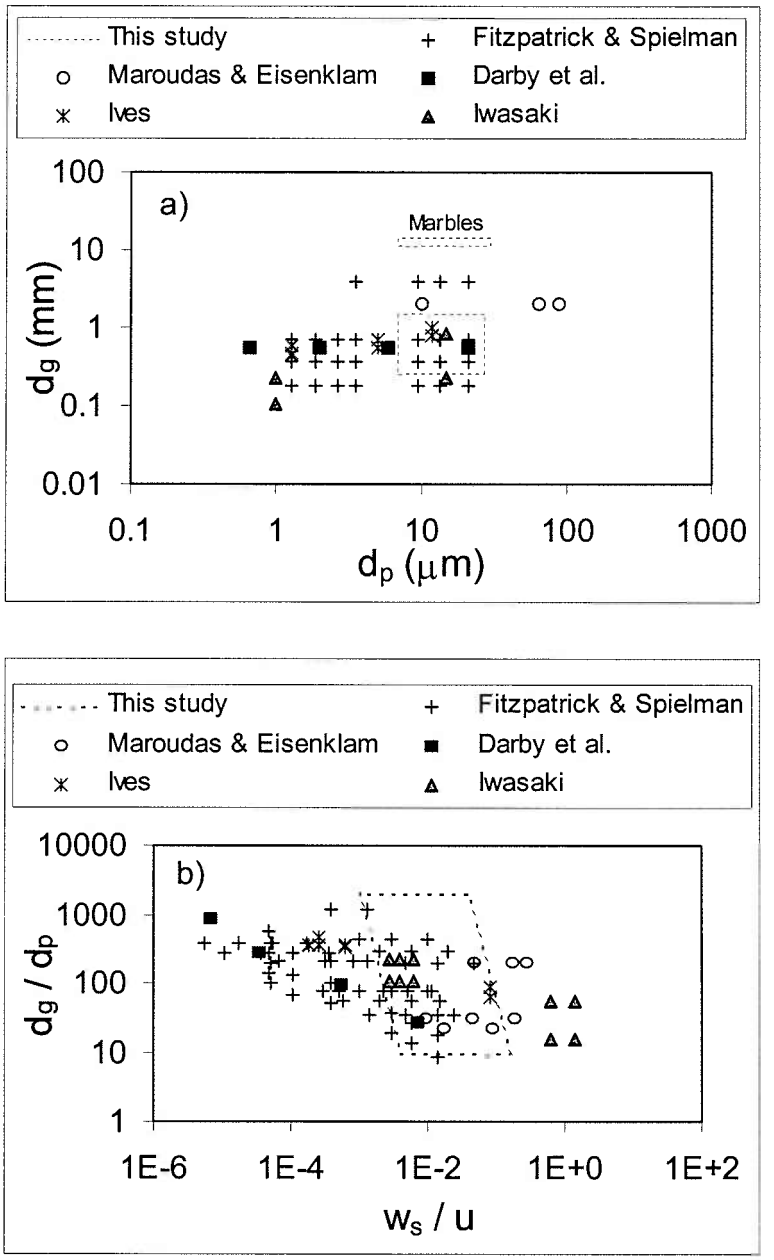

Figure 3.6. Parameter comparison between this study and previous investigations. a) Grain and particle sizes. b) Dimensionless parameters for settling and bed grain ratio. Dashed line boxes represent range of values from this study. Points are plotted for studies conducted by Fitzpatrick and Spielman (1973), Maroudas and Eisenklam (1964), Darby et al. (1992), Ives (1967), and Iwasaki (1937).

The balance between diffusion and filtration described by (3.23) relies on filtration driven by the local velocities. This balance is described by a coupled differential equation for flow and concentration,

$$\nu_b \frac{\partial^2 C(z)}{\partial z^2} = \lambda_T C(z) = \lambda u(z) C(z), \tag{3.34}$$

The solution of this equation is detailed in Appendix B. The concentration profile is

$$\frac{C(z)}{\overline{C}} \cong I_0 \left\{ \sqrt{R_K \lambda \sqrt{10K}} \exp\left(\frac{\sqrt{10}}{2R_K} \frac{z}{\sqrt{K}} \right) \right\}, \tag{3.35}$$

where I_0 is a modified Bessel function of the first kind of order zero (Hildebrand, 1976). The final expression for the deposition enhancement from the definition of flux (3.22) is

$$E_d - 1 = R_K^2 \frac{\lambda \nu}{w_s}. \tag{3.36}$$

3.3.4. Numerical model of particle concentration

A numerical model of the governing equation (3.20) was designed to fully understand the dynamics of the concentration profile within the sediment bed. Methods described by Patankar (1980) were employed. The model domain was initialized without any particles and the boundary conditions (3.21) were applied. Each node in the model domain was subject to diffusion (3.17) and filtration (3.26 and 3.30). The mass of particles at each node was divided into two groups: in the pores and on the grains (filtered). This distinction allows for conclusions regarding the particle fate.

The numerical model predicts the profile shape through time and answered two important questions. First, the time dependence and scales of penetration could be

determined. Second, the appropriate governing equation for the interface and deep in the sediment could be identified. Two cases of flow and concentration in 400-μm sand will be considered as a basis for discussion: deposition without filtration to simulate the diffusive penetration limit (3.23) and a series of filtration efficiencies under the same conditions to explore the role of the quasi-steady limit (3.24).

The numerical experiments without filtration clearly verify the error function profile (3.32) for concentration within the sediment (Figure 3.7a). This result demonstrates the importance of the diffusivity for delivering particles to deeper regions of the sediment bed. The penetration scales from the numerical model runs (Figure 3.7b) increased with fluid forcing and were consistent with the observations of mm-scale penetration (Figure 2.17). Both of these results support the assertion that diffusive processes deliver particles to the sediment bed.

Profiles of particle concentration with filtration are modified by the removal of particles in the thin region of flow near the sediment water interface. The profile is altered from the diffusive shape (3.32) to the Bessel function solution (3.36) within this region (Figure 3.8a). This change affects a very thin layer at the interface, but is important in the definition of flux. Due to the use of the interfacial concentration gradient in the flux definition (3.22), the proper solution to the deposition enhancement is (3.36), even though a majority of the profile is based on diffusive penetration. Confirmation of this was drawn from the numerical results by comparing the filtration efficiency used as model input to the efficiency calculated from the flux estimate based on the concentration gradient (3.22). This comparison shows a correlation between the

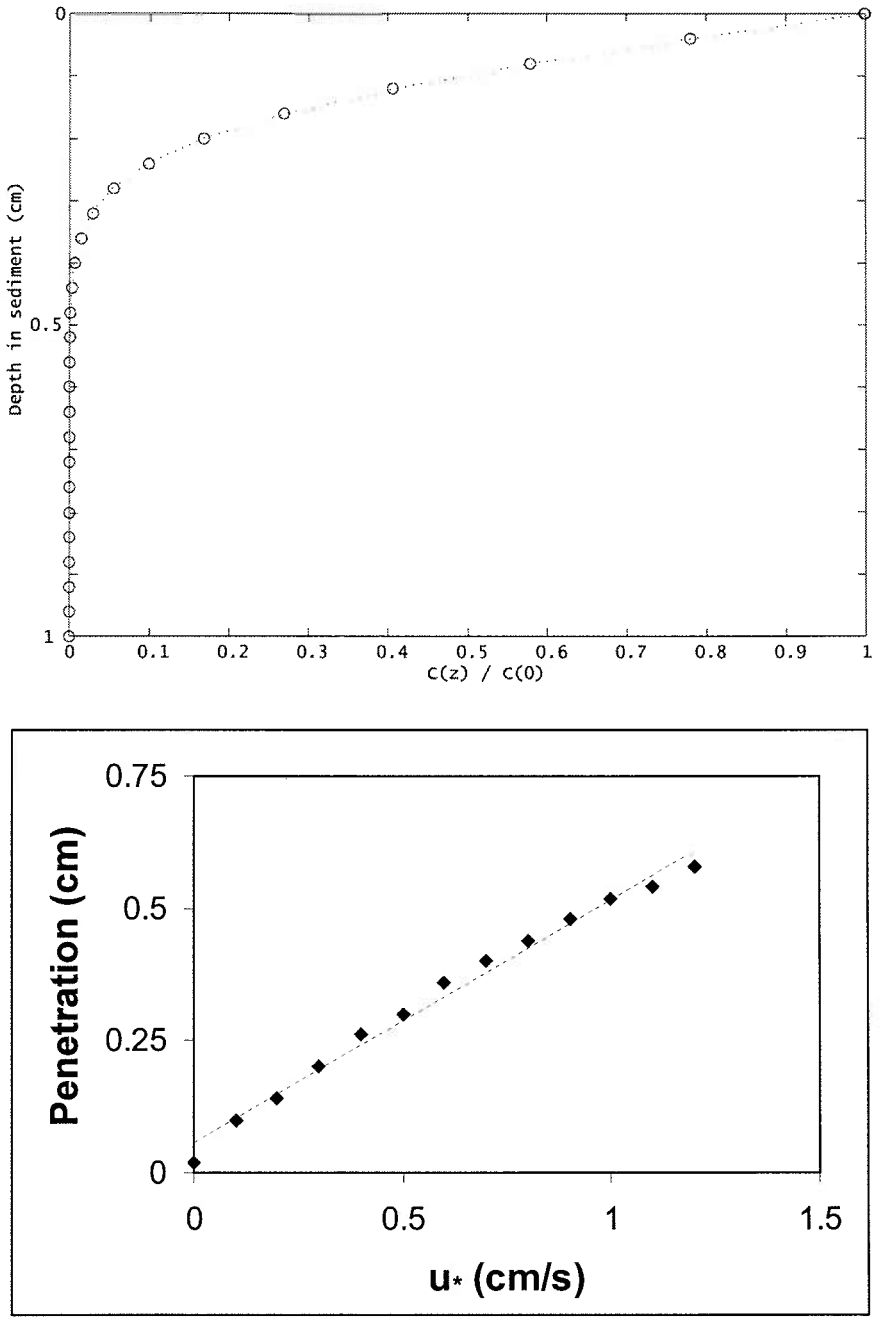

Figure 3.7. Numerical model results for no filtration (3.23). a) Comparison of model profile and analytical solution (3.32). b) Penetration as a function of shear velocity. The dashed curve represents a linear regression of the data ($r^2 = 0.99$).

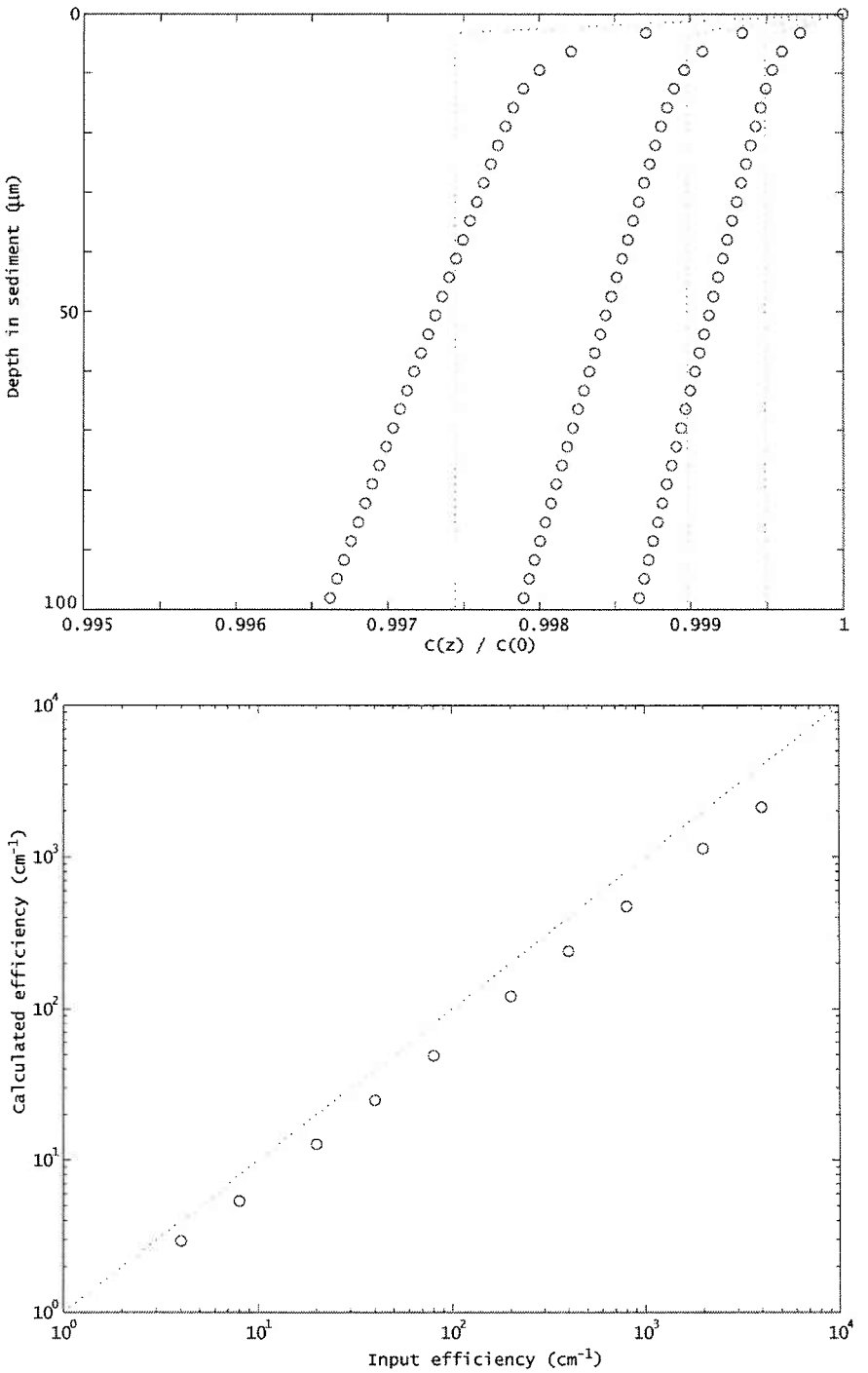

Figure 3.8. Numerical model results with filtration (3.24). a) Comparison of model profile and analytical solution (3.35) for three efficiencies. b) Comparison of efficiencies from interfacial gradient to those used as input. The dashed curve represents a 1:1 line.

values with a small offset for smaller calculated values (Figure 3.8b). This reduction in efficiency is due to the reduction in gradient due to the small, but visibly evident (Figure 3.8a), role of the time derivative in smoothing the profile relative to the Bessel function.

Results from the numerical model contribute to a general understanding of the penetration and fate of deposited particles. The shape of the profile is defined by diffusive penetration of fluid into the sediment. At the interface, filtration balances the delivery, altering the concentration profile. The flux is defined in terms of this filtration (3.36). In the following assessment of the model performance, the filtration efficiency of the bed is treated as the unknown quantity as a function of the measured flux,

$$\lambda = \frac{w_s}{\nu}(E_d - 1)R_K^{-2} \tag{3.37}$$

3.4. Application of model form to oxygen data

The model for fine particle deposition may be applicable to the transport of other constituents, such as oxygen. Many observations of diffusive boundary layers for oxygen extending across the sediment water interface are reported in the literature (e.g., Jorgensen and Revsbech, 1985; Booij et al., 1994). These observations have led to the conclusion that diffusive processes typically control the transport of oxygen into sediment. Therefore, when flux measurements exceed predictions based on diffusion, explanations including irrigation by animals or errors introduced by instrumentation (e.g., Booij et al., 1991) are proposed. It remains possible that an alternate hypothesis could explain these discrepancies.

An appropriate model for solute distribution within the sediment bed could be described by the same governing equation as particles by substituting consumption rate (Θ) for the filtration decay. Another variable change is the use of a piston velocity (k) instead of the deposition velocity. These values are defined in the same fashion and provide consistency with earlier work on oxygen transport. The solution for piston velocity resembles that for particles if filtration were independent of concentration,

$$k = \sqrt{\Theta \nu_b} \,. \tag{3.38}$$

Using the diffusivity expression (3.17) for ν_b, then the flux becomes

$$\frac{k}{u_*} = \sqrt{\frac{\Theta K}{10\nu}} \,. \tag{3.39}$$

Four published studies of sedimentary oxygen flux have been selected to test the idea of dispersion-forced enhancement of the flux. These studies were selected because the investigators report the appropriate quantities (u_*, k and K). The studies cover a breadth of techniques and sediment types, including in-situ benthic chambers (Booij et al., 1991; Booij et al., 1994) and flume experiments with cores (Guss, 1998) or manipulated sediment beds (Hondzo, 1998). All of these studies demonstrate an approximately linear dependence of k on u_*. Table 3.1 summarizes the calculated consumption rates from these fits. Comparison of sand (Booij et al., 1991) and mud (Booij et al., 1994) reveal an expected increase for the finer, potentially richer in organics, sediment. Natural river sediments, chosen to have high oxygen demand by Hondzo (1998), consumed at a greater rate than artificial sediments. The seasonal cores tested by Guss (1998) demonstrated a predictable variation in consumption from late

spring (low) to summer (high) to late fall (low). These data provide strong evidence for a general theory regarding the enhancement of flux due to flows across the sediment water interface.

3.5. Summary of chapter

A new model is presented to predict the enhancement of fine particle deposition to sediment beds. The notable improvement of this model over those previously published (e.g., Dade et al., 1991) is the inclusion of interfacial flows and the controls of permeability and filtration on the deposition rate.

Table 3.1. Models for relevant velocity scale in diffusivity estimate.

Source	Method	Treatment	$\frac{\sqrt{K}}{d_g}$	$\frac{k}{u_*}$ x 10^4	Θ (s^{-1})
Booij et al., 1991	In-situ chamber	Sand	0.07	8.0 ± 1.5	0.036
Booij et al., 1994	In-situ chamber	Mud	0.22	4.2 ± 1.0	0.060
Hondzo, 1998	Flume	Artificial	0.09	8.0 ± 0.4	0.006
		River	0.05	8.7 ± 1.6	0.062
Guss, 1998	Flume-cores	Late spring	0.05*	2.1 ± 1.7	0.001
	(all sand)	Summer	0.05*	16 ± 3.9	0.075
		Fall	0.05*	6.5 ± 1.5	0.013
		Late fall	0.05*	2.5 ± 0.5	0.002

* - estimated from porosity

Measurements made by Richardson and Parr (1988) are the basis of the flow component of the model. This formulation imposes a constant viscosity in the sediment bed. Fluid penetration data collected by Huettel et al. (1996) agree well with the selected flow model, but coincident particle penetrations suggest that filtration limits the depth.

Numerical modeling of the governing equations for particle concentration led to some insights into the dynamics of the profile within the sediment bed. It is apparent that two regions exist. Deep in the bed, filtration is negligible and the diffusive penetration of particles increases the concentration in the pores. This penetration is consistent with flume observations. At the interface, filtration balances delivery, altering the profile shape. Although this layer is thin, it defines the flux and, subsequently, the required filtration efficiency.

An intriguing aspect of this modeling effort was the recognition that the intrusion of fluid into the sediment may affect the flow profile above the sediment due to slip. This effect may be measurable for certain bed and flow treatments, in particular for smooth turbulent flows. This would provide an independent test of the flow model without relying of particles as a fluid tracer.

The model was applied to available data on oxygen transport to permeable sediments (Booij et al., 1991; Booij et al., 1994; Guss, 1998; Hondzo, 1998). These data sets conform well to a model with constant consumption in the bed. Resultant consumption rates qualitatively follow trends that are predictable from treatment descriptions. The next step is to apply this model to deposition data to assess the interactions of particle delivery and filtration.

4. Comparison of experimental measurements with fine particle deposition model

4.1. Introduction

Understanding of flow across the sediment water interface is an important part of predicting many other interfacial transport processes. These flows have been implicated in driving the enhancement of fine particle deposition within a proposed model (Chapter 3). Critical to assessing the performance of this model is the comparison with data from deposition experiments (Chapter 2) and flow measurements (this Chapter).

Dade et al. (1991) present a model to predict the enhancement of fine particle deposition due to bed roughness. This model describes the controls on particle delivery and identifies modes for capture, but this model fails to predict the relatively large enhancements measured in recent flume experiments (see Chapter 2). The model presented in Chapter 3 considers the sedimentary controls on deposition (i.e. permeability). This model predicts significant enhancement of fine particle deposition to flat permeable bed.

Previous efforts to uncover the mechanisms of fluid transport into permeable beds have focused on the role of topography (e.g., Packman and Brooks, 1995; Huettel et al., 1996), biological activity (e.g., Huettel and Gust, 1992; Martin and Banta, 1992), and experimental artifacts (e.g., Khalili et al., 1997; Basu, 1999). This chapter targets the simple scenario of a turbulent, open channel flow over a flat sediment bed (Figure 4.1). In this case, the potential for fluid and, subsequently, particle transport into the bed exists.

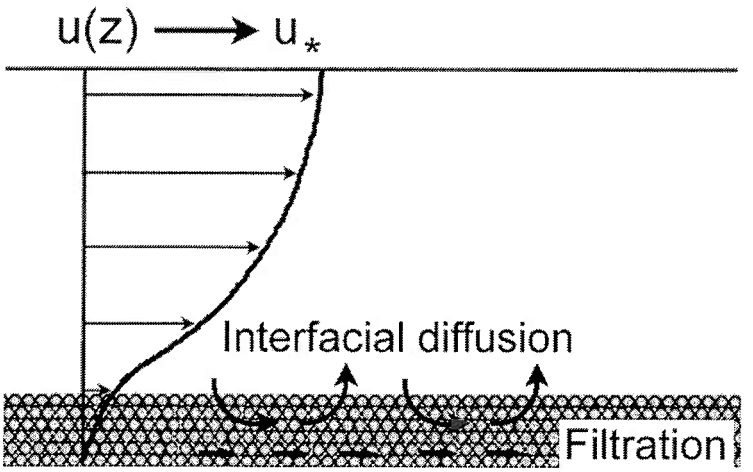

Figure 4.1. Schematic of the fine particle deposition system targeted in this study. All variables are described in the text.

Flow across the sediment water interface is difficult to detect directly without altering the flow itself. Most flow measurement devices rely on homogeneous media, not the case for fluid-sediment mixtures. Investigators that have had success with these types of measurements have focused on high permeability cases (Ruff and Gelhar, 1972; Nagoka and Ohgaki, 1990) or depended on tracers to indicate fluid velocities and pathways (Thibodeaux and Boyle, 1987; Huettel and Rusch, 2000). For flat sand beds, the exchange mechanisms have not been directly observed to date.

A method to detect the fluid exchange between a boundary layer and the sediment bed is critical comparison of fluid velocity profiles near the interface. The shape of the boundary layer profile is indicative of the bottom drag exerted on the fluid. Beavers and Joseph (1967) observed reduction of drag attributable to slip at the boundary. The drag reduction is similar to the case of a solid boundary that is allowed to move with the fluid. This boundary would exhibit less drag than one that is fixed. Richardson and Parr (1991)

qualitatively describe the competition between drag reduction via slip and drag increases from form drag in the bed.

Another option for altering the flow profile to accommodate changes in the roughness length is to add a vertical shift in the elevation coordinate. This method is typically applied to correct for experimental errors in instrument placement or to assess the effect of roughness on the flow profile (e.g., Jackson, 1981). Zagni and Smith (1976) considered the effect of permeability on the displacement over large bed grains, therefore, the resultant displacement was due to bed roughness (i.e., form drag), not permeability.

Critical to describing the flow within the bed is the selection of an appropriate boundary condition. Previous attempts have included matching velocity, viscosity, shear stress, pressure, or a combination of these (e.g., Ochoa-Tapia and Whitaker, 1995). The primary difficulty with all of these techniques is the understanding of the appropriate scales for some of the environmental parameters. For example, the sediment is characterized by the grain size and permeability from bulk samples. These properties could be drastically different on the small scales where the significant flows exist, especially near the sediment water interface (e.g., Schalchi, 1992). Given these difficulties, the detection of fluid exchange between the flow and sediment via flow measurements seems as appropriate as estimating flows through complicated model formulations with the necessary assumptions.

The goal of this chapter is to document the detection of changes in the velocity profile due to the presence of a permeable bed, with a focus on the implications to the deposition of fine particles. The description of this research is divided into four sections.

First, the flow profile model selected to fit experimental data is introduced. Second, the flume facilities are described. Third, the experimental data are condensed into the relevant parameters for comparing solid and permeable boundaries. Fourth, the results are applied to other transport systems, including fine particle deposition. By constraining the changes in interfacial fluid flux via profile measurements, this study provides a framework for inferring the effects of this transport without directly measuring them.

4.2. Summary of fluid flow and particle deposition model

Experimental flow data were fit to an expression for open channel, turbulent boundary layers, necessitating collection of several points in elevation (z). The profile expression for a smooth turbulent boundary layer over a permeable boundary can be expressed as

$$u(z) = \frac{u_*}{\kappa}\ln(z_+) + 5.5u_* + W(z) + u_s, \tag{4.1}$$

$$\text{where } z_+ = \frac{u_* z}{\nu}. \tag{4.2}$$

where u_* is the shear velocity, κ is the von Karman constant, ν is the fluid viscosity, u_s is the slip velocity, W is the profile due to the wake layer,

$$W(z) = \frac{2\Pi}{\kappa}u_* \sin^2\left(\frac{\pi z}{2h}\right), \tag{4.3}$$

Π is a fit parameter that ranges from 0 to 0.4 (Coles, 1956), and h is the channel depth. Note that smooth boundaries are those that fit the following criterion:

$$R_* = \frac{u_* d_g}{\nu} < 10 \tag{4.4}$$

where d_g is the grain size of the bed, R_* is called the roughness Reynolds number. Integration of this profile leads to a general expression for the drag coefficient,

$$C_D = \kappa^2 \left[\ln(R_h) + (5.5\kappa + \Pi - 1) + \kappa \frac{u_s}{u_*} \right]^{-2}. \tag{4.5}$$

where R_h is the channel Reynolds number defined as

$$R_h = \frac{Uh}{\nu}. \tag{4.6}$$

and U is the depth averaged velocity. The drag expression (4.5) demonstrates that the addition of slip to the profile reduces the drag coefficient.

The conversion of slip to a displacement depends on measurements taken within the viscous sublayer. The displacement from the profile,

$$u(z_+) = u_* (z_+ + \Delta_+) = u_* z_+ + u_* \Delta_+, \tag{4.7}$$

$$\text{where } \Delta_+ = \frac{u_* \Delta}{\nu}, \tag{4.8}$$

is directly analogous to the slip velocity,

$$\frac{u_s}{u_*} = \Delta_+ \tag{4.9}$$

The displacement from the log layer profile is expected to reflect the roughness size and geometry (Jackson, 1981). A possible link between this displacement and slip is the apparent reduction of the equivalent roughness (k_s) for fully rough beds where the profile is

$$u(z) = \frac{u_*}{\kappa} \ln\left(\frac{z+\Delta}{k_s}\right) + 8.5u_* + W(z) + u_s . \tag{4.10}$$

By definition, k_s is the same as d_g in this expression. If the slip is neglected and this assumption relaxed, then the slip and change in roughness are related,

$$\frac{k_s}{d_g} = \exp\left(-\kappa \frac{u_s}{u_*}\right). \tag{4.11}$$

The roughness from a profile neglecting slip would appear to be less rough than the sediment grain size.

Typically, a model for flow within the sediment bed assigns an eddy viscosity of the fluid within the sediment (ν_b) that drives the flow (e.g., Ruff and Gelhar, 1972; Nagoka and Ohgaki, 1990). An experimental relationship for interfacial diffusion was developed in Chapter 3 based on data collected by Richardson and Parr (1988),

$$\frac{\nu_b}{\nu} \cong \frac{R_K^2}{10}, \tag{4.12}$$

$$\text{where } R_K = \frac{u_* \sqrt{K}}{\nu} \tag{4.13}$$

and K is the bed permeability. Relating the slip velocity,

$$\frac{u_s}{u_*} = R_K \sqrt{\frac{\nu}{\nu_b}} \cong \sqrt{10} \tag{4.14}$$

to the displacement provides a means for testing the flow model which drives the enhancement of fine particle deposition,

$$\frac{\Delta}{d_g} = \frac{u_s}{u_* R_*} \cong \frac{\sqrt{10}}{R_*}. \tag{4.15}$$

The deposition expressions based on this flow model is described in detail in Chapter 3. The basic framework is the balance of delivery driven by interfacial diffusion (ν_b) and the retention of particles via filtration. The final expression for the enhancement of deposition is

$$E_d - 1 = R_K^2 \frac{\lambda \nu}{w_s}, \tag{4.16}$$

$$\text{where } E_d = \frac{w_d}{w_s}, \tag{4.17}$$

λ is the filtration efficiency in the bed, w_d is the deposition velocity, and w_s is the particle settling velocity.

4.3. Research facilities

Observations were made in the flume facilities located in the Reinhart Coastal Research Laboratory at the Woods Hole Oceanographic Institution. Particle deposition experiments are described in Chapter 2. Flow data from a majority of these experiments have also been analyzed using the methods described herein. Additional flow profile experiments were conducted in the "Racetrack Flume" — a recirculating, seawater (Figure 4.2). Flow is driven by a linear paddle-drive designed to maintain vertical paddle orientation while in the flow. The test section is positioned on the opposite side (7.5 m long, 75 cm wide, 30 cm deep). Water depth was in the range of 12 to 15 cm for these experiments. All flume experiments used 10-μm filtered seawater or freshwater seeded with fine (<10 μm) glass beads (supplied by MoSci Corporation, Rolla, MO). These

particles had a fall velocity of 0.01 cm/s, significantly smaller than the flow velocities measured. The flume was built with a PVC bottom that was used as the control (smooth) boundary for comparison with sediment beds. The turns include vanes with a spacing to evenly split the total volume flow through the channel.

Sediment beds were installed over the flume bottom to a depth of 4 cm. Upstream of the sediment, ramp panels were installed to bring the flume bottom level with the sediment surface. Two types of natural sediments (350-μm sand and 1.3-mm gravel) were used in this study. To test very rough flow conditions, artificial sediment (1.23-cm marbles) was also used. Permeability values were determined using falling or constant head permeability tests (Al-Khafaji and Andersland, 1992). Bottom topography was manually eliminated and flat bed conditions were verified by visual inspection from above and through sidewall windows. A complete list of treatments used to evaluate the flow at the sediment water interface is included in Table 4.1.

Velocity measurements were made with a Laser Doppler Velocimeter (LDV) (Agrawal and Belting, 1988) approximately 1 m upstream of the end of the test section. Profiles of flow were taken in two fashions: 'LOG' profiles of both horizontal and vertical components for a majority of the water column (from 10 to 1.5 cm above bottom) and 'VSL' profiles of the horizontal component with measurements very close to the boundary (from 10 cm to 2 mm above bottom). The profile measurements were fit to a

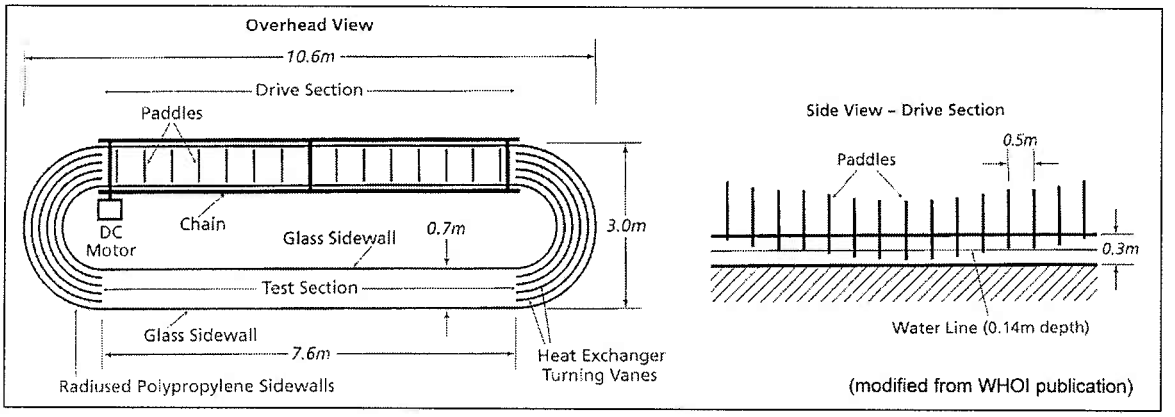

Figure 4.2. Layout of Racetrack Flume. Sediment bed was installed in test section. Sampling location for LDV near end of test section (6.2 m from upstream turn).

Table 4.1. Summary of treatments for flow study.

Bed	# runs	u_* (cm/s)	h (cm)	d_g	K (cm^2)
PVC	17	0.10 to 0.92	13.2 to 13.5	---	---
Sand	15	0.10 to 0.65	12.1 to 12.6	400 μm	2.7×10^{-7}
Gravel	15	0.10 to 0.42	12.3 to 12.8	1.3 mm	2.8×10^{-6}

model developed by Reichardt (1951) that includes the viscous sublayer, log layer, and wake layer with an additional allowance for the displacement of this profile,

$$\frac{u(z)}{u_*} = \frac{1}{\kappa}\ln(1+\kappa(z_+ + \Delta_+)) + 7.8\left(1 - e^{\frac{-(z_+ + \Delta_+)}{11}} - \frac{(z_+ + \Delta_+)}{11} e^{\frac{-(z_+ + \Delta_+)}{3}}\right). \qquad (4.18)$$

The shear velocity may be obtained from other flow statistics. Flow profiles of both the horizontal and vertical (w) flow components were collected and the correlation of the fluctuations was computed. This quantity is called the Reynolds stress and should fit a linear profile in the logarithmic portion of the boundary layer,

$$-\rho\,\overline{u'w'} = \rho u_*^2\left(1 - \frac{z}{h}\right). \qquad (4.19)$$

Similarity between these fit values and those from the mean profile fits (Figure 4.3) supports the use of boundary layer profile fits to estimate bottom shear stress.

Another flow statistic that may reveal an effect of bed permeability is the fluctuation intensity of the velocity, measured as the root mean square (RMS). If the permeability of the sediment allows flows to cross the interface, then the fluctuating flows near the bed should exceed those expected for solid boundaries. Nezu and Rodi (1986) present a model for the RMS of the horizontal velocity for turbulent boundary layers,

$$u_r(z) = 2u_* \exp\left(\frac{-z}{h}\right)\left[1 - \exp\left(\frac{-z_+}{10}\right) + 0.15 z_+ \exp\left(\frac{-R_h}{10}\right)\right]. \qquad (4.20)$$

Deviations from this model profile would also indicate changes in the flow field for permeable beds relative to solid boundaries.

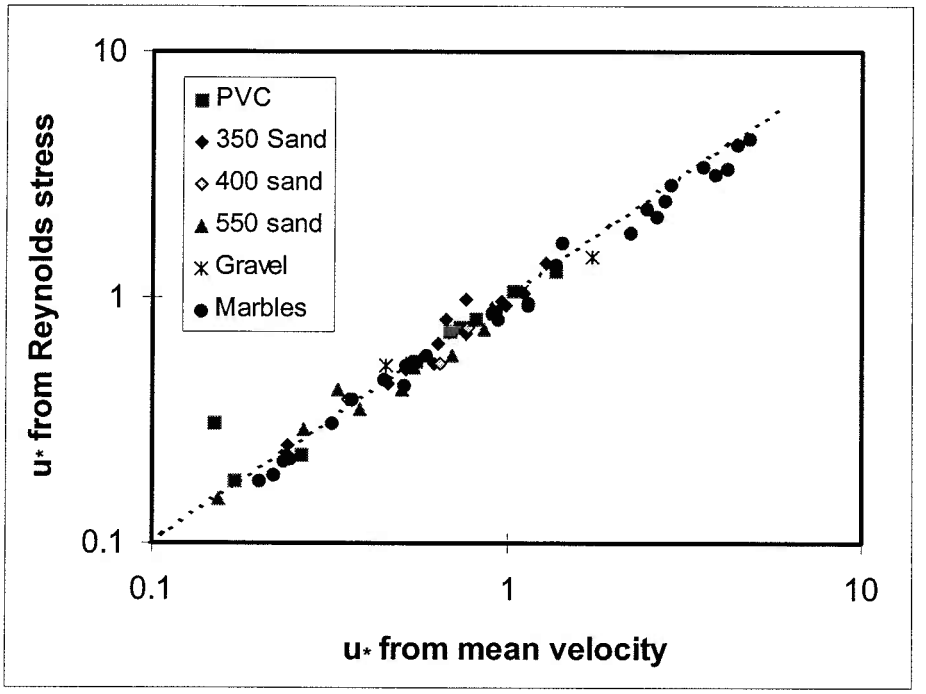

Figure 4.3. Comparison of shear velocity estimates from mean velocity and Reynolds stress profiles for all deposition treatments. Points indicate boundary material: squares = PVC, diamonds = 350- and 400-μm sand, triangles = 550-μm sand, asterisks = 1.3-mm gravel, and circles = 1.2-cm marbles.

4.4. Results

4.4.1. Measurements of displacement

Vertical displacement in the velocity profile (Δ) was measured for flows over both solid (PVC) and permeable beds. The data from experiments with measurements within the viscous sublayer are summarized in Table 4.2. Profiles of velocity over PVC show excellent agreement with the empirical model (4.18) well into the viscous sublayer (Figure 4.4). The PVC results indicate that there is negligible displacement for flow over solid boundaries for the range of flows used in this study (Figure 4.5). The

Figure 4.4. Mean velocities for PVC experiments. Profiles for (a) u* = 0.17 cm/s, (b) u* = 0.55 cm/s, and (c) u* = 0.92 cm/s. Multiple points represent repeated measurements at each elevation.

(a)
u* = 0.17 cm/s
u mean
u model
Elevation (cmab)
Velocity (cm/s)
(b)
u* = 0.55 cm/s
u mean
u model
Elevation (cmab)
Velocity (cm/s)
(c)
u* = 0.92 cm/s
u mean
u model
Elevation (cmab)
Velocity (cm/s)

average displacement for PVC boundaries was 90 ± 100 μm. For reference, the vertical scale of the sample volume for velocity measurement was 800 μm.

For the natural sediment bed experiments, the displacement was often evident as departures from the model in the mean profiles (Figure 4.6). The fit values of displacement were usually larger than the grain size (Figure 4.7). These data seem to indicate that the influence of slip in the boundary on the flow profile is most significant at lower R_*. Data from LOG fits are summarized in Table 4.3. The general trend of displacement suggests a minimum detectable value. A visual fit to the data places this limit at $\Delta_+ = 11$, equivalent to the viscous sublayer thickness.

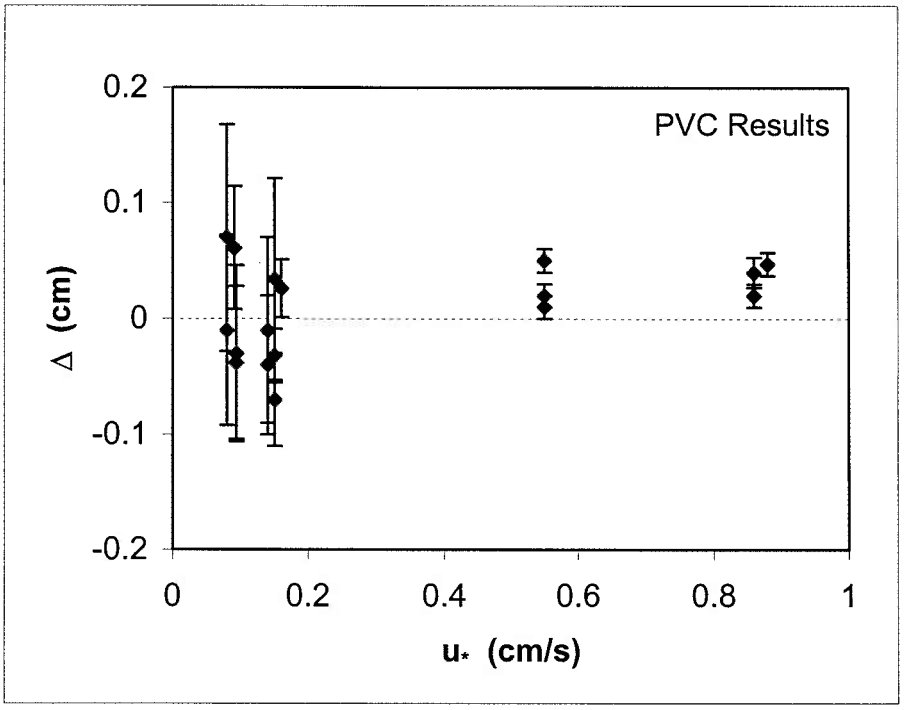

Figure 4.5. Displacements from profiles over PVC. Error bars are ±1 SD.

Table 4.2. Flow experiment data summary.

d_g (μm)	u_* (cm/s)	h (cm)	R_*	R_h	Δ (cm)	C_D
PVC	0.08	13.2	0	106	0.07	0.0044
PVC	0.08	13.2	0	106	-0.01	0.0053
PVC	0.09	13.5	0	123	0.06	0.0037
PVC	0.09	13.5	0	127	-0.04	0.0045
PVC	0.09	13.5	0	127	-0.03	0.0045
PVC	0.14	13.5	0	189	-0.04	0.0034
PVC	0.14	13.5	0	189	-0.01	0.0039
PVC	0.15	13.5	0	202	-0.03	0.0043
PVC	0.15	13.5	0	202	0.03	0.0046
PVC	0.15	13.5	0	202	-0.07	0.0041
PVC	0.16	13.5	0	216	0.03	0.0039
PVC	0.55	13.2	0	726	0.01	0.0024
PVC	0.55	13.2	0	726	0.02	0.0024
PVC	0.55	13.2	0	726	0.05	0.0025
PVC	0.86	13.2	0	1135	0.04	0.0020
PVC	0.86	13.2	0	1135	0.02	0.0020
PVC	0.88	13.2	0	1162	0.05	0.0021
400	0.07	12.3	0.25	86.1	0.22	0.0041
400	0.08	12.3	0.28	98.4	0.13	0.0053
400	0.08	12.3	0.28	98.4	0.11	0.0050
400	0.13	12.4	0.46	161.2	0.06	0.0035
400	0.13	12.4	0.46	161.2	0.19	0.0024
400	0.16	12.4	0.56	198.4	0.20	0.0031
400	0.23	12.4	0.81	285.2	0.08	0.0033
400	0.24	12.3	0.84	295.2	0.09	0.0035
400	0.24	12.3	0.84	295.2	0.26	0.0040
400	0.24	12.3	0.84	295.2	0.34	0.0036
400	0.34	12.6	1.19	428.4	0.22	0.0028
400	0.34	12.6	1.19	428.4	0.31	0.0030
400	0.65	12.1	2.28	786.5	0.19	0.0025
400	0.65	12.1	2.28	786.5	0.32	0.0025
400	0.65	12.1	2.28	786.5	0.33	0.0025
1300	0.11	12.3	1.43	135	0.05	0.0028
1300	0.11	12.3	1.43	135	0.02	0.0035
1300	0.11	12.3	1.43	135	0.06	0.0024
1300	0.12	12.8	1.56	154	0.20	0.0032
1300	0.12	12.8	1.56	154	0.24	0.0028
1300	0.12	12.8	1.56	154	0.12	0.0029
1300	0.14	12.5	1.82	175	0.24	0.0027
1300	0.16	12.5	2.08	200	0.18	0.0035
1300	0.19	12.8	2.47	243	0.04	0.0027
1300	0.22	12.8	2.86	282	0.10	0.0039
1300	0.22	12.8	2.86	282	0.04	0.0036
1300	0.30	12.5	3.90	375	0.18	0.0025
1300	0.30	12.5	3.90	375	0.17	0.0028
1300	0.30	12.5	3.90	375	0.20	0.0027
1300	0.42	12.8	5.46	538	0.15	0.0025

Figure 4.6. Mean velocities for sediment experiments. Sand profiles for (a) u* = 0.23 cm/s, (b) u* = 0.34 cm/s, and (c) u* = 0.65 cm/s. Gravel profiles for (d) u* = 0.16 cm/s, (e) u* = 0.22 cm/s, and (f) u* = 0.33 cm/s. Multiple points represent repeated measurements at each elevation.

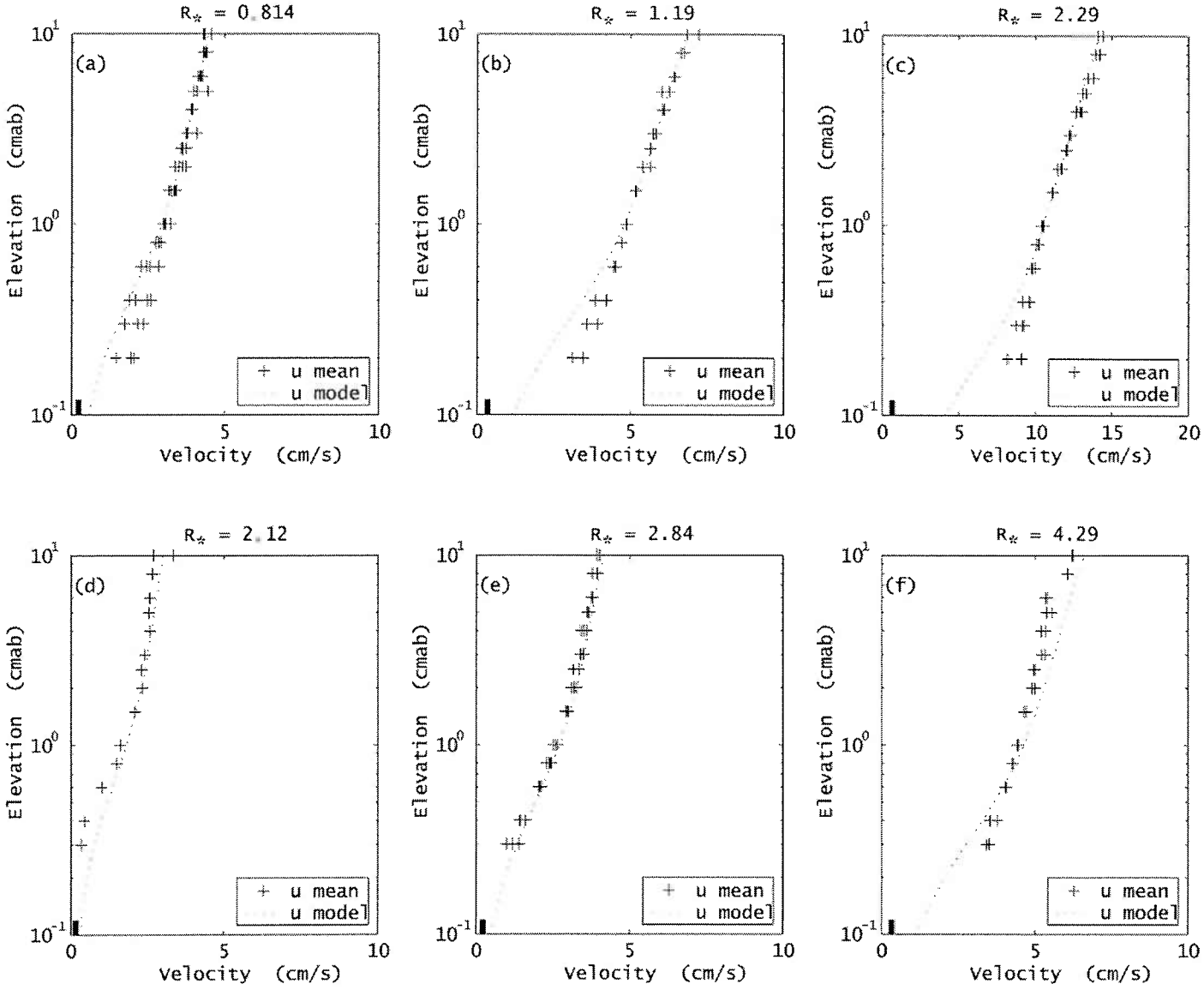
R* = 0.814
(a)
R* = 1.19
(b)
R* = 2.29
(c)
R* = 2.12
(d)
R* = 2.84
(e)
R* = 4.29
(f)
Elevation (cmab)
Velocity (cm/s)
u mean
u model

Table 4.3. Summary of flow data from deposition experiments.

d_g (μm)	u_* (cm/s)	h (cm)	R_*	R_h	Δ (cm)	Δ' (cm)
350	0.34	13.0	1.19	442	0.12	0.53
350	0.50	13.2	1.75	660	0.12	0.48
350	0.53	13.0	1.86	689	0.04	0.23
350	0.60	13.0	2.10	780	0.07	0.30
350	0.86	13.0	3.01	1118	0.14	0.48
350	0.98	13.0	3.43	1274	0.05	0.20
350	1.00	13.0	3.50	1300	0.05	0.22
350	1.11	13.0	3.89	1443	0.06	0.23
350	1.15	13.0	4.03	1495	0.20	0.60
350	1.49	13.0	5.22	1937	0.03	0.14
400	0.34	12.6	1.19	428	0.07	0.36
400	0.50	13.0	1.75	650	0.05	0.27
400	0.69	12.3	2.42	849	0.08	0.32
400	0.80	12.5	2.80	1000	0.01	0.05
550	0.28	12.2	1.54	342	0.05	0.30
550	0.34	12.1	1.87	411	0.03	0.20
550	0.42	12.2	2.31	512	0.03	0.18
550	0.47	12.0	2.59	564	0.18	0.64
550	0.51	11.8	2.81	602	0.08	0.32
550	0.69	12.5	3.80	863	0.03	0.16
550	0.72	12.4	3.96	893	0.07	0.29
550	0.91	12.3	5.01	1119	0.03	0.15
550	0.94	12.1	5.17	1137	0.05	0.20
1300	0.43	12.8	5.6	550	0.02	0.13
1300*	0.56	13.5	7.3	756	0.01	0.06
1300*	0.72	13.5	9.4	972	0.01	0.10
1300	0.82	12.3	10.7	1009	0.06	0.25
1300*	0.85	13.5	11.1	1148	0.01	0.09
1300*	1.01	13.5	13.1	1364	0.03	0.15
1300	1.25	12.6	16.2	1575	0.01	0.07
1300*	1.40	13.5	18.2	1890	0.06	0.23
12300	0.20	12.2	24.6	244	0.08	0.46
12300	0.21	12.1	25.8	254	0.16	0.72
12300	0.34	12.0	41.8	408	0.03	0.21
12300	0.38	12.1	46.7	460	0.23	0.82
12300	0.40	12.1	49.2	484	0.12	0.48
12300	0.58	12.1	71.3	702	0.13	0.48
12300	0.76	12.2	93.5	927	0.09	0.35
12300	0.84	12.1	103	1016	0.06	0.25
12300	1.29	12.2	159	1574	0.14	0.42
12300	1.48	12.0	182	1776	0.17	0.47
12300	2.43	12.0	299	2916	0.05	0.17
12300	2.67	12.0	328	3204	0.05	0.15
12300	3.36	12.1	413	4066	0.16	0.40
12300	4.08	12.0	502	4896	0.20	0.45
12300	4.19	12.0	515	5028	0.23	0.52

* = pilot experiment without particles

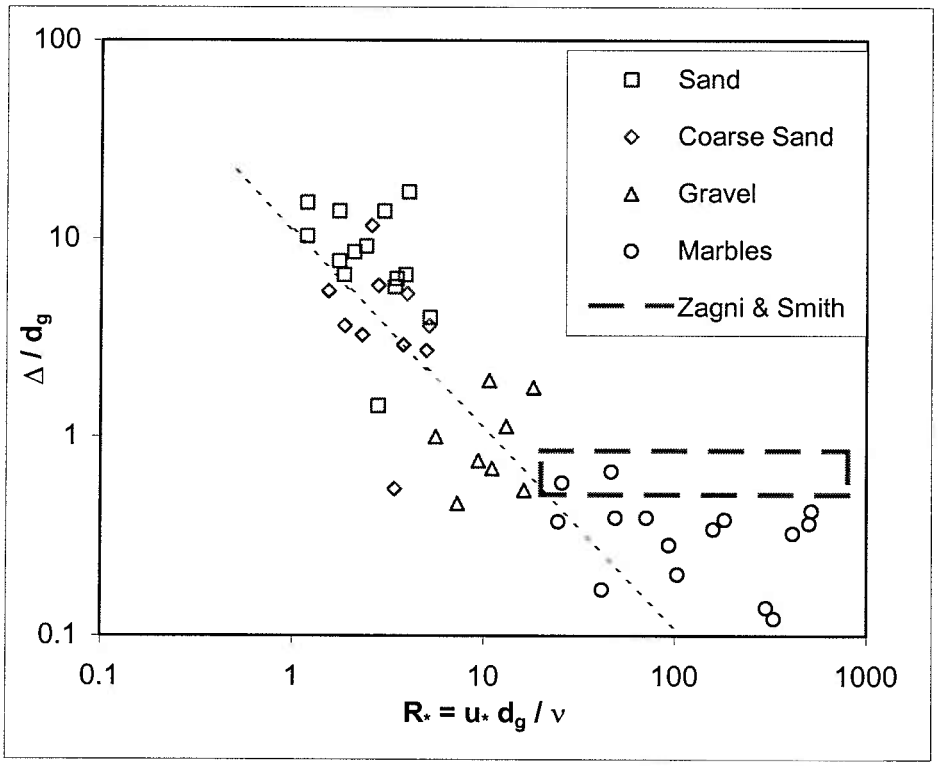

Figure 4.7. Displacements from profiles over sediment. All results are from LOG profile fits. Point shapes represent sediment type: squares = sand; diamonds = coarse sand; triangles = gravel; circles = marbles. Error bars are +-1 SD. Data from Zagni and Smith (1976) fall within rectangular region. Line represents a curve defined by $\Delta_+ = 11$.

The displacements for marble beds exhibited a significant and nearly constant displacement for all flows tested (0.38 ± 0.06 cm). This value of Δ is consistent with the displacement due to roughness geometry ($0.3\ d_g$) predicted by previous investigators (e.g., Jackson, 1981). A relatively constant displacement for rough boundaries is consistent with the measurements by Zagni and Smith (1976) for beds of similar roughness.

4.4.2. Changes in channel resistance

The drag coefficients from all flow experiments are presented in Figure 4.8. The PVC results resemble the predicted curve for smooth turbulent boundary layers with no slip. The permeable bed results all fall on or below the predicted curve, supporting the idea that slip leads to measurable drag reduction. Note that this reduction is solely due to the choice of drag coefficient, based on the mean velocity in the channel. Beavers and

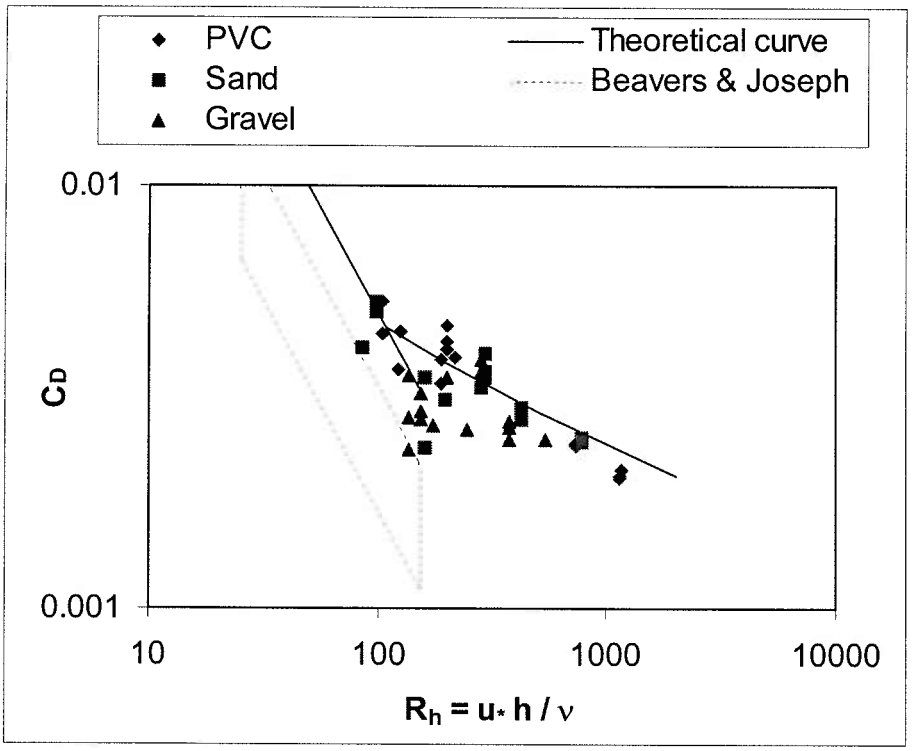

Figure 4.8. Summary of drag coefficient results plotted as a function of the channel Reynolds number. Point shapes represent sediment type: diamonds = PVC; squares = sand; triangles = gravel. Data from Beavers and Joseph fall within rectangular region.

Joseph (1967) also present data supporting drag reduction due to a permeable boundary of similar magnitude. Their work was under laminar flow conditions unlike the turbulent conditions described for this work.

A test of the ability to detect changes in apparent roughness was conducted using marble beds. A small reduction in roughness was detected ($k_s = 0.78 \pm 0.05\ d_g$) that would translate to a slip of $0.65u_*$. It is not certain that this is attributable to slip, because other theories to explain this result include artifacts due to roughness regularity.

4.4.3. RMS velocity results

Profiles of the RMS velocity over solid (PVC) boundaries followed the model (4.20) closely for the range of flows used in this study (Figure 4.9). The same model fits the profiles over sediment beds as well (Figure 4.10). It is remarkable that these profiles fit the model so well given that the value for u_* used in calculating the model profile was obtained from the mean velocity data and profile fits (Figures 4.4 and 4.6).

4.5. Discussion

4.5.1. Diffusion driven by interfacial flows

One of the goals of this study is to apply these flow results to predictions of transport across the sediment water interface. The comparison of measured displacements within the viscous sublayer to previously derived estimates of interfacial diffusivity is critical to this discussion. Measurements of slip were recovered from VSL fits with at least 3 measurements in the viscous sublayer. The observed slip velocities fall

Figure 4.9. RMS velocities for PVC experiments. Profiles for (a) u* = 0.17 cm/s, (b) u* = 0.55 cm/s, and (c) u* = 0.92 cm/s. Multiple points represent repeated measurements at each elevation.

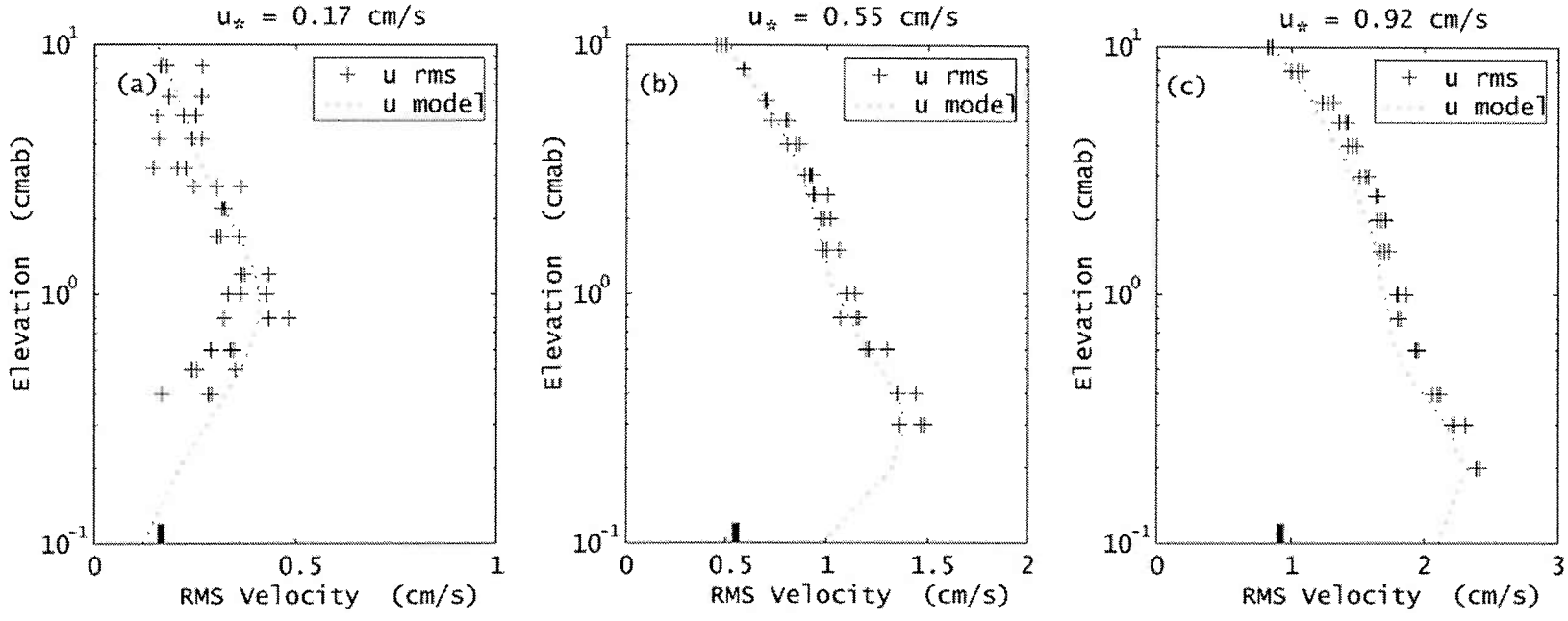
u* = 0.17 cm/s
u* = 0.55 cm/s
u* = 0.92 cm/s
(a)
(b)
(c)
u rms
u model
Elevation (cmab)
RMS Velocity (cm/s)

Figure 4.10. RMS velocities for sediment experiments. Sand profiles for (a) u* = 0.23 cm/s, (b) u* = 0.34 cm/s, and (c) u* = 0.65 cm/s. Gravel profiles for (d) u* = 0.16 cm/s, (e) u* = 0.22 cm/s, and (f) u* = 0.33 cm/s. Multiple points represent repeated measurements at each elevation.

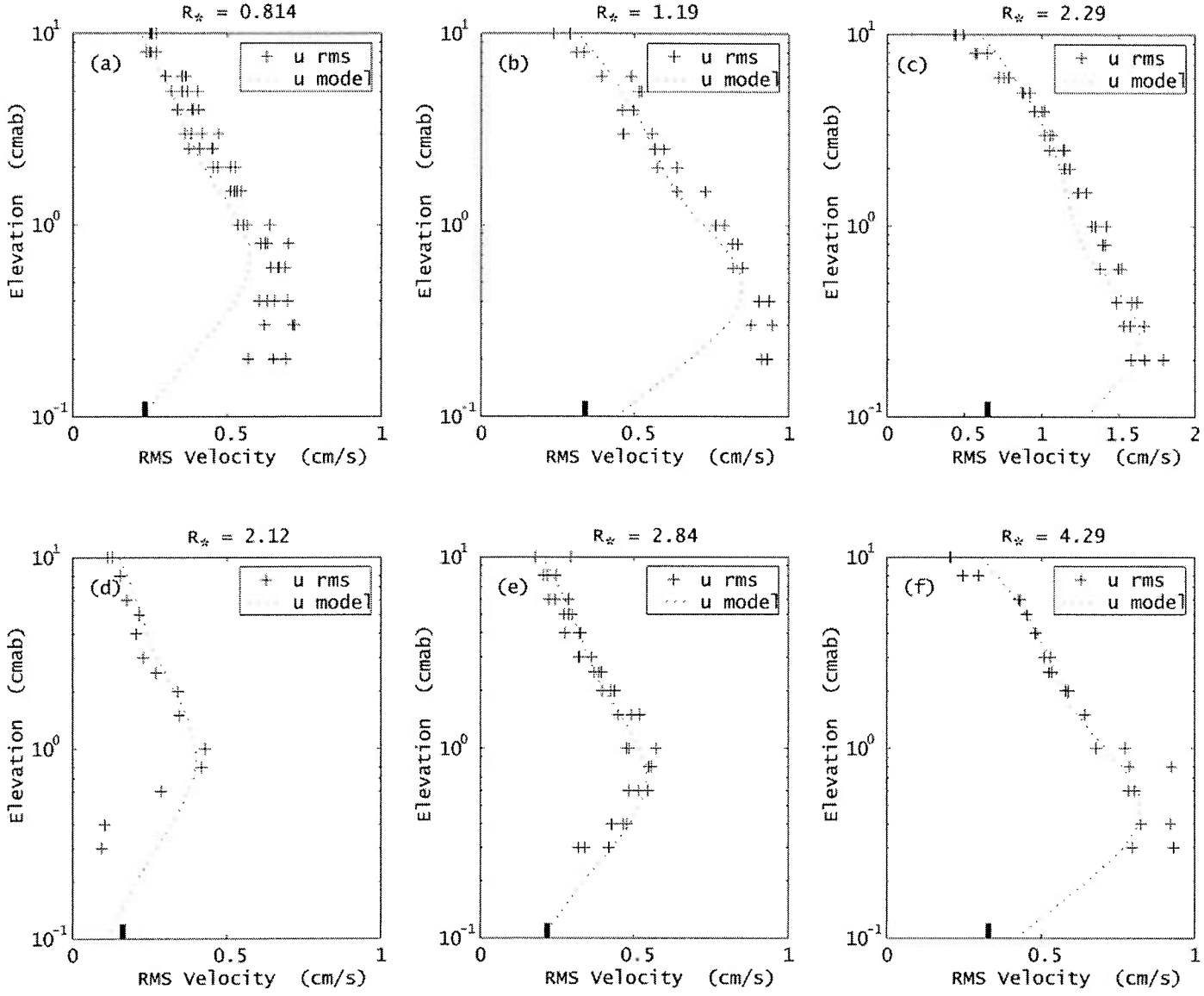
R* = 0.814
(a)
u rms
u model
Elevation (cmab)
RMS Velocity (cm/s)
R* = 1.19
(b)
R* = 2.29
(c)
R* = 2.12
(d)
R* = 2.84
(e)
R* = 4.29
(f)

in between the models using constant diffusivity and dispersion-based expressions (Figure 4.11). The average slip velocities, normalized by the shear velocity, were 3.08 ± 0.97 for sand and 2.26 ± 0.60 for gravel. These values are consistent with the value ($\sqrt{10} = 3.16$) predicted using a constant diffusivity (3.18b), and agree with the average result for slip for marble beds (3.40 ± 0.45) measured directly by Nagoka and Ohgaki (1990). This agreement is surprising considering the large R_K associated with their experiments. On the other hand, the result obtained for foam walls (1.21 ± 0.05) by Ruff and Gelhar (1972) fall well below the predicted constant.

In order to explain this difference, the contrast between sediment beds and blocks of permeable materials needs to be explored. The materials tested by previous investigators are summarized in Table 4.4. For sediment beds, the void scale (B) describes the average pore size. This scale was approximated using a geometric relationship presented by Nagoka and Ohgaki (1990),

$$B = \frac{2\phi^2}{3(1-\phi)} d_g , \tag{4.21}$$

and the ratio varies from 17 to 25% (data from List and Brooks, 1967; Richardson and Parr, 1988; Nagoka and Ohgaki, 1990). The ratio of the void scale to the permeability reveals a clear distinction between material porosities. These values are much larger than those for the high porosity materials (aloxite from Beavers and Joseph, 1967; Ruff and Gelhar, 1972). A lower ratio may be due to more energetic processes driving the fluid into the bed due to a more open structure within the block, suggesting that a process

different than the viscous drag assumed within the flow model would define the slip velocity.

Table 4.4. Contrast of matrix structure between permeable materials and sediment beds.

Source	Boundary	d_g (cm)	B (cm)	K (cm^2)	ϕ	$\sqrt{K}/B$
Beavers & Joseph (1967)	foametal	N/A	0.041	9.7E-05	42.7%	0.242
		N/A	0.086	3.9E-04	47.3%	0.230
		N/A	0.114	8.2E-04	40.0%	0.250
	aloxite	N/A	0.033	6.5E-06	95.7%	0.077
		N/A	0.069	1.6E-05	97.4%	0.058
Ruff & Gelhar (1972)	foam	N/A	0.309	3.8E-04	97.0%	0.06
List & Brooks (1967)	sediment	0.096	0.013	5.8E-06	36.0%	0.19
		0.025	0.005	6.9E-07	41.0%	0.17
		0.007	0.001	4.3E-08	38.0%	0.18
		0.150	0.023	1.7E-05	37.5%	0.18
		0.018	0.001	2.3E-08	20.0%	0.25
		0.048	0.007	1.6E-06	37.0%	0.18
		0.054	0.005	1.0E-06	31.0%	0.20
		0.054	0.005	1.1E-06	32.0%	0.20
		0.093	0.015	7.4E-06	38.7%	0.18
		0.159	0.039	4.1E-05	44.8%	0.17
		0.338	0.055	9.7E-05	38.6%	0.18
		0.167	0.023	1.8E-05	36.0%	0.19
Richardson & Parr (1988)	sediment	0.300	0.047	7.1E-05	38.0%	0.18
		0.103	0.015	7.9E-06	37.4%	0.18
		0.048	0.007	1.6E-06	36.6%	0.19
		0.028	0.004	5.4E-07	36.7%	0.19
		0.011	0.002	1.7E-07	43.4%	0.17
Nagoka & Ohgaki (1990)	marbles	1.9	0.191	1.4E-03	32.0%	0.20
		4.08	0.559	1.1E-02	36.2%	0.19
This study	sediment	0.035	0.002	2.5E-07	27.0%	0.21
		0.040	0.002	2.7E-07	25.5%	0.22
		0.055	0.002	3.0E-07	22.2%	0.24
		0.130	0.008	2.8E-06	25.5%	0.22
	marbles	1.23	0.209	1.40E-03	39.3%	0.18

All shaded values calculated from other values (in this table) from the original studies.

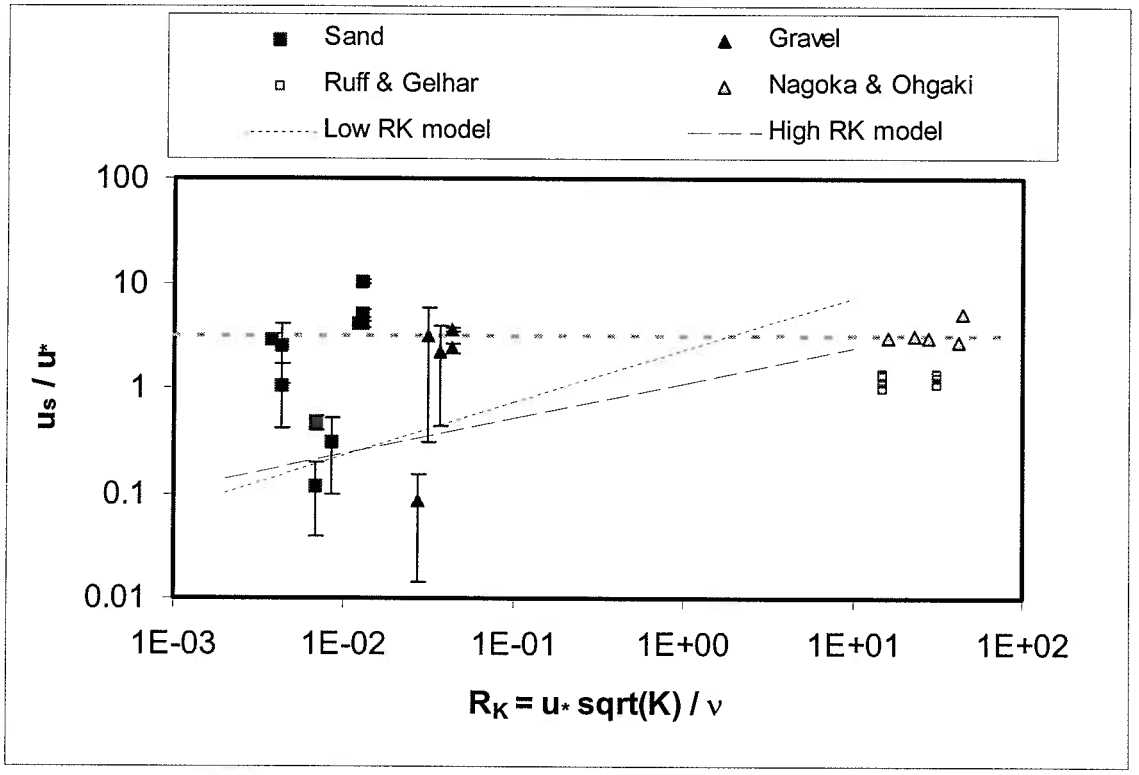

Figure 4.11. Slip velocities from measured displacements and other investigators. Only results from VSL profile fits presented. Point shapes represent sediment type: solid squares = sand and solid triangles = gravel. Open points represent data from other investigators (see discussion in text). Error bars are ± 1 SD. Dashed horizontal line represents constant diffusivity model prediction for slip. Thin dashed curves are predictions from low and high R_K models described in text.

4.5.2. Detection of flow near the interface

The deviation of the mean and RMS velocities from the model profiles in Figures 4.6 and 4.10 is indicative of the relaxation of the no-slip condition at a permeable interface. The change in profiles is noticeable within the viscous sublayer, where the fluctuations begin to decrease towards the boundary, supporting the idea that the viscous sublayer should be present in order to detect the alteration of the flow profile by slip.

This result does not preclude slip for beds under flows with higher R_*, but defines when the slip can be detected via the methods presented herein.

4.5.3. Performance of deposition model

Without specific measurements of the fate of the particles within the bed, there is no definite test of the deposition model, however, there is the opportunity to assess the relative contributions of the two potential capture mechanisms: filtration and accumulation in the pore fluid. The model expression for deposition (4.16) can be rearranged to express filtration efficiency in terms of the measured deposition rate,

$$\lambda = \frac{w_s}{\nu}(E_d - 1)R_K^{-2}. \qquad (4.22)$$

The calculated efficiencies from deposition measurements exceeded the efficiencies based on filtration alone for all treatments in this study (Figure 4.12a). The predicted efficiency includes filtration by both interception (3.26) and sedimentation (3.30). For sand beds, including the data from Huettel et al. (1996), the predicted efficiencies are predominantly due to interception. Sedimentation was the larger contributor to the predicted efficiency for the marble beds and coarse sediments tested by Einstein (1968).

While it is clear that the sediment water interface acts as a very efficient filter relative to columns containing the same sediment, the controlling mechanisms are not evident. On possible control is the geometry of the bed grains and particles represented by the bed grain ratio (D_R). This parameter plays a significant role in the filtration of particles via interception (3.26). Data from this study and Einstein (1968) appear to follow a similar trend with respect to D_R (Figure 4.12b). The vertical scatter in the data

plotted in Figure 4.12b is due to another, flow dependent, parameter that is not resolved in this analysis. The power of D_R in the best fit (-3.4 ± 0.1) is smaller than the power in the interception expression (-2). This difference represents an increased dependence on the bed geometry, possibly due to the difference between packed sediment columns and the sediment water interface.

4.5.4. Potential for future study

This study was successful in applying a frequently used technique (LDV) to indirectly measure quantities that were deemed too difficult to directly observe. However, the potential exists for development of new techniques to tackle the problem of measuring interfacial flux. Visualization should be possible with techniques such as Particle Tracking Velocimetry (PTV) with magnified optics to measures flow fields at the grain scale (see Anderson et al., 2001 for an example of mm-scale PTV). Another avenue would involve the pursuit of sediment-fluid combinations with the same index of refraction (e.g., Nicholai et al., 1995), allowing optical techniques, including LDV, to work across the sediment water interface. This would also provide a means for determining the fate of deposited particles. Unfortunately, these materials were not available within the acceptable ranges of other environmental parameters for this study (e.g., low fluid viscosity). These options should be kept in mind as the greatest potential methods for direct detection of fluid velocities along and across the interface.

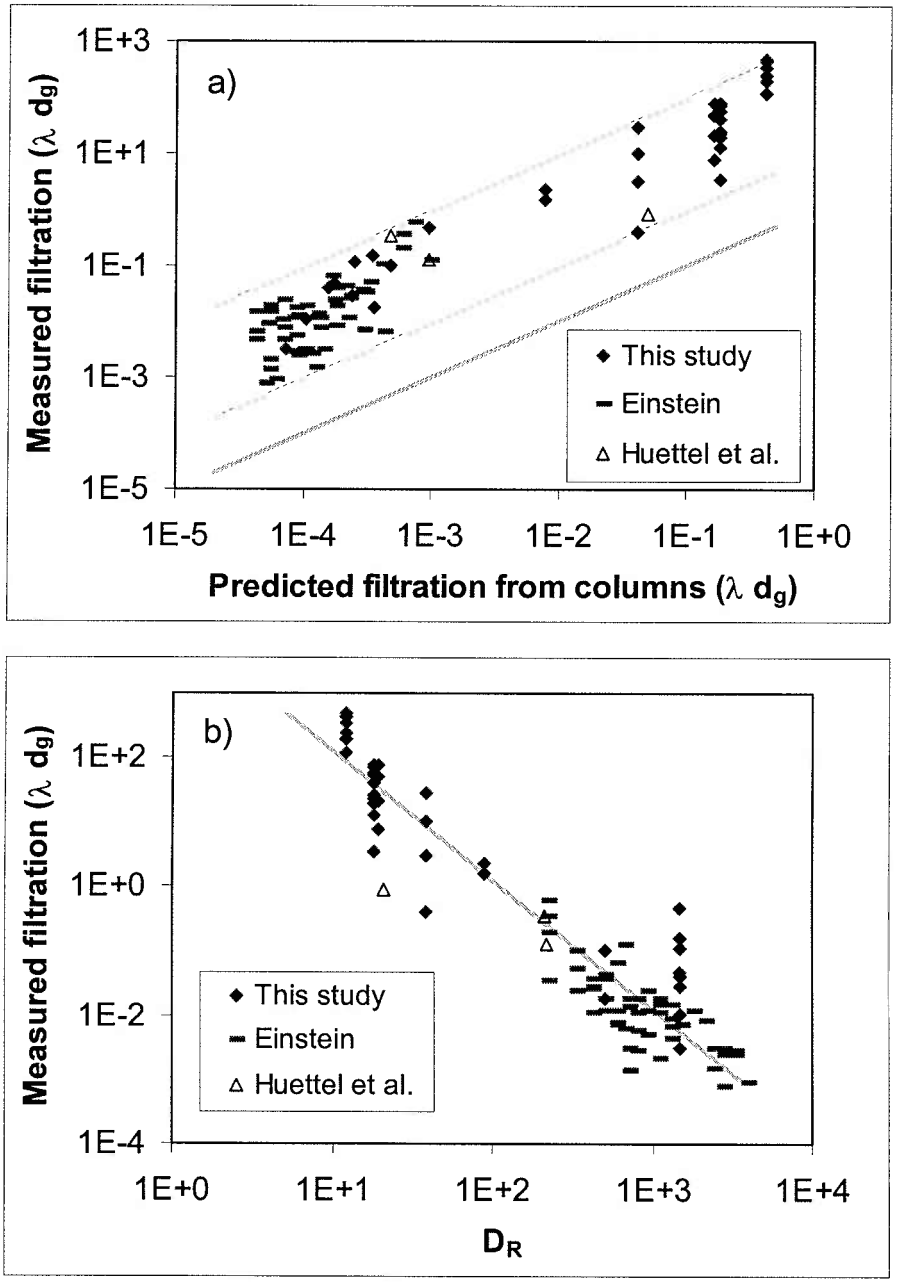

Figure 4.12. Filtration measured in flume experiments. a) Comparison of measurements with the predictions for filtration from sediment columns (3.26 and 3.30). Gray line is 1:1 and dashed curves represent 10:1 and 1000:1. b) Decay relative to bed grain ratio. Gray line represents –2 slope typical of filtration via interception (3.26). Diamonds represent this study, triangles from Huettel et al. (1996) and bars represent data collected by Einstein (1968).

4.6. Conclusion

This chapter directly tested the fluid and particle components of a fine particle model proposed in Chapter 3. In particular, measurements were made of the changes in flow velocities above the sediment water interface to infer the interfacial momentum flux. These observations support the concept of interfacial diffusive fluxes of fluid capable of transporting solutes and fine particles into the sediment. While these results fall short of direct observation, evidence of coupling between the boundary layer and the changes in bed permeability supports the proposed model. Additional support is found in the potential agreement between particle deposition measurements and the model predictions. While the direct comparison revealed a under estimation in the filtration term, the trend in flow was consistent with observations. The model could be modified to provide the necessary increase in filtration in order to match observations. Two options include imposing a constant filtration velocity or considering capture in the very slow flows below the uppermost grains. Therefore, with modification, the proposed model provides predictions for the conditions that enhance fine particle deposition.

5. Summary of observations and model to predict fine particle deposition to permeable sediments

5.1. Introduction

The concept of a no-slip condition at solid boundaries is a central tenet of fluid mechanics. For sediment beds that are permeable, there can be flows both within and into the sediment (i.e., interfacial flows). Many recent studies (e.g., Huettel et al., 1996; Packman et al., 1997) have explored the capability of interfacial flows to alter the deposition of fine particles near bed roughness. By focusing on roughness, the potential for interfacial flows to modulate deposition to flat permeable beds has been neglected. The common assumption that particles simply settle under gravity to flat sediment beds (Einstein, 1968) has also deflected attention away from interfacial flows. Richardson and Parr (1988), however, postulated that the release of solutes from sediment under runoff flows was due to a diffusive flux across the sediment water interface. This diffusion drives an exchange of overlaying and interstitial fluids and could enhance the delivery of particles to the sediment bed.

Interfacial diffusion depends on both the fluid forcing and the characteristics of the sediment bed. In this context, the bed shear stress and the permeability of the sediment bed are used to describe the amount of fluid intrusion and, therefore, the interfacial diffusion. Once particles enter the bed, they are either retained via filtration or subject to resuspension. Therefore, the process of enhanced deposition is composed of two parts: delivery by interfacial diffusion and retention by bed filtration.

Deposition rates to flat sediment beds were measured in order to identify the mechanisms responsible for controlling them. Specific conditions led to enhanced deposition that was not predicted by models that depend on roughness to increase delivery (Dade et al., 1991), therefore, a new model was proposed based on the balance between interfacial diffusion and bed filtration. The model performed well in predicting fluid flow attributes, such as slip at the sediment water interface. This model also reproduced the dependence on flow seen in the deposition data and particle penetration into the sediment. Additional observations using new experimental techniques may verify the mechanisms responsible for enhanced deposition and the fate of the deposited particles.

5.2. Observations of enhanced deposition

The basic assumption in fine particle deposition studies is that the rate of deposition is equivalent to the particle settling velocity (e.g., Einstein, 1968; Self et al., 1989). This assumption leads to the definition of enhancement as the increase in deposition rate relative to settling. Experiments with impermeable beds confirmed that settling is an appropriate baseline for the overall deposition rate. Observations for flat sediment beds revealed conditions where clear enhancement of deposition occurred. The amount of enhancement appeared to be dependent on the flow as well as the bed and particle properties. Experiments also confirmed the lack of enhancement observed by Einstein (1968) for large sediments.

An attempt was made to fit this data to a fine particle deposition model proposed by Dade et al. (1991) that describes the enhancement of deposition due to turbulent processes and the capture of particles by bed roughness. The Dade model predicts changes to delivery due to roughness, neglecting any processes that may depend on the structure of the sediment below the interface and, subsequently, fails to describe the observed deposition rates due to the small roughness scales for flat sediment beds.

Additional information was also collected during deposition experiments. Sediment cores revealed that the deposited particles are primarily in the upper cm of the bed. These results suggest a depth of penetration for interfacial flows. Changes in the median diameter of the suspension indicate the dependence of the principal mechanism of deposition and the particle diameter. Results were inconclusive due to the inability to separate the model options, but the general conclusion is that the process is dependent on particle size to some power between 0 and 2.

Other mechanisms that could be responsible for altering the deposition rate were discussed. The effects of aggregation and topography were dismissed due to careful experimental design and additional flume tests. These tests also revealed a negative trend between enhancement and drag in the channel for some treatments. The opposite (positive) trend was anticipated for deposition driven by topography. Therefore, the observed deposition rates are due to a transport mechanism that also reduces the drag coefficient.

5.3. Model for predicting conditions for enhancement

A new model to predict the enhancement of fine particle deposition was proposed. The idea behind this model is that deposition to permeable beds is composed of two parts: fine particle delivery to and retention in the sediment bed. The processes for each of these parts were extracted from previous research exploring the flow-induced diffusion across the sediment water interface and the filtration of particles in granular beds.

The adoption of interfacial diffusion to describe fluid and particle flux to the bed was inspired by the correlation between drag and deposition observed in flume experiments. The same diffusion responsible for particle delivery also transports flow momentum into the sediment, driving an interstitial flow that is detectable as a slip at the interface. This slip would decrease the drag coefficient in the channel and, therefore, generate a negative correlation between drag and deposition.

The final component of the model is a general theoretical mechanism that corresponds to the empirical diffusion expression. Two model expressions were derived, distinguished by the role of filtration assumed to be occurring. In one case, no filtration occurs and deposition rates depend on the accumulation of particles in the bed (3.32). In the other, the filtration balances delivery and is coupled to the flow profile within the sediment (3.36). Numerical models revealed that a combination of these models is appropriate for different regions of the sediment. The former describes the penetration of particles deep into the bed and the later describes the flux at the interface.

5.4. Evaluation of the model in terms of fluid and particle transport

The proposed model includes predictions regarding the fluid transport into the sediment bed and the filtration of particles by the sediment. These two attributes can be evaluated through comparison with experiments directed at the detection of interfacial flow and the observations of deposition described earlier. By evaluating the model in two parts, the reasons behind success or failure are easier to identify.

Flow experiments to explore the influence of a permeable boundary on the overlaying flow targeted the detection of slip at the interface. Slip, driven by interfacial flows, would reduce the drag in the channel with interfacial flux increase. Measurements within the viscous sublayer provided direct measures of the displacement of the flow profile. This displacement is directly comparable to the slip velocity. These measurements were consistent with previous measurements of diffusion (Richardson and Parr, 1988) and slip (Nagoka and Ohgaki, 1990) for sediment beds. A limitation of this method is the need to make measurements in the viscous sublayer. For rough beds or large shear velocities, the viscous sublayer becomes too thin for measurement or disrupts altogether. The majority of cases where deposition enhancement was observed were in flow regimes where this technique is possible.

The evaluation of the particle filtration component of the model revealed a shortcoming. Model predictions were lower than the observed values, but followed the general trend of the data suggesting an error in the constants within the efficiency expressions. This error may be due to the presence of strong velocity gradients within the sediment. This gradient does not exist in experimental setups used to derive the filtration

expressions where flow is approximately uniform. It is reasonable to think that the particles are falling into slower flows deeper in the bed where filtration is more efficient. The addition of a filtration velocity to the efficiency term brought model and data into agreement. This alteration should be used with caution given the limited relevance of the Darcy velocity in general oceanographic scenarios (large depth).

5.5. Alternative methods for further evaluation

Two limitations existed within this study that should be remedied in future work targeting the interfacial exchange of fluid and particles. First, several measurements within this work were limited by inherently weak signals. Second, the indirect nature of some of the observations leaves room for improvement through the design of direct methods. Both of these shortcomings could be eliminated with alternate methods.

Weak signals for some critical measurements could have been avoided through the use of different methods. For instance, a broader particle size distribution and longer experimental runs might have improved the determination of which median diameter model was the best fit. The downfall of this adjustment would have been the requirement of larger concentrations to assure detectable amounts of particles in water samples over time. Large concentrations may have induced other mechanisms (i.e., aggregation) that were excluded from the study. Another improvement on the work would have been the allowance for higher flows over the sand bed. If the enhancement truly increases with the flow, then large enhancements would occur with high shear velocities. The critical erosion threshold for the sediment limits the observations in this study. By using fixed

beds, this limit would be eliminated; however, fixed matrices may be very different than loose sediment at the grain scale. These differences may be critical to the transport processes that are the target of the work.

Direct observations of these mechanisms would have been preferred. During work on this thesis, the difficulty of making these observations was not overcome. The most promising techniques for making direct measurements of flow or concentration in sediment beds is the application of index of refraction matched sediment and fluid with optical flow measurement (e.g., Nicholai et al., 1995). The benefit of using indirect methods is the relative ease of making the measurements and the applicability of the technique to other investigators. In this study, profiles of velocity above the interface were used to estimate the slip at and interstitial flow below the interface.

5.6. Summary of thesis

This thesis contributes new evidence for the potential control of deposition of fine particles to flat sediment beds by the near bed flows and sedimentary characteristics of the bed. A new model to describe the rate of deposition was proposed based on the recognition of a balance between interfacial diffusion and bed filtration. This model adequately predicts the flow attributes at the interface, providing verification of the description of fluid and momentum transport into the bed; however, the implementation of filtration may be inadequate due to the unique flow characteristics at the sediment water interface. Additional research using emerging techniques to observe flow and particle motion at the grain scale may provide the details required to bring the model and

data into agreement. This thesis documents the importance of permeable sediments, regardless of the bed shape, on the mediation of particle flux from the water column to the bed.

References

Agrawal, Y.C. and Belting, C.J., 1988. Laser velocimetry for benthic sediment transport. Deep-Sea Research, 35(6): 1047-1067.

Ahuja, L.R. and Lehman, O.R., 1983. The extent and nature of rainfall-soil interaction in the release of chemicals of runoff. J. Environ. Qual., 12(1): 34-40.

Al-Khafaji, A.W. and Andersland, O.B., 1992. Geotechnical engineering and soil testing. Saunders College Publishing, Fort Worth.

Anderson, E.J., McGillis, W.R. and Grosenbaugh, M.A., 2001. The boundary layer of swimming fish. J. Exp. Biol., 204(1): 81-102.

Bandyopadhyay, P.R., 1987. Rough-wall turbulent boundary layers in the transition regime. J. Fluid Mech., 180: 231-266.

Basu, A.J., 1999. Computation of flow through a fluid-sediment interface in a benthic chamber. Phys. Fluids, 11(6): 1395-1405.

Bear, J., 1972. Dynamics of fluids in porous media. Dover Publications, New York.

Beavers, G.S. and Joseph, D.D., 1967. Boundary conditions at a naturally permeable wall. J. Fluid Mech., 30(1): 197-207.

Booij, K., Helder, W. and Sundby, B., 1991. Rapid redistribution of oxygen in a sandy sediment induced by changes in the flow velocity of the overlying water. Neth. J. Sea Res., 28(3): 149-165.

Booij, K., Sundby, B. and Helder, W., 1994. Measuring the flux of oxygen to a muddy sediment with a cylindrical microcosm. Neth. J. Sea Res., 32(1): 1-11.

Boudreau, B.P., 1997. Diagenetic models and their implications. Springer-Verlag, Berlin.

Brinkman, H.C., 1947. A calculation of the viscous force exerted by a flowing fluid on a dense swarm of particles. Appl. Sci. Res., A1: 27-34.

Browne, L.W.B., 1974. Deposition of particles on rough surfaces during turbulent gas-flow in a pipe. Atmos. Environment, 8: 801-816.

Butman, C.A., 1987. Larval settlement of soft-sediment invertebrates: the spatial scales of pattern explained by active habitat selection and the emerging role of hydrodynamical processes. Oceanogr. Mar. Biol. Annu. Rev., 25: 113-165.

Butman, C.A. and Chapman, R.J., 1989. The 17-Meter Flume at the Coastal Research Laboratory. Part I: Description and user's manual. WHOI Tech. Rept., 89-10(CRC Tech. Rept. 89-2): 31 pp.

Butman, C. A., 1989. Sediment-trap experiments on the importance of hydrodynamical processes in distributing settling invertebrate larvae in near-bottom waters. J. Exp. Mar. Biol. Ecol. 134: 37-88.

Carling, P.A., 1984. Deposition of fine and coarse sand in an open-work gravel bed. Can. J. Fish. Aquat. Sci., 41: 263-270.

Cleaver, J.W. and Yates, B., 1975. A sub layer model for the deposition of particles from a turbulent flow. Chem. Eng. Sci., 30: 983-992.

Coles, D., 1956. The law of the wake in the turbulent boundary layer. J. Fluid Mech., 1: 191-226.

Dade, W.B., 1993. Near-bed turbulence and hydrodynamic control of diffusional mass transfer at the sea floor. Limnol. Oceanogr., 38(1): 52-69.

Dade, W.B., Nowell, A.R.M. and Jumars, P.A., 1991. Mass arrival mechanisms and clay deposition at the seafloor. In: R.H. Bennett and others (Editors), Microstructure of fine-grained sediments. Springer-Verlag, New York, pp. 161-165.

Darby, J.L., Attanasio, R.E. and Lawler, D.F., 1992. Filtration of heterodisperse suspensions: modeling of particle removal and head loss. Water Research, 26(6): 711-726.

Darcy, H., 1856. Les Fountaines Publiques de la Ville de Dijon. Dalmont, Paris.

Davies, C.N., 1966. Deposition from moving aerosols. In: C.N. Davies (Editor), Aerosol Science. Academic Press, New York, pp. 393-445.

Drake, D.E. and Cacchione, D.A., 1989. Estimates of the suspended sediment reference concentration (Ca) and the resuspension coefficient (go) from near-bottom observations on the California shelf. Cont. Shelf Res., 9(1): 51-64.

Eckelmann, H., 1974. The structure of the viscous sublayer and the adjacent wall region in a turbulent channel flow. J. Fluid Mech., 65(part 3): 439-459.

Einstein, A., 1906, reprinted 1956. On the theory of Brownian movement. In: R. Furth (Editor), Investigations on the theory of Brownian movement. Dover Publications, New York, pp. 19-35.

Einstein, H.A., 1968. Deposition of suspended particles in a gravel bed. J. Hydr. Div., ASCE, 94: 1197-1205.

Einstein, H.A. and Li, H., 1956. The viscous sublayer along a smooth boundary. J. Engrg. Mech. Div., ASCE, 82(2): Paper 945.

Eylers, H., Brooks, N.H. and Morgan, J.J., 1995. Transport of adsorbing metals from

stream water to a stationary sand-bed in a laboratory flume. Mar. Freshwater Res., 46: 209-14.

Fitzpatrick, J.A. and Spielman, L.A., 1973. Filtration of aqueous latex suspensions through beds of glass spheres. J. Colloid Interface Sci., 43(2): 350-369.

Gonzalez, E.A. and Hill, P.S., 1998. A method for estimating the flocculation time of monodispersed sediment suspensions. Deep-Sea Research, 45: 1931-1945.

Grass, A.J., 1971. Structural features of turbulent flow over smooth and rough boundaries. J. Fluid Mech., 50(part 2): 233-255.

Grass, A.J., Stuart, R.J. and Mansour-Tehrani, M., 1991. Vortical structures and coherent motion in turbulent flow over smooth and rough boundaries. Phil. Trans. R. Soc. Lond. A, 336: 35-65.

Gruesbeck, C. and Collins, R.E., 1982. Entrainment and deposition of fine particles in porous media. Soc. Pet. Eng. J., 22(6): 847-856.

Guss, S., 1998. Oxygen uptake at the sediment-water interface simultaneously measured using a flux chamber method and microelectrodes: must a diffusive boundary layer exist? Est. Coast. Shelf Sci., 46: 143-156.

Harleman, D.R.F. and Rumer, R.R., 1963. Longitudinal and lateral dispersion in an isotropic porous medium. J. Fluid Mech., 16: 385-394.

Hedges, J.I., 1992. Global biogeochemical cycles: progress and problems. Mar. Chem., 39: 67-93.

Herzig, J.P., Leclerc, D.M. and Goff, P.L., 1970. Flow of suspensions through porous media - application to deep filtration. Ind. Eng. Chem., 62(5): 8-35.

Hildebrand, F.B., 1976. Advanced calculus for applications. Prentice-Hall, Englewood Cliffs.

Hondzo, M., 1998. Dissolved oxygen transfer at the sediment-water interface in a turbulent flow. Water Resour. Res. 34(12): 3525-3533.

Hoyal, D.C.J.D., Bursik, M.I., Atkinson, J.F. and Depinto, J.V., 1997. Filtration enhances suspended sediment deposition from surface water to granular permeable beds. Water Air Soil Pollut., 99(1-4): 157-171.

Huettel, M. and Gust, G., 1992. Impact of bioroughness on interfacial solute exchange in permeable sediments. Mar. Ecol. Prog. Ser., 89: 253-267.

Huettel, M. and Rusch, A., 2000. Transport and degradation of phytoplankton in permeable sediment. Limnol. Oceanogr., 45(3): 534-549.

Huettel, M., Ziebis, W. and Forster, S., 1996. Flow-induced uptake of particulate matter in permeable sediments. Limnol. Oceanogr., 41(2): 309-322.

Ives, K.J., 1967. Deep filters. Filtr. Separ.(Mar/Apr): 125-135.

Iwasaki, T., 1937. Some notes on sand filtration. J. Am. Water Works Assoc., 29(10): 1591-1602.

Jackson, P.S., 1981. On the displacement height in the logarithmic velocity profile. J. Fluid Mech., 111: 15-25.

Jorgensen, B.B. and des Marais, D.J., 1990. The diffusive boundary layer of sediments: oxygen microgradients over a microbial mat. Limnol. Oceanogr., 35(6): 1343-1355.

Jorgensen, B.B. and Revsbech, N.P., 1985. Diffusive boundary layer and the oxygen uptake of sediments and detritus. Limnol. Oceanogr., 30(1): 111-122.

Keulegan, G.H., 1938. Laws of turbulent flow in open channels. J. Research, National Bureau of Standards, 121.

Khalili, A., Basu, A.J. and Huettel, M., 1997. A non-Darcy model for recirculating flow though a fluid-sediment interface in a cylindrical container. Acta Mech., 123: 75-87.

Kozeny, J., 1927. Uber kapillare Leitung des Wassers im Boden. Sitzungsber. Akad. Wiss. Wein, 136: 271-306.

Larsen, S.E. et al., 1995. Dry deposition of particles to ocean surfaces. Ophelia, 42: 193-204.

Leonard, L.A. and Luther, M.E., 1995. Flow hydrodynamics in tidal marsh canopies. Limnol. Oceanogr., 40(8): 1474-1484.

Lerman, A., 1978. Chemical exchange across sediment-water interface. Ann. Rev. Earth Planet. Sci., 6: 281-303.

Ligrani, P.M. and Moffat, R.J., 1986. Structure of transitionally rough and fully rough turbulent boundary layers. J. Fluid Mech., 162: 69-98.

List, E.J. and Brooks, N.H., 1967. Lateral dispersion in saturated porous media. J. Geophys. Res., 72(10): 2531-2541.

Maroudas, A. and Eisenklam, P., 1964. Clarification of suspensions: a study of particle deposition in granular media. Part I - some observations on particle deposition. Chem. Eng. Sci., 20: 867-873.

Maroudas, A. and Eisenklam, P., 1964. Clarification of suspensions: a study of particle deposition in granular media. Part II - a theory of clarification. Chem. Eng. Sci., 20: 875-888.

Martin, C.S., 1970. Effect of a porous sand bed on incipient sediment motion. Water Resour. Res., 6(4): 1162-1174.

Martin, W.R. and Banta, G.T., 1992. The measurement of sediment irrigation rates: A comparison of the BR- tracer and 222RN/226RA disequilibrium techniques. J. Mar. Res., 50: 125-154.

McCave, I.N. and Swift, S.A., 1976. A physical model for the rate of deposition of fine-grained sediments in the deep sea. Geol. Soc. Am. Bull., 87: 541-546.

McDowell-Boyer, L.M., Hunt, J.R. and Sitar, N., 1986. Particle transport through porous media. Water Resour. Res., 22(13): 1901-1921.

Nagoka, H. and Ohgaki, S., 1990. Mass transfer mechanism in a porous riverbed. Water Research, 24(4): 417-425.

Nezu, I. and Rodi, W., 1986. Open-channel flow measurements with a laser doppler anemometer. J. Hydr. Engrg., ASCE, 112(5): 335-355.

Nicholai, H., Herzhaft, B., Hinch, E.J., Oger, L. and Guazzelli, E., 1995. Particle velocity fluctuations and hydrodynamic self-diffusion of sedimenting non-Brownian spheres. Phys. Fluids, 7(1): 12-23.

Nicholson, K.W., 1988. The dry deposition of small particles: a review of experimental measurements. Atmos. Environment, 22(12): 2653-2666.

Nielsen, P., 1993. Turbulence effects on the settling of suspended particles. J. Sed. Petrol., 63(5): 835-838.

Nikuradse, J., 1933. Stromungsgesetze in rauhen Rohren: VDI Forschungsheft 361, 22 pp.

Nino, Y. and Garcia, M.H., 1996. Experiments on particle-turbulence interactions in the near-wall region of an open channel flow: implications for sediment transport. J. Fluid Mech., 326: 285-319.

Nittrouer, C. A. and Wright, L.D., 1994. Transport of particles across continental shelves. Review of Geophysics 32(1): 85-113.

Ochoa-Tapia, J.A. and Whitaker, S., 1995. Momentum transfer at the boundary between a porous medium and a homogeneous fluid - II. Comparison with experiment. Int. J. Heat Mass Transfer, 38(14): 2647-2655.

Packman, A.I. and Brooks, N.H., 1995. Colloidal particle exchange between stream and stream bed in a laboratory flume. Mar. Freshwater Res., 46: 233-236.

Packman, A.I., Brooks, N.H. and Morgan, J.J., 1997. Experimental techniques for laboratory investigation of clay colloid transport and filtration in a stream with a sand bed. Water Air Soil Pollut., 99: 113-122.

Packman, A.I., Brooks, N.H. and Morgan, J.J., 2000. A physicochemical model for colloid exchange between a steam and a sand streambed with bed forms. Water Resour. Res., 36(8): 2351-2361.

Parr, A.D., Richardson, C., Lane, D.D. and Baughman, D., 1987. Pore water uptake by agricultural runoff. J. Environ. Eng., 113(1): 49-63.

Patankar, S.V., 1980. Numerical Heat Transfer and Fluid Flow. Series in Computational Methods in Mechanics and Thermal Sciences. Hemisphere Publishing Corporation, Washington, 197 pp.

Prandtl, L., 1925. Uber die ausgebildete Turbulenzen. Z. Ang. Math., 5: 136-139.

Reichardt, H., 1951. Vollstandige darstellung der turbulenten geschwindigkeitsverteilung in glatten leitungen. Z. angew. Math. Mech., 31(7): 208-219.

Richardson, C.P. and Parr, A.D., 1988. Modified fickian model for solute uptake by runoff. J. Environ. Eng., 114(4): 792-809.

Richardson, C.P. and Parr, A.D., 1991. Friction and free-surface flow over porous media. J. Hydr. Engrg., ASCE, 117(11): 1496-1512.

Rouse, H., 1937. Modern conceptions of the mechanics of fluid turbulence. Transactions ASCE, 102(463-541).

Ruff, J.F. and Gelhar, L.W., 1972. Turbulent shear flow in porous boundary. J. Engrg. Mech. Div., ASCE, 98(EM4): 975-991.

Sakthivadivel, R. and Einstein, H.A., 1970. Clogging of porous column of spheres by sediment. J. Hydr. Div., ASCE 96(HY2): 461-472.

Schalchi, U., 1992. The clogging of coarse gravel river beds by fine sediment. Hydrobiologia 235/6: 189-197.

Schlichting, H., 1960. Boundary-layer theory. McGraw-Hill, New York.

Self, R.F.L., Nowell, A.R.M. and Jumars, P.A., 1989. Factors controlling critical shears for deposition and erosion of individual grains. Mar. Geol., 86: 181-199.

Sherard, J.L., Dunnigan, L.P. and Talbot, J.R., 1984a. Filters for silts and clays. J.

Geotech. Engrg., 110(6): 701-718.

Sherard, J.L., Dunnigan, L.P. and Talbot, J.R., 1984b. Basic properties of sand and gravel filters. J. Geotech. Engrg., 110(6): 684-700.

Shimada, M., Okuyama, K., Kousaka, Y. and Ohshima, K., 1987. Turbulent and brownian diffusive deposition of aerosol particles onto a rough wall. J. Chem. Eng. Japan, 20(1): 57-64.

Stolzenbach, K.D., Newman, K.A. and Wong, C.S., 1992. Aggregation of fine particles at the sediment-water interface. J. Geophys. Res., 97: 17889-17898.

Svensson, U. and Rahm, L., 1991. Toward a mathematical model of oxygen transfer to and within bottom sediments. J. Geophys. Res., 96(C2): 2777-2783.

Thibodeaux, L.J. and Boyle, J.D., 1987. Bedform-generated convective transport in bottom sediment. Nature, 325: 341-343.

Ward, J.C., 1964. Turbulent flow in porous media. J. Hydr. Div., ASCE, 90(HY5): 1-12.

Wheatcroft, R. A., Borgeld, J.C., Born, R.S., Drake, D.E., Leithold, E.L., Nittrouer, C.A. and Sommerfield, C.K., 1996. The anatomy of an ocean flood deposit. Oceanography 9(3): 158-162.

Wood, N.B., 1981. A simple method for the calculation of turbulent deposition to smooth and rough surfaces. J. Aerosol Sci., 12(3): 275-290.

Zagni, A.F.E. and Smith, K.V.H., 1976. Channel flow over permeable beds of graded spheres. J. Hydr. Div., ASCE, 102(HY2): 207-222.

Appendix A. Flow profile solutions for depth dependent diffusivity based on dispersion relationships

This appendix details the solution of an equation that governs the flow component of the model proposed in Chapter 3 of this thesis that determines the influence of diffusion on the interstitial flow profile. This solution based on work by Trowbridge (pers. comm.) in the pursuit of alternate flow models. The model expression can be expressed as a general differential equation,

$$\frac{\partial}{\partial z}\left(\nu_b \frac{\partial u}{\partial z}\right) = \frac{\nu}{K} u, \tag{A.1}$$

with the boundary conditions

$$u \to 0 \text{ as } z \to -\infty \tag{A.2a}$$

$$\nu_b \left.\frac{\partial u}{\partial z}\right|_{z=0} = u_*^2. \tag{A.2b}$$

The expressions for diffusivity from dispersion research differ slightly, but a general form would be

$$\nu_b = A \nu R_{K,b}^m = A \nu \left(\frac{u\sqrt{K}}{\nu}\right)^m, \tag{A.3}$$

where A and m are introduced as constants. By expanding the derivative, the differential equation becomes

$$u\frac{\partial^2 u}{dz^2} + m\left(\frac{\partial u}{dz}\right)^2 = \frac{\nu^m}{AK^{1+m/2}} u^{2-m}. \tag{A.4}$$

This equation is autonomous, allowing the substitution

$$\tilde{\phi} = \frac{\partial u}{\partial z}. \tag{A.5}$$

The differential equation can now be expressed as

$$\frac{u}{2}\frac{d\tilde{\phi}^2}{du} + m\tilde{\phi}^2 = \frac{\nu^m}{AK^{1+m/2}}u^{2-m}. \tag{A.6}$$

The solution for $\tilde{\phi}$ is obtained through altering the powers of u in the above expression,

$$\frac{d}{du}\left(u^{2m}\tilde{\phi}^2\right) = \frac{2\nu^m}{AK^{1+m/2}}u^{m+1}, \tag{A.7}$$

and integrating to obtain

$$u^{2m}\tilde{\phi}^2 = \frac{2\nu^m}{A(m+2)K^{1+m/2}}u^{m+2} + c_1, \tag{A.8}$$

where c_1 is an integration constant. This constant disappears in the limit of small u deep in the bed. This leads to

$$\tilde{\phi} = \frac{\partial u}{\partial z} = \sqrt{\frac{2}{A(m+2)}}\frac{\nu^{m/2}}{K^{1/2+m/4}}u^{1-m/2}, \tag{A.9}$$

and an expression for the flow,

$$u^{m/2} = \frac{m}{2}\sqrt{\frac{2}{A(m+2)}}\frac{\nu^{m/2}}{K^{1/2+m/4}}z + c_2, \tag{A.10}$$

where c_2 is an integration constant that is related to the slip velocity (u_s),

$$c_2 = u_s^{m/2}. \tag{A.11}$$

The solution for slip can be attained from the boundary condition at the interface,

$$u^{2m}\tilde{\phi}^2 = u_*^4 \frac{\nu^{2m-2}}{A^2 K} = \frac{2\nu^m}{A(m+2)K^{1+m/2}} u_s^{m+2}. \tag{A.12}$$

Therefore, the slip velocity is

$$u_s = \left(\frac{m+2}{2A}\right)^{1/m+2} \left(\frac{u_*^4 K^{1-m/2}}{\nu^{2-m}}\right)^{1/m+2} \tag{A.13}$$

$$\text{or } \frac{u_s}{u_*} = \left(\frac{m+2}{2A}\right)^{1/m+2} R_K^{\left(\frac{2-m}{2+m}\right)}. \tag{A.14}$$

This expression can be substituted into the profile expression to generate a solution,

$$\frac{u(z)}{u_*} = \frac{u_s}{u_*}\left(1+\frac{z}{\delta}\right)^{2/m}. \tag{A.15}$$

where δ is the flow penetration depth,

$$\frac{\delta}{\sqrt{K}} = (2A)^{1/m+2}(m+2)^{\left(\frac{2m+2}{2m+4}\right)} R_K^{\left(\frac{2m}{2+m}\right)} \tag{A.16}$$

Specific solutions for the dispersion models are presented in the text (Chapter 3) and Table A.1.

Table A.1. Summary of flow profile solutions for dispersion models.

Low $R_{K,b}$	High $R_{K,b}$
$A = 0.14;\ m = \frac{2}{3}$	$A = 1;\ m = 1$
$\frac{u(z)}{u_*} = \frac{u_s}{u_*}\left(1 + \frac{z}{\delta}\right)^3$	$\frac{u(z)}{u_*} = \frac{u_s}{u_*}\left(1 + \frac{z}{\delta}\right)^2$
$\frac{u_s}{u_*} \cong 2.3 R_K^{1/2}$	$\frac{u_s}{u_*} \cong 1.1 R_K^{1/3}$
$\frac{\delta}{\sqrt{K}} = 1.2 R_K^{1/2}$	$\frac{\delta}{\sqrt{K}} = 2.6 R_K^{2/3}$

Appendix B. Bessel function solution pertinent to the particle filtration model

This appendix details the solution of an equation that governs the filtration model proposed in Chapter 3 of this thesis which determines the amount of particle filtration due to a subsurface, particle-laden flow. The model expression can be expressed as a general differential equation,

$$\frac{\partial^2 \chi}{\partial \xi^2} = \Phi \chi \exp(\gamma \xi), \tag{B.1}$$

where all parameters are dimensionless and expressed in terms of the original variables,

$$\chi = \frac{C}{C_0}, \tag{B.2}$$

$$\xi = \frac{z}{d_g}, \tag{B.3}$$

$$\Phi = \frac{\lambda u_s d_g^2}{\nu_b}, \text{ and} \tag{B.4}$$

$$\gamma = 2 d_g \sqrt{\frac{\nu}{\nu_b K}}. \tag{B.5}$$

This equation is subject to the following boundary conditions:

$$\chi = 1 \text{ at } \xi = 0 \text{ and } \chi \to 0 \text{ at } \xi \to -\infty . \tag{B.6}$$

A substitution was used to alter the governing equation into a form whose solution is known. The substitution,

$$\zeta = \exp\left(\frac{\gamma \xi}{2}\right), \tag{B.7}$$

changes (B.1) into

$$\zeta^2 \frac{\partial^2 \chi}{\partial \zeta^2} + \zeta \frac{\partial \chi}{\partial \zeta} - \zeta^2 \frac{4\Phi}{\gamma^2} \chi = 0, \tag{B.8}$$

with the following new boundary conditions:

$$\chi = 1 \text{ at } \zeta = 1 \text{ and } \chi \to 0 \text{ at } \zeta \to 0 \ . \tag{B.9}$$

The solution of this equation is

$$\chi = c_3 I_0 \left\{ \frac{2}{\gamma} \sqrt{\zeta \Phi} \right\}. \tag{B.10}$$

I_0 is a modified Bessel function of the first kind of order zero (Hildebrand, 1976) and c_3 is a constant. From the boundary condition at $\zeta = 1$, the final expression becomes

$$\chi = \frac{I_0 \left\{ \frac{2}{\gamma} \sqrt{\zeta \Phi} \right\}}{I_0 \left\{ \frac{2}{\gamma} \sqrt{\Phi} \right\}} \ . \tag{B.11}$$

A flux at the boundary is prescribed that can be represented by an additional dimensionless variable ($\widetilde{F}$) and the gradient at $\xi = 0$,

$$\widetilde{F} = \frac{(w_d - w_s) d_g}{\nu_b} = \left(\frac{\partial \chi}{\partial \xi} \right)_{\xi = 0}, \tag{B.12}$$

Substituting (B.11) into (B.12), the flux expression becomes

$$\widetilde{F} = \left[\sqrt{\zeta \Phi} \frac{I_1 \left\{ \frac{2}{\gamma} \sqrt{\zeta \Phi} \right\}}{I_0 \left\{ \frac{2}{\gamma} \sqrt{\Phi} \right\}} \right]_{\zeta = 1} = \sqrt{\Phi} \frac{I_1}{I_0} \left\{ \frac{2}{\gamma} \sqrt{\Phi} \right\}. \tag{B.13}$$

For small arguments, confirmed in Figure B.1, the flux can be estimated as

$$\widetilde{F} \cong \frac{\Phi}{\gamma} \tag{B.14}$$

$$\text{or } \widetilde{F} = \frac{(w_d - w_s)d_g}{\nu_b} = \frac{\lambda u_s d_g^2}{2\nu_b}\sqrt{\frac{\nu_b K}{\nu d_g^2}} = \frac{\lambda u_s d_g}{2}\sqrt{\frac{K}{\nu\nu_b}}, \tag{B.15}$$

Substituting for u_s, the final form becomes,

$$E_d - 1 = R_K^2\left(\frac{\lambda\nu}{w_s}\right). \tag{B.16}$$

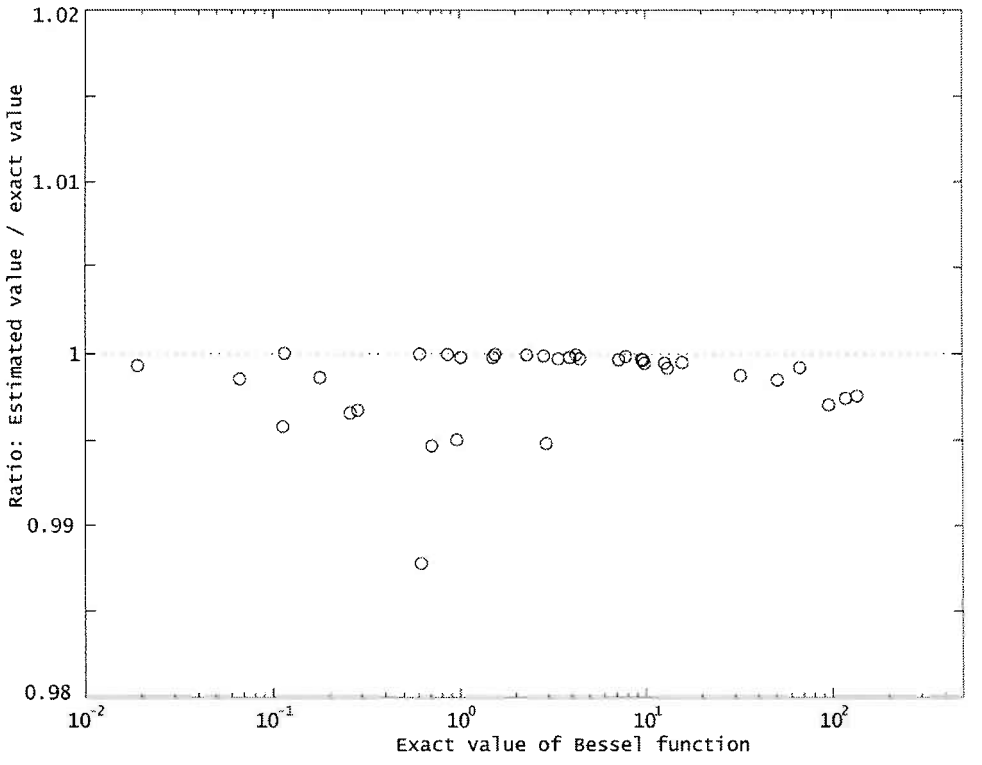

Figure B.1. Ratio of estimated value to the exact value of the Bessel function from (B.13). The ratio is plotted with respect to the exact value of the Bessel function. The points represent all experimental treatments presented in Chapter 2.

Appendix C. Notation used in thesis

Variable Name	Units	Description	Introduced in Chapter / Appendix
A	(-)	Coefficient in dispersion relationship	A
A_c	(L^2)	Surface area of cores	2
B	(L)	Void scale in sediment bed	4
b_f	(L)	Width of flume channel	2
C	$(M\ L^{-3})$	Particle concentration	1
$\overline{C}$	$(M\ L^{-3})$	Mean concentration of suspension	1
$\overline{C}_a$	$(M\ L^{-3})$	Ambient concentration	2
C_D	(-)	Channel drag coefficient	1
$\overline{C}_{H/T}$	$(M\ L^{-3})$	Concentration at HEAD or TAIL	2
C_r	$(M\ L^{-3})$	Reference concentration	1
$\overline{C}_0$	$(M\ L^{-3})$	Initial concentration in time series	2
C_Δ	$(M\ L^{-3})$	Concentration at capture distance	2
c	(-)	Constant for turbulent drag in sediment	3
D	$(L^2\ T^{-1})$	Particle diffusivity	1
D_R	(-)	Grain diameter ratio	1
d_g	(L)	Grain diameter	1
d_{g15}	(L)	Diameter for 15^{th} percentile of grain size dist.	3
d_{min}	(L)	Minimum particle diameter	2
d_p	(L)	Particle diameter	1
d_{p50}	(L)	Median particle diameter	2
E_D	(-)	Enhancement factor	1
e_A	$(M\ L^2\ T^{-2})$	Electrical affinity between grains and particles	3
F	$(M\ L^{-2}\ T^{-1})$	Depositional flux	1
$\tilde{F}$	(-)	Dimensionless flux	B
Fr	(-)	Froude number	1
f_I	(-)	Coefficient for interception	3
f_S	(-)	Coefficient for sedimentation	3

Variable Name	Units	Description	Introduced in Chapter / Appendix
g	$(L\ T^{-2})$	Gravitational acceleration	1
h	(L)	Depth of flow	1
h'	(L)	Adjusted water depth	2
K	(L^2)	Permeability	1
k	$(L\ T^{-1})$	Piston velocity for oxygen	3
k_s	(L)	Equivalent grain roughness	4
L	(L)	Channel length	2
L_L	(L)	Length for loss determination	2
$M_{pre/post}$	(M)	Total mass of sediment in PRE or POST cores	2
m	(-)	Power in dispersion relationship	A
m_{add}	(M)	Mass of particle addition to flume	2
m_c	(M)	Corrected mass of particles in core	2
$m_{pre/post}$	(M)	Mass of particles in PRE or POST cores	2
m_w	(M)	Predicted mass of particles in core from loss	2
n	(-)	Fraction of particle size distribution	2
p	$(M\ L^{-2}\ T^{-2})$	Pressure in sediment	3
R	(-)	Rouse number	1
R_*	(-)	Grain Reynolds number	1
R_h	(-)	Channel Reynolds number	1
R_K	(-)	Bed Reynolds number	1
$R_{K,b}$	(-)	Bed Reynolds number for local velocity	3
Sc	(-)	Schmidt number	1
t	(T)	Time	2
t_{core}	(T)	Elapsed run time prior to coring	2
t_{p+}	(-)	Particle relaxation time	1
t_R	(T)	Run time	3
$t_{0,H/T}$	(T)	Lag time for time series at HEAD or TAIL	2
U	$(L\ T^{-1})$	Mean horizontal velocity	1
u	$(L\ T^{-1})$	Local fluid velocity in sediment	3
u_*	$(L\ T^{-1})$	Shear velocity	1

Variable Name	Units	Description	Introduced in Chapter / Appendix
$\overline{u'w'}$	$(L^2\ T^{-2})$	Time averaged velocity covariance	4
u_d	$(L\ T^{-1})$	Darcy velocity	3
u_f	$(L\ T^{-1})$	Filtration velocity	3
u_r	$(L\ T^{-1})$	RMS of horizontal velocity	4
u_s	$(L\ T^{-1})$	Slip velocity	2
V_f	(L3)	Volume of flume	2
W	$(L\ T^{-1})$	Wake velocity profile	2
w_d	$(L\ T^{-1})$	Deposition velocity	1
w_L	$(L\ T^{-1})$	Loss velocity	2
w_s	$(L\ T^{-1})$	Settling velocity of particles	1
x	(L)	Alongstream distance	2
z	(L)	Elevation or depth in bed	1
z_+	(-)	Dimensionless elevation	2
z_r	(L)	Reference elevation	1
α	(T^{-1})	General decay for concentration time series	2
$\alpha_{H/T}$	(T^{-1})	Decay of concentration at HEAD or TAIL	2
γ	(-)	Dimensionless decay of flow profile	B
Δ	(L)	Displacement in profile	4
Δ_+	(-)	Dimensionless displacement	4
Δ_D	(L)	Capture distance	2
δ	(L)	Flow penetration scale	3
δ_f	(L)	Total fluid penetration	3
δ_p	(L)	Particle penetration	3
δ_D	(L)	Diffusive sublayer thickness	1
ε	(-)	Correction term for spatial variability of cores	2
ζ	(-)	Exponential scale in Bessel function	B
η_D	(-)	Capture efficiency	2
Θ	(T^{-1})	Consumption rate for oxygen	3
κ	(-)	von Karman's constant	1

Variable Name	Units	Description	Introduced in Chapter / Appendix
λ	(L^{-1})	Filtration efficiency	3
λ'	(T^{-1})	Filtration decay	3
λ_I	(L^{-1})	Filtration efficiency for interception	3
λ_S	(L^{-1})	Filtration efficiency for sedimentation	3
ν	$(L^2\ T^{-1})$	Fluid kinematic viscosity	1
ν_b	$(L^2\ T^{-1})$	Diffusivity in sediment bed	3
ν_t	$(L^2\ T^{-1})$	Turbulent diffusivity	2
ξ	(-)	Dimensionless depth in bed	B
Π	(-)	Wake parameter	2
ρ	$(M\ L^{-3})$	Fluid density	1
ρ'	(-)	Suspension density anomaly	1
ρ_p	$(M\ L^{-3})$	Particle density	1
σ	(L)	Integration variable for particle diameter	2
τ_b	$(M\ L^{-1}\ T^{-2})$	Bed shear stress	1
Φ	(-)	Dimensionless filtration term	B
ϕ	(-)	Porosity	1
$\tilde{\phi}$	(T^{-1})	Gradient of velocity in bed	A
χ	(-)	Dimensionless concentration	B

Units consist of mass (M), length (L), and time (T).